RELATIONSHIP BETWEEN MICROSTRUCTURE AND COLD DEFORMATION BEHAVIOR OF ALUMINUM ALLOYS USING THERMODYNAMIC MODELING METHOD

By

Nazia Nafsin

Student Number – 0411112026P

A thesis paper submitted to the Department of Materials and Metallurgical Engineering of Bangladesh University of Engineering and Technology, Dhaka in partial fulfillment of the requirements for the Degree of Master of Science in Materials and Metallurgical Engineering.

Department of Materials and Metallurgical Engineering

Bangladesh University of Engineering and Technology

June, 2013

The thesis titled "**Relationship between Microstructure and Cold Deformation Behavior of Aluminum Alloys Using Thermodynamic Modeling Method"** submitted by **Nazia Nafsin**, Student No. 0411112026P, Session-April 2011, has been accepted as satisfactory in partial fulfillment of the requirements for the degree of Master of Science in Materials and Metallurgical Engineering on June, 2013.

BOARD OF EXAMINERS

1. Dr. Hossain Mohammad Mamun Al Rashed — Chairman (Supervisor)
   Assistant Professor
   Department of Materials and Metallurgical Engineering
   BUET, Dhaka - 1000

2. Dr. Md. Mohar Ali — Member (Ex-officio)
   Professor and Head
   Department of Materials and Metallurgical Engineering
   BUET, Dhaka - 1000

3. Dr. Kazi Md. Shorowordi — Member
   Assistant Professor
   Department of Materials and Metallurgical Engineering
   BUET, Dhaka - 1000

4. Dr. Md. Abdul Gafur — Member (External)
   Senior Engineer, PP and PDC
   Bangladesh Council of Science and Industrial Research (BCSIR)
   Dhaka - 1205

Declaration

It is hereby declared that this thesis or any part of it has not been submitted elsewhere for the award of any degree or diploma.

Nazia Nafsin

This work is dedicated to

My Parents

ACKNOWLEDGEMENT

The author is deeply indebted to her supervisor Dr. Hossain Mohammad Mamun Al Rashed, Assistant Professor, Department of Materials and Metallurgical Engineering (MME), Bangladesh University of Engineering and Technology (BUET) for his continuous guidance, help, suggestions and encouragement throughout the progress of the project work.

The author expresses her sincere gratitude to the Head of Department of MME, Professor Dr. Md. Mohar Ali, for providing her with the laboratory facilities to carry out this research work. The author also expresses her heartiest thanks to all teachers and employees of the Department of MME who directly or indirectly help her during this work.

The author deeply acknowledges the help rendered by Dr. Md. Abdul Gafur, Senior Engineer, PP and PDC, BCSIR, Dhaka for his help for obtaining Differential Thermal Analysis. The author is thankful to Materials Science Division, Atomic Energy Centre, especially to Mr. Md. Al Mamun, for his support in Energy Dispersive X-Ray analysis.

The author is highly thankful to Mr. Abdullah Al Maksud for helping her with the operation and handling of Optical Emission Spectroscopy.

The author is also thankful to Mr. Md. Washim Uddin, Mr. Md. Harun-Ur- Rashid, Mr. Md. Shamsul Alam and Mr. Ahmad Ullah for their kind assistance with the laboratory works.

Finally, the author is deeply indebted to her parents, sibling and especially to Md. Mahbubul Hasan for providing mental strength to continue the research work smoothly.

TABLE OF CONTENTS

LIST OF FIGURES

CHAPTER 2

CHAPTER 3

CHAPTER 4

LIST OF TABLES

LIST OF ABBREVIATIONS

DTA:	Differential Thermal Analysis
EDX:	Energy Dispersive X-Ray
EQM:	Equilibrium Solidification
SEM:	Scanning Electron Microscope
SG:	Scheil-Gulliver Solidification
UTM:	Universal Testing Machine

ABSTRACT

The current work emphasizes establishment of relationship between microstructure and cold deformation behavior of aluminum-copper -magnesium alloys. Aluminum-copper-magnesium alloys with varying Cu% and Mg% were casted and undergone cold deformation after homogenization, and their microstructures were examined using optical microscope. Using CALPHAD method, phases developed for different levels of Cu and Mg were modeled in JMatPro software package. It has been found that the prediction performed in equilibrium condition matches closely to phase fraction simulation. It can predict several extra phases in comparison to the equilibrium simulation. Image analysis by ImageJ also confirms this finding experimentally. Finally, the effects of deformation were studied by measuring the hardness of those alloys.

From this study it was possible to predict the weight fractions of phases formed during solidification and homogenization using CALPHAD modeling. EDX results confirmed the formation of Al_2Cu phase (white phase) and Al_7Cu_2M and Mg_2Si phases (black phases) as modeled in CALPHAD. With increasing amount of copper and magnesium in the binary aluminum-copper alloy system, fraction of Al_2Cu, Al_7Cu_2M, Al_2CuMg and Mg_2Si phases increased which increased hardness values. However, those additions lowered liquidus and solidus temperatures of alloys as investigated from DTA and modeling.

The phase fractions of different alloys obtained from CALPHAD were verified using image analysis techniques. Image analysis data showed a convincing conformation of phases that formed during solidification and through solid state diffusion.

Homogenization and solution treatment had a negative effect on the hardness values of investigated aluminum alloys due to dissolution of Al_2Cu and Mg_2Si phases in to the aluminum matrix. On the other hand, deformation increased the number of dislocations by interactions of dislocation during deformation and other defects, which caused an enhancement of hardness values. Deformation also causes microstructural changes by

destroying the necklace like shape of Al-Cu-Mg phases initially obtained in as-cast and homogenized alloys. For this reason, with larger amount of deformation, the increment of hardness may not be very significant. After comparing the effects of all the processing parameters i.e. homogenization, deformation and alloy addition on hardness, it was revealed using ANOVA modeling, that magnesium addition and amount of deformation affects hardness of Al-Cu-Mg alloys to a large extent compared to addition of copper and homogenization.

CHAPTER 1
INTRODUCTION

Environmental legislation to reduce emission of greenhouse gases is forcing transportation industries to find out substitutes of steels – currently profoundly used in vehicle production. Aluminum, being lighter than steel, is considered as an exciting alternative material in such applications. The environmental issue of emissions has triggered the requirement to minimize vehicle weight, but at the same time increased performance is required to satisfy customer expectations. The performance of vehicle engines is limited by the piston material's ability to sustain surrounding pressure and temperature. This drives the continuous development of new alloys.

For this development, an examination of effects of different alloying elements on microstructure is necessary. As statistical experiments on multi-component systems are expensive and complex, the use of thermodynamic and kinetic software is popular to calculate models of phase fractions and properties. Phases can be predicted for both equilibrium and non-equilibrium Scheil-Gulliver solidification conditions with varying amount of alloying elements. The accuracy of the model is, therefore, very important. An effort is made to analyze predicted models with experimental microstructural results to verify the performance of modeling under various solidification conditions.

The most important cast aluminum alloy system is Al-Cu alloys. The addition of copper as main alloying element (mostly ranges between 3 and 6 wt %, but can be much higher), with or without magnesium as alloying constituent (range up to 2 wt %), allows material strengthening by precipitation hardening, resulting in good strengthening. Also the fatigue properties are very good for this series [1]. Nevertheless, the corrosion properties may degrade for such composition.

Up to 12 wt. % copper the strength of the alloy can increase through precipitation hardening, with or without the presence of Mg; Hardening is achieved through the precipitation of Al_2Cu or Al_2CuMg intermetallic phases during ageing which leads to strengths second only to the highest strength 7xxx series alloys [1-2]. Above 12 wt. % Cu the alloy becomes brittle. These alloys can also be used for high strength structural applications, such as aircraft fittings and wheels, military vehicles and bridges, forgings for trucks [1-2]. The main benefit of adding magnesium to aluminum-copper alloys is the increased strength and hardness following solution heat treatment and quenching [1].

The present study includes the microstructural effects on deformation of aluminum alloys. Aluminum alloys of specified composition were casted and homogenized at 400^{o}C for four hours. Then microstructures of as cast and homogenized alloys were observed. Compression tests involving 10%, 20% and 50% deformations were performed at room temperature on the homogenized samples. Finally the effects of changes in microstructure and hardness on deformation of aluminum alloys were studied using thermodynamic modeling software and image analysis.

From this research it will be possible to fabricate aluminum alloys using different alloying elements. Homogenization temperatures of these alloys will also be possible to determine using thermodynamic modeling. These might provide important information regarding the influence of alloying elements on microstructure and mechanical properties.

The reminder of the thesis is divided into a number of chapters. Chapter Two is a review of previous works relevant to this study. Initially it describes aluminum alloys, classification of aluminum alloys, effects of major and minor alloying elements on aluminum alloys, aluminum-copper phase diagram, homogenization of aluminum alloys, CALPHAD modeling software, solidification techniques: equilibrium and Scheil-Gulliver solidification, plastic deformation and work hardening.

Chapter Three describes the materials and equipment used in the present work, alloy preparation technique, homogenization and cold deformation processes, phase quantification techniques: image analysis and thermodynamic modeling. Then procedure of determination of hardness is described.

Chapter Four describes the results and discussion on all mechanical, structural and morphological properties.

Finally, chapter Five summarizes the major conclusions from the results of the present research.

CHAPTER 2
LITERATURE REVIEW

This chapter presents a brief review on the literature related to the aluminum alloys, effects of various alloying elements on aluminum, their solidification mechanism, heat treatment processes, cold deformation and thermodynamic modeling techniques of these aluminum alloys.

2.1 Aluminum Alloys

Aluminum alloys are alloys in which aluminum (Al) is the predominant metal. The typical alloying elements are copper, magnesium, manganese, silicon and zinc. There are two principal classifications, namely casting alloys and wrought alloys, both of which are further subdivided into the categories heat-treatable and non-heat-treatable. About 85% of aluminum is used for wrought products, for example rolled plate, foils and extrusions. Cast aluminum alloys yield cost effective products due to the low melting point, although they generally have lower tensile strengths than wrought alloys [3]. Aluminum alloys are widely used in engineering structures and components where light weight or corrosion resistance is required [3].

At high temperatures (200-250 °C) aluminum alloys tend to lose some of their strength. However, at subzero temperatures, their strength increases while retaining their ductility, making aluminum an extremely useful low-temperature alloy [4].

Aluminum alloys have a strong resistance to corrosion which is a result of an oxide skin that forms as a result of reactions with the atmosphere [4]. This corrosive skin protects aluminum from most chemicals, weathering conditions, and even many acids, however alkaline substances are known to penetrate the protective skin and corrode the metal [4].

Aluminum alloys with a wide range of properties are used in engineering structures. Alloy systems are classified by a number system (ANSI) or by names indicating their main alloying constituents. Selecting the right alloy for a given application entails considerations of its tensile strength, density, ductility, formability, workability, weldability, and corrosion resistance, to name a few. A brief historical overview of alloys and manufacturing technologies is given in R.E. Sanders, 2001 [5]. Aluminum alloys are used extensively in aircraft industries due to their high strength-to-weight ratio. On the other hand, pure aluminum metal is much too soft for such usage, and it does not have the high tensile strength that is needed for airplanes and helicopters [5].

2.2 Classification of Aluminum Alloys

As mentioned earlier, there are two main classes of aluminum alloy:

- Cast alloys are directly cast into their final form by one of various methods such as sand-casting, die or pressure die casting. Casting is used for complex product shapes. These alloys contain high levels of silicon to improve their castability.
- Wrought alloys, which are initially cast as ingots or billets and subsequently hot and/or cold-worked mechanically into the desired form. i.e.

    - rolling to produce sheet, foil or plate
    - extrusion to produce profiles, tubes or rods
    - forming to produce more complex shapes from rolled or extruded stock
    - forging to produce complex shapes with superior mechanical properties

These two main classes of alloys have different systems of classification. Generally similar alloy elements are added, but in different quantities [6].

2.2.1 Cast alloys

The aluminum Association (AA) has adopted a nomenclature similar to that of wrought alloys. British Standard and DIN have different designations. In the AA system, the second two digits reveal the minimum percentage of aluminum, e.g. 150.x corresponds to a minimum of 99.50% aluminum. The digit after the decimal point takes a value of 0 or 1,

denoting casting and ingot respectively [3]. The main alloying elements in the AA system are as follows:

- 1xx.x series are (minimum 99% aluminum)
- 2xx.x series (copper)
- 3xx.x series (silicon, copper and/or magnesium)
- 4xx.x series (silicon)
- 5xx.x series (magnesium)
- 7xx.x series (zinc)
- 8xx.x series (tin)

2.2.2 Wrought alloys

The International Alloy Designation System is the most widely accepted naming scheme for wrought alloys. Each alloy is given a four-digit number, where the first digit indicates the major alloying elements [3].

- 1000 series are essentially pure aluminum with a minimum 99% aluminum content by weight and can be work hardened.
- 2000 series are alloyed with copper, can be precipitation hardened to strengths comparable to steel. Formerly referred to as duralumin, they were once the most common aerospace alloys, but were susceptible to stress corrosion cracking and are increasingly replaced by 7000 series in new designs.
- 3000 series are alloyed with manganese, and can be work hardened.
- 4000 series are alloyed with silicon. They are also known as silumin.
- 5000 series are alloyed with magnesium.
- 6000 series are alloyed with magnesium and silicon, are easy to machine, and can be precipitation hardened, but not to the high strengths that 2000 and 7000 can reach.
- 7000 series are alloyed with zinc, and can be precipitation hardened to the highest strengths of any aluminum alloy.
- 8000 series is a category mainly used for lithium alloys.

2.3 Effects of Alloying Elements

A brief discussion of alloying elements commonly used in aluminum alloys is described below. An extensive survey on few major alloying elements is described in Section 2.4.1.

2.3.1 Silicon

Pure aluminum melts at 660.3 °C. It is not suitable for casting and is only used for electrical applications (where high conductivity is essential), and a few other special applications. Most casting alloys contain silicon as the major alloying element. Silicon forms a eutectic with aluminum at 11.7% Si, 577°C. Silicon additions improve casting characteristics by improving fluidity, feeding and hot tear resistance. The silicon-rich phase is hard, so the hardness of the alloy is increased with silicon content but ductility and machinability are reduced [7].

The eutectic alloys have the highest fluidity for a given casting temperature and having a short freezing range, they solidify with primary shrinkage. They are good for thin section castings. Where higher strength is needed, the lower silicon alloys are used. The hypereutectic alloys are difficult to machine, they are used for wear-resistant applications such as pistons.

2.3.2 Copper

Improves strength, hardness, machinability and thermal conductivity. Heat treatment is most effective with 4–6% copper alloys. Copper decreases castability and hot tear resistance together with corrosion resistance.

2.3.3 Magnesium

Small additions of 0.25–0.5% magnesium allow Al–Si alloys to be hardened by heat treatment, improving mechanical properties through the precipitation of Mg_2Si in a finely dispersed form. Their proof stress can be almost doubled.

Mg is used at levels of around 1% in high silicon piston alloys. Higher levels still, around 3–6% magnesium, are used in low silicon alloys to improve the anodizing characteristics and give a bright surface finish for decorative components. Magnesium content is kept low

in pressure die casting alloys to avoid embrittlement. The presence of magnesium increases the oxidation losses of liquid aluminum [7].

2.3.4 Iron

Levels of 0.9–1.0% iron are used in pressure die casting alloys to prevent die sticking. High iron contents decrease ductility, shock resistance and machinability.

Castability is decreased by iron due to the formation of sludge phases with manganese and chromium etc. For this reason, alloys for processes other than pressure die casting are limited to less than 0.8% iron [7].

2.3.5 Manganese

Manganese improves casting soundness at levels over 0.5%. Manganese controls the intermetallic form of iron in the alloy, leading to improved ductility and shrinkage characteristics [7].

2.3.6 Nickel

When combined with copper, nickel enhances strength and hardness at elevated temperature.

2.3.7 Zinc

When zinc is combined with copper and magnesium, heat treatment and natural ageing characteristics are improved. The fluidity is increased but shrinkage problems may occur [7].

2.3.8 Lead

Lead improves machinability at levels over 0.1%.

2.3.9 Titanium

Titanium refines the grain structure when combined with boron.

2.3.10 Phosphorus

Phosphorus refines the primary silicon phase in hypereutectic alloys. In hypoeutectic alloys, low levels of phosphorus coarsen the eutectic structure and reduce the effect of sodium and strontium eutectic modifiers [7].

2.3.11 Strontium

If used in levels of 0.008–0.04%, strontium modifies the Al–Si eutectic structure.

2.3.12 Sodium

Sodium is used to modify the eutectic structure.

2.3.13 Lithium

The great advantage of lithium is the reduction of weight of the alloy system. While lithium up to 3% may be used to improve the properties of wrought aluminum alloys, it has a generally harmful effect on casting properties by reducing the effectiveness of sodium or strontium modifiers at levels above 0.5%. At even lower levels, above 0.01%, porosity problems are experienced. It is recommended that lithium levels below 0.003% are used for casting alloys [7].

2.4 Effects of Alloying Elements on Cast Aluminum Alloys

'The Aluminum Association's Designations and Chemical Composition Limits for Aluminum Alloys in the Form of Castings and Ingot' lists for each alloy 10 specific alloying elements. Not all of the listed elements are major alloying ingredients in terms of an alloys intended uses; some major elements in one alloy are not major elements in another. Also, some elements, like Sr for example, can be very important to microstructure control and mechanical properties but are not specifically identified in the Aluminum Association document and are instead are merely included in the category of very minor additions [8].

For purposes of understanding their effects and importance, alloying elements for the majority of alloys are probably best classified as major, minor, microstructure modifiers or

impurities; understanding, however, those impurity elements in some alloys might be major elements in others:

• Major elements typically include silicon (Si), copper (Cu) and magnesium (Mg)

• Minor elements include nickel (Ni) and tin (Sn) - found largely in alloys that likely would not be used in high integrity die castings

• Microstructure modifying elements include titanium (Ti), boron (B), strontium (Sr), phosphorus (P), beryllium (Be), manganese (Mn) and chromium (Cr)

• Impurity elements would typically include iron (Fe), chromium (Cr) and zinc (Zn).

2.4.1 Major Elements

2.4.1.1 Silicon

Silicon (Si) is unquestionably the most important single alloying ingredient in the vast majority of aluminum casting alloys. Silicon is primarily responsible for so-called “good castability”; i.e., the ability to readily fill dies and to solidify castings with no hot tearing or hot cracking issues.

Silicon’s important role as an alloying ingredient is several-fold:

• Silicon’s high heat of fusion contributes immensely to an alloy’s “fluidity” or “fluid life”.

• The fact that silicon has limited solid solubility (maximum 1.65%) and yet forms a eutectic with aluminum at a significantly high level (11.7%) means that alloys with more than a few percent silicon undergo a relatively large volume fraction of isothermal solidification, thus they gain significant strength while undergoing little or no thermal contraction-very important to avoiding hot tearing or hot cracking issues [8, 10].

• The more silicon an alloy contains, the lower is its thermal expansion coefficient.

• Silicon is a very hard phase, thus it contributes significantly to an alloy’s wear resistance.

• Silicon combines with other elements to improve an alloy's strength and to make alloys heat treatable.

• Silicon can cause a permanent increase in a casting's dimensions if the part is not thermally stabilized before being put into elevated temperature service.

Isothermal solidification — pure aluminum (Al) solidifies "isothermally", that is, at a single temperature. Eutectic compositions (Al with 11.7% Si, such as 413 alloy for example) also solidify essentially "isothermally", that is, within a very narrow temperature window. They tend to solidify progressively from the die surface toward the thermal center of the casting's cross-section. There exists a very narrow plane of demarcation between the solidified portion and the remaining liquid. That solidification pattern alone provides a minimum tendency to hot tear during casting. The planar front solidification of very narrow freezing range alloys produces a sound skin extending toward the thermal center of the casting section. At the end of solidification, any liquid to solid transition shrinkage is confined along the thermal centerline of the casting [8, 10].

Because solidification shrinkage is not connected to the surface of the casting, castings produced from such alloys are usually pressure tight.

The presence of Si generally overcomes the hot-shortness and also the poor fluidity of casting alloys. As little as 5% silicon in an alloy provides a sufficient degree of isothermal solidification to overcome any major hot shortness issues and, at the same time, improves fluidity. Metal casters often label broad freezing range aluminum alloys as being quite "difficult to cast." It is not, however, their solidification temperature range that makes them difficult, but rather, their characteristic cooling curve shapes (little isothermal solidification) and their lack of fluidity, both brought on by their lack of sufficient silicon [10].

Alloys 333 (Al-8.0/10.0Si-1Fe-3/4Cu) also have relatively broad solidification temperature ranges, but those alloys contain significant quantities of silicon, to have excellent fluidity and they undergo a substantial degree of relatively isothermal solidification [8].

All 3XX and 4XX alloys undergo a significant degree of relatively isothermal solidification at their major Al-Si eutectic arrest. By the time cooling resumes below that arrest

temperature, the bulk of the solid has already formed and only the lowest melting temperature phases remain liquid (generally, the copper and/or magnesium bearing eutectics). The 3XX and 4XX alloys already have, at that point, sufficient structure and strength to overcome whatever cooling-contraction restrictions the mold might impose as the casting continues to solidify from the Al-Si eutectic arrest to the solidus temperature [10].

3XX and 4XX alloys have almost no tendency to hot tear or hot crack, except where some form of imposed “hot spot” might exist in the die during late stages of solidification.

Strength — Silicon alone contributes very little to the strength of aluminum casting alloys. However, when combined with magnesium to form Mg_2Si, Si provides a very effective strengthening mechanism in aluminum castings. Mg_2Si is soluble in the solid alloy to a limit of about 0.7% Mg, and provides the precipitation strengthening basis for an entire family of heat-treatable alloys (alloy numbers 356 through 360 and their many variations).

Thermal Expansion Coefficient — increasing the silicon level in an alloy decreases its thermal expansion coefficient as well as its specific gravity.

Wear Resistance — Silicon also increases an alloy’s wear resistance, which has often made aluminum silicon alloy castings attractive substitutes for gray iron in automotive applications. The hypereutectic Al-Si alloys, such as B390, are used extensively in premium aluminum bare-bore engine blocks, for example, as well as in numerous pumps, compressors, pistons and automatic transmission components [10].

Silicon and Cutting Tool Wear - As important as silicon’s contributions are to improved casting characteristics, there exists a downside as well. The more silicon an alloy contains, especially into the hypereutectic range, the greater the tool wear during machining, With the current popularity of polycrystalline diamond cutting tools, tool wear has become less and less of an issue when selecting casting alloys. It continues to be an important consideration however where high-speed steel (HSS), carbide or other less wear-resistant tool materials are employed [10].

2.4.1.2 Copper

Copper (Cu) has the single greatest impact of all alloying elements on the strength and hardness of aluminum casting alloys, both heat-treated and not heat-treated and at both ambient and elevated service temperatures. Copper also improves the machinability of alloys by increasing matrix hardness, making it easier to generate small cutting chips and fine machined finishes. On the downside, copper generally reduces the corrosion resistance of aluminum; and, in certain alloys and tempers, it increases stress corrosion susceptibility [1, 10].

Aluminum-copper alloys that do not also contain at least moderate amounts of silicon have relatively poor fluidity and resistance to hot tearing during solidification. Although alloys with up to 10% copper were popular in the very early years of the aluminum foundry industry, they have now been replaced by silicon containing alloys, with the exception of the very-high-strength alloy 206 that is described later.

2.4.1.3 Magnesium

Magnesium's (Mg) role is also to strengthen and harden aluminum castings. Silicon combines with magnesium to form the hardening phase, Mg_2Si that provides the strengthening and heat treatment basis for the popular 356 family of alloys. Magnesium is also the strengthening ingredient in the high magnesium 5XX alloys that contain very little silicon [1, 8 and 10]. Those alloys too depend on Mg_2Si, but gain additionally from other magnesium-bearing phases.

The Al-Mg alloys 515 through 518 are designated for die casting, as are the proprietary Al-Mg alloys "Magsimal-59" developed by Rheinfelden Aluminum in Germany, "Maxxalloy 59" developed by SAG in Austria and Aural 11 by Alcan [6]. The strength of binary Al-Mg compositions is not generally improved by heat-treating, however, these alloys have excellent strength and ductility in the as-cast and room temperature self-aged condition. Al-Mg alloys have marginal castability (they are aggressive toward tools, they lack fluidity because of their low silicon and they tend to be hot-short). However, they have excellent

corrosion resistance and they tend to anodize to a natural aluminum color. Machinability of these alloys is also excellent [10].

Magnesium's greatest influence on strength occurs, not in the 5XX alloy series, but rather when it is combined with silicon in 3XX alloys to form Mg_2Si and/or with copper in 3XX or 2XX alloys, forming the precipitation-hardening phase, Al_2CuMg.

2.4.2 Minor Elements

2.4.2.1 Nickel

Nickel (Ni) enhances the elevated temperature service strength and hardness of 2XX alloys. It is employed for the same purpose in some 3XX alloys, but its effectiveness in the silicon-containing alloys is less dramatic.

2.4.2.2 Tin

Tin (Sn) in 8XX aluminum casting alloys is for the purpose of reducing friction in bearing and bushing applications. The tin phase in those alloys melts at a very low temperature (227.7 ^{o}C). Tin can exudes under emergency conditions to provide short-term liquid lubrication to rubbing surfaces if such bearings/bushings severely overheat in service.

The 8XX series alloys are not generally applicable to die casting or its variations and thus are not shown among the alloys suitable for high integrity die casting [10].

2.4.3 Microstructure Modifying Elements

2.4.3.1 Titanium and Boron

Titanium (Ti) and boron (B) are used to refine primary aluminum grains. Titanium alone, added as a titanium aluminum master alloy, forms $TiAl_3$, which serves to nucleate primary aluminum dendrites. More frequent nucleation or initiation of dendrites means a larger number of smaller grains. Grain refinement is illustrated in Figure 2.1.

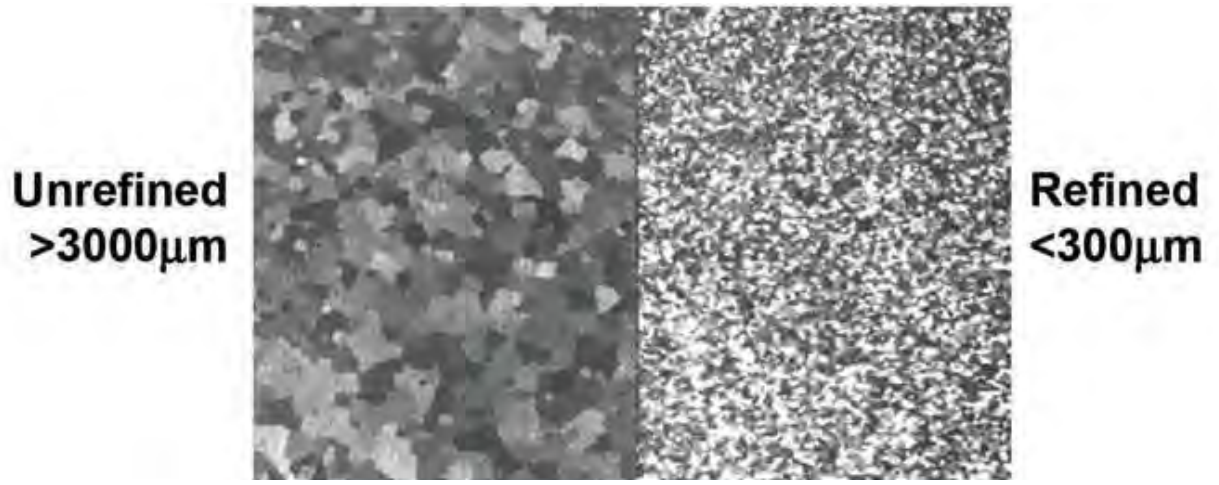

Figure 2.1: Illustration of grain-refined aluminum by Titanium and Boron [10].

Grain refining efficiency is better when titanium and boron are used in combination. Master alloys of aluminum with 5% titanium and 1% boron are commonly used additives for this purpose. They form TiB_2 and $TiAl_3$, which together are more effective grain refiners than $TiAl_3$ alone. The most efficient grain refiner for Al-Si alloys has a Ti:B ratio closer to 1.5:1. That is a special case, applicable to 3XX and 4XX alloys and not to the other alloy systems [10].

2.4.3.2 Strontium, Sodium, Calcium and Antimony

These elements (one or another, and not in combination) are added to eutectic or hypoeutectic aluminum silicon casting alloys to modify the morphology of the eutectic silicon phase. Without the benefit of a modifying treatment, eutectic silicon solidifies in a relatively coarse continuous network of thin platelets, shown in Figures 2.2-2.4. That morphology provides abundant stress risers and thus limits the attainment of maximum strength and ductility. Modification with one of the above elements changes the eutectic silicon into a fine fibrous or lamellar structure (Figures 2.2 and 2.3).

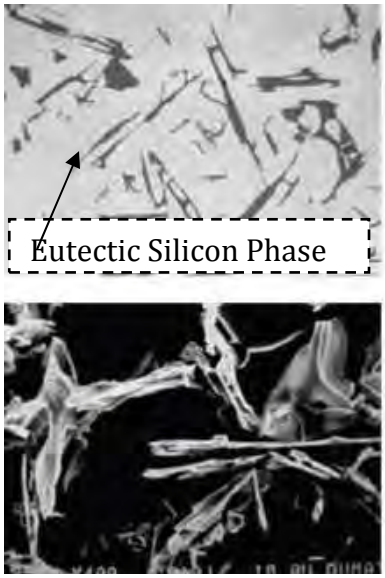

Figure 2.2: Unmodified silicon Phase [10].

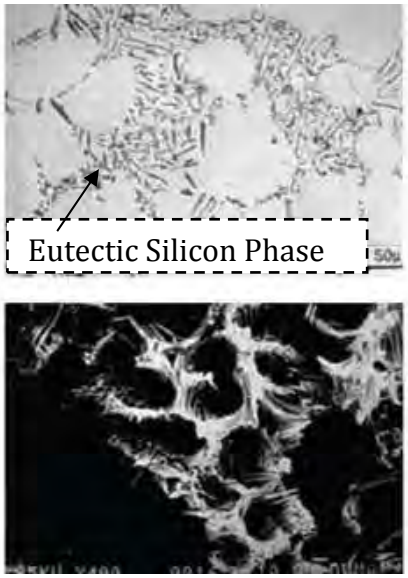

Figure 2.3: Modified silicon phase [10].

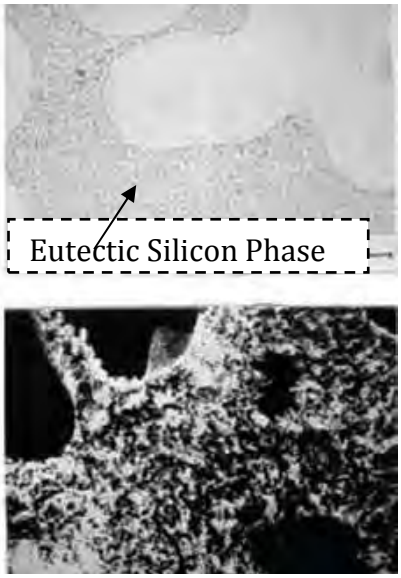

Figure 2.4: Super-modified silicon phase [10].

2.4.3.3 Strontium

Strontium accomplishes the same modified eutectic silicon structure as sodium, but strontium's effect fades at a much slower rate. Strontium is usually added to somewhat higher retained levels than sodium (0.01 - 0.025%); but strontium can generally be counted on to remain effective for many hours and through numerous re-melts. Because of this, strontium has become the preferred modifier now-a-days.

2.4.3.4 Manganese & Chromium

Alone or in combination, manganese (Mn) and/or chromium (Cr) change the morphology of the iron-rich Al_5FeSi phase (Figure 2.5) from its typical platelet/acicular form to a more cubic $Al_{15}(MnFe)_3Si_2$ form (Figure 2.6) that is less harmful to ductility. That forms the rationale for the 'Designations and Chemical Composition Limits for Aluminum Alloys in the Form of Castings and Ingot' stipulation in 356.1 alloy; "if iron exceeds 0.45%, manganese content shall not be less than one-half the iron content." As with the platelet/acicular Al_5FeSi phase, the volume fraction and size of the cubic $Al_{15}(MnFe)_3Si_2$ phase is also a function of concentration levels and solidification rate. Greater concentrations of iron, manganese and/or chromium are tolerable at higher solidification rates.

While manganese and/or chromium cause a beneficial change to the morphology of iron phases, it is that change in combination with large concentrations of iron, manganese and chromium that leads to “sludge” in traditional secondary die casting alloys. Manganese has proven to be a suitable substitute for iron to minimize "soldering" of the cast melt to steel tooling during die casting [10].

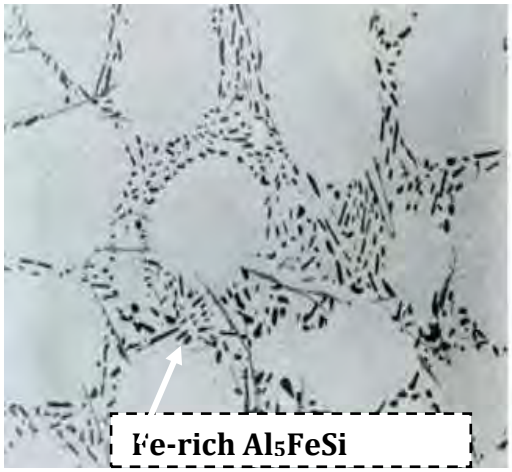

Figure 2.5: Fe-rich Al_5FeSi [10].

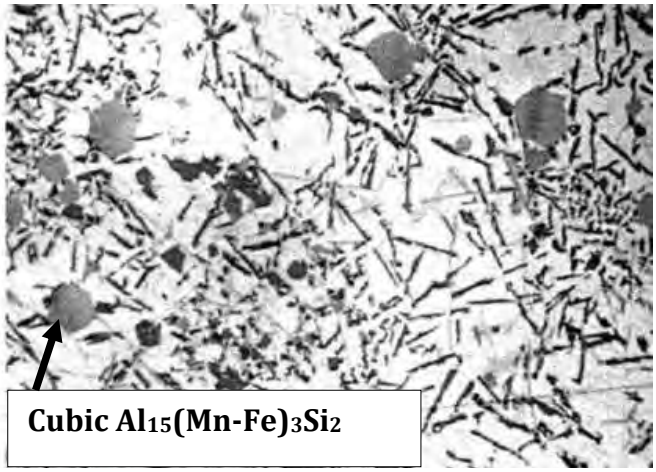

Figure 2.6: Cubic $Al_{15}(Mn\text{-}Fe)_3Si_2$ form phase in platelet form [10].

Manganese and/or chromium also tend to stabilize some 2XX and 7XX alloys at elevated service temperatures. Chromium especially suppresses grain growth in those systems. Manganese and chromium impart a bronze to gold color to 7XX alloys that are anodized.

2.4.4 Impurity Elements

2.4.4.1 Iron

Iron (Fe) is present in most traditional die casting alloys as an impurity, yet a very useful impurity. Iron in concentrations of 0.8% or more greatly reduces the tendency of an alloy to solder to die casting tooling. The Al-Fe-Si ternary eutectic composition occurs at about 0.8% Fe. Theoretically, when iron is alloyed to a little above that amount, the supersaturated molten alloy has little tendency to dissolve the relatively unprotected tool steel while the molten alloy and die are in intimate contact.

Iron in a moderate range intended to reduce soldering is also credited with improving somewhat the resistance of die casting alloys to hot tearing during solidifications in rigid die cast tooling. That characteristic may, however, be overstated as some die casters say iron at the upper end of the typical range actually increases hot-tearing issues.

Iron combines with aluminum, silicon, and other elements to form a variety of hard, complex insoluble phases. The beta Al_5FeSi phase forms as very thin platelets, which appear acicular or needle-like in a polished cross section (Figure 2.5). Such morphologies provide stress risers that significantly reduce the ductility of an alloy.

Their volume fraction and size are functions of not only the iron concentration but also the solidification conditions (rate). The platelets tend to be fewer and smaller at higher solidification rates; thus, die casting is able to tolerate higher iron levels than other casting processes.

Iron at high concentrations cannot be tolerated in high-integrity die casting variations such as high-vacuum, squeeze and semi-solid casting. In those cases, a major goal is usually high ductility, and beta Al_5FeSi platelets destroy ductility by providing numerous stress risers and points of crack initiation. In those cases, primary alloys more traditionally used in sand and permanent mold casting have become the popular choices for high integrity die casting as well. Those alloys avoid Al_5FeSi platelets by limiting iron to very low limits. In some cases, high-integrity die castings have tolerated less pure alloys than required in sand and permanent mold by simply abiding by the rule “if iron exceeds 0.45%, manganese content shall not be less than one-half the iron content” [10].

As noted earlier, manganese at concentrations above 0.4% has now been demonstrated to provide adequate protection against soldering, so alloys intended for high integrity vacuum die casting, such as 365 and Alcan's Aural alloys, avoid harmful Al_5FeSi platelets by manganese substitution for iron.

2.4.4.2 Zinc

The only intentional and controlled additions of zinc (Zn) to aluminum casting alloys are in the 7XX series, and those are not yet suitable for die casting or any of its variations.

Otherwise, zinc is present merely as an acceptable impurity element in many secondary (scrap-based) die casting alloys. As such, zinc is quite neutral; it neither enhances nor detracts from an alloy's properties.

It should be recognized that zinc is a relatively dense (heavy) element, and as such it increases an alloy's mass density. High-zinc alloys usually seem attractive because they cost somewhat less than low-zinc versions. However, that attractiveness can be deceiving if the cost differential is too small; it can make little sense to purchase lower cost alloys if doing so means shipping a higher weight of material with each casting [9, 10].

2.5 Solidification of Aluminum Copper Alloys:

The Al-Cu phase diagram is a simple binary diagram. The aluminum rich end of the aluminum copper equilibrium diagram is shown in Figure 2.7. The maximum solubility of copper in aluminum is 5.65wt% at 548 ^{o}C, and the solubility decreases to 0.45wt% at 300 ^{o}C. The eutectic composition is around 33wt% copper. Therefore alloys containing between 2.5 and 5wt% copper will respond to heat treatment by age hardening. The theta (θ) phase is an intermediate phase whose composition corresponds closely to Al_2Cu. Solution treatment is carried out by heating the alloy in the alpha (α) single-phase region followed by a rapid cooling. Subsequent aging, either natural or artificial, will allow precipitation of θ phase, thus increasing the strength of the alloy [11].

The quality of the cast product is largely governed by the solidification conditions which determine the final microstructure. Solidification starts when the melt temperature goes below the liquidus temperature. Solid nucleates and grows in different directions. Some nuclei grow preferentially in certain directions in a form known as dendrites and branching also occurs. An increase in degree of undercooling favors dendrite formation. After solidification the microstructure will contain a varying amount of eutectic depending on the

alloy composition. This eutectic has an irregular pattern as branching and termination of the flakes occur and growth occurs at a non-isothermal interface.

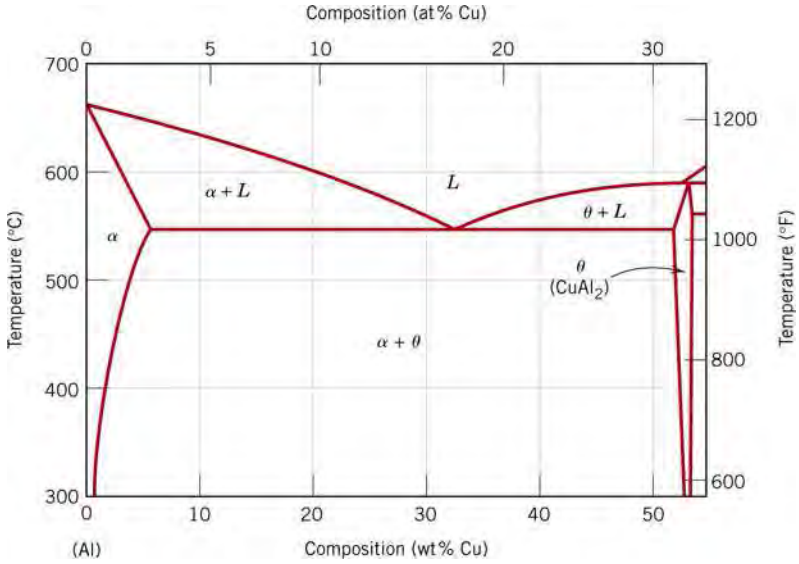

Figure 2.7: Phase Diagram of Al-Cu binary alloy (hypoeutectic alloy -25%Cu/75%Al hypereutectic alloy-36%Cu/64%Al) [12].

2.5.1 Micrographs: Eutectic Alloy

Micrographs are high-resolution microscope pictures which may be produced by techniques such as reflect light microscopy (RLM, Figure 2.8), scanning electron microscopy (SEM, Figure 2.9) or scanning transmission microscopy (STM).

As a liquid is cooled at the eutectic composition, the two phases grow simultaneously as an interconnected structure which forms the solid eutectic phase. The phase has a lamellar structure, which consists of many thin alternating layers of the two components.

The lamellar structure ensures that there are very small diffusion fields head of the solid-liquid interface, meaning that atoms do not travel over very significant distances for the two phases to simultaneously form.

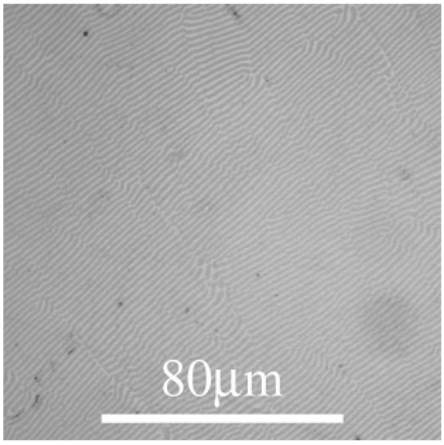

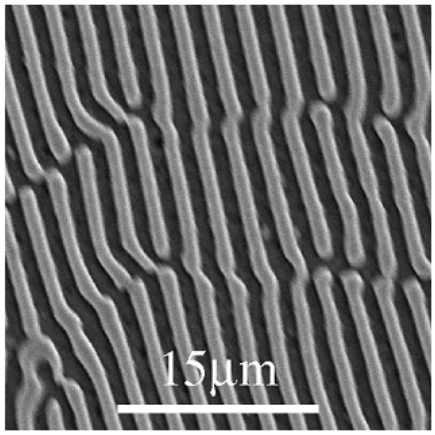

Figure 2.8: Eutectic Al-Cu alloy (RLM) [12]. Figure 2.9: Eutectic Al-Cu alloy (SEM) [12].

The RLM picture (Figure 2.8) shows the co-operative formation of θ and Al phases which form the eutectic lamellae. The SEM picture (Figure 2.9) shows an interlamellar spacing of about 1µm, as well as some imperfections which form from irregularities and disturbances during growth [12].

This specimen was made by unidirectional cooling and was metallographically prepared (mounted, ground and polished) and etched in dilute NaOH which stains the surface of the θ phase brown/black while leaving the "phase unattacked (appearing white).

2.5.2 Micrographs: Hypoeutectic Alloy

The RLM micrograph (Figure 2.10) of the 25%Cu/75%Al sample shows primary Al dendrite arms (white). The dendrite trunk has been intersected at an angle by the plane of polishing to give the observed morphology.

Primary phases often form as dendrites. These are solid structures forming from a liquid, which solidify in a branched manner because it is energetically favorable. A dendrite will rarely form in a completely regular manner [12]. A diagram of such an idealized regular dendrite is pictured in Figure 2.12.

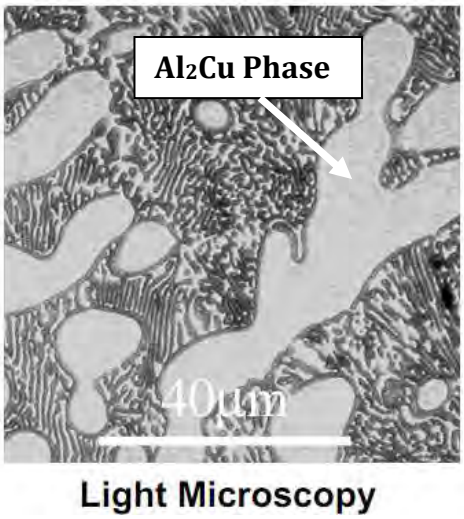

Figure 2.10: Hypoeutectic Al-Cu alloy (RLM) [12] .

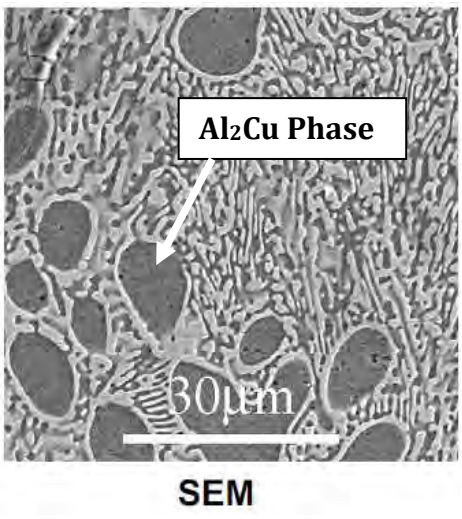

Figure 2.11: Hypoeutectic Al-Cu alloy (SEM) [12].

Figure 2.12: Schematic diagram of dendritic structure [12].

Between the dendrites is the Al-$CuAl_2$ eutectic. Initially dendrites would have formed from the liquid, the regions between the dendrite arms known as the mushy zone transforming to a eutectic solid (L to Al + $CuAl_2$). These two phases form cooperatively as neighboring lamellae with the lateral diffusion of material across the growing interface. The relative amounts of the two phases (Al and θ) in the eutectic are determined by applying the Lever Rule at the eutectic temperature [12].

2.5.3 Micrographs: Hypereutectic Alloy

The RLM micrograph (Figure 2.13) of the 36%Cu/64%Al sample, just to the right of the eutectic (known as the hypereutectic) shows primary dendrite formation from the θ ($CuAl_2$) phase. The remaining liquid transforms to the eutectic at the eutectic temperature [12].

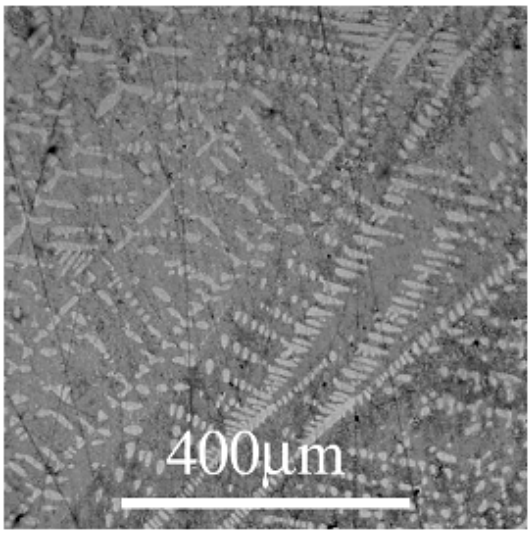

Figure 2.13: Hypereutectic Al-Cu alloy (RML) [12].

2.6 Heat Treatment of Aluminum Alloys

Heat treating processes for aluminum are precision processes. They must be carried out in furnaces properly designed and built to provide the thermal conditions required, and adequately equipped with control instruments to insure the desired continuity and uniformity of temperature-time cycles. To insure the final desired characteristics, process details must be established and controlled carefully for each type of product [13].

The general types of heat treatments applied to aluminum and its alloys are:

- Preheating or homogenizing, to reduce chemical segregation of cast structures and to improve their workability
- Annealing, to soften strain-hardened (work-hardened) and heat treated alloy structures, to relieve stresses, and to stabilize properties and dimensions

- Solution heat treatments, to effect solid solution of alloying constituents and improve mechanical properties
- Precipitation heat treatments, to provide hardening by precipitation of constituents from solid solution.

2.6.1 Homogenization Heat Treatment:

As-cast aluminum alloys tend to have very non-uniform microstructures. Wrought alloys for rolling or extrusion are given an ingot heat treatment to modify the cast structure. This is often referred to as homogenization.

Features of the cast structure that affect subsequent processing and/or properties can be altered by soaking for several hours at a temperature in the range 500-620 °C [13].

After casting, most aluminum alloys are typically subjected to homogenizing heat treatment, which for casting alloys can be combined with isothermal tempering before quenching. Its primary goal is to eliminate the consequences of microsegregation, as well as to raise the level of properties of shaped castings. In the case of wrought aluminum alloys, another advantage is in increased technological formability before subsequent thermo mechanical treatment such as rolling, extrusion etc.

In the course of homogenization of aluminum alloys the following processes take place [14 and 15]:

- Dissolution of non-equilibrium phases and corresponding constituent particles
- Elimination of concentration inhomogeneities for the alloying elements (micro segregation)
- Changes in phase composition and constituent particle morphology
- Changes in grain and dislocation microstructures of aluminum solid solution
- Decomposition of aluminum solid solution in the course of isothermal heat treatment accompanied by the formation of dispersoids (in alloys containing addition of transition metals)
- Development of secondary porosity

- Decomposition of solid solution with respect to the principal alloying elements upon cooling after isothermal heat treatment.

2.7 Thermodynamic Modeling of Phases

2.7.1 CALPHAD Description

The understanding and use of equilibrium phase diagrams is an essential component of nearly all materials science applications. An equilibrium phase diagram graphically represents the stable phases existing within a designated system as a function of specific conditions, namely: temperature, pressure, and for multicomponent systems, composition. Non-equilibrium phase diagrams can also be determined and are extremely useful as they can illustrate the existence of metastable phases under non-equilibrium conditions. The output of any phase diagram is contingent upon obeying the Gibbs phase rule [16]:

$$P + F = C + 2 \qquad (2.1)$$

where P = number of phases, F = degrees of freedom, and C = number of components.

In many cases, one is considering a system under constant pressure. Assuming constant pressure, the phase rule is reduced to P + F = C + 1. Phase diagrams can be thought of as an initial “road map” for alloy design.

Practical limitations of experimental phase diagrams are the time necessary to accurately reproduce the diagrams through experiment, as well as the increasing difficulty, cost and time consumption to do so, as the complexity (components) of the phase diagram increases. For condensed systems, binary phase diagrams are easily depicted in two dimensions, temperature versus composition. Ternary systems are more complex, utilizing a Gibbs triangle to express the compositions of the three components in two dimensions. To consider temperature as well, one has to introduce a third dimension into the diagram, or more often, plot the phase diagrams in two dimensions at a constant temperature or composition (isothermal or isopleth phase diagram).

Since many alloy systems having significant practical and industrial applications contain more than three elements, the creation, depiction, and ultimately, use of experimental phase diagrams becomes more difficult and convoluted, as one cannot graphically conceptualize

beyond three dimensions. Through the use of computational methods via the CALPHAD method, the equilibrium conditions of more complex systems can be more easily visualized and applied.

The CALPHAD (CALculation of PHAse Diagrams) approach was pioneered by Kaufman in the early 1970's [16]. In this approach, the Gibbs energy of each within a system is modeled, producing an accurate description of the system in database form.

From this database, it is possible to calculate all types of thermodynamic information: phase diagrams, free energy curves, enthalpy of formation and entropy of formation curves, and so on.

The drawback of CALPHAD approach is that it is not predictive, and thus, can't predict new phases. As such, it must still rely on experimental information. The process is shown schematically in Figure 2.14. Parameters for each known phase are entered, and scrutinized with respect to all available experimental information (invariant points, liquidus lines, formation enthalpy, activity, etc). The CALPHAD approach is an iterative one, as the free energies of each phase are collectively changing while reducing the sum of the error between the calculated values and the experimental data.

While the calculated phase diagram won't predict the existence of any new phases, it will often predict subtle and sometimes extremely significant changes within the system. Such changes are considered more correct since the thermodynamic assessment considers the interactions of all of the phases with respect to their free energies, rather than independent experimental measurements, indirectly related to thermodynamics.

Recently, a combined first-principles / CALPHAD approach has been under development to reduce the amount of experimental information needed with the ultimate goal of needing no experimental input [17]. At current, first-principles calculations can provide accurate formation enthalpy information, and in some cases formation entropy information. As discussed above, such "experimental" information will aid in the thermodynamic accuracy and overall robustness of the thermodynamic modeling.

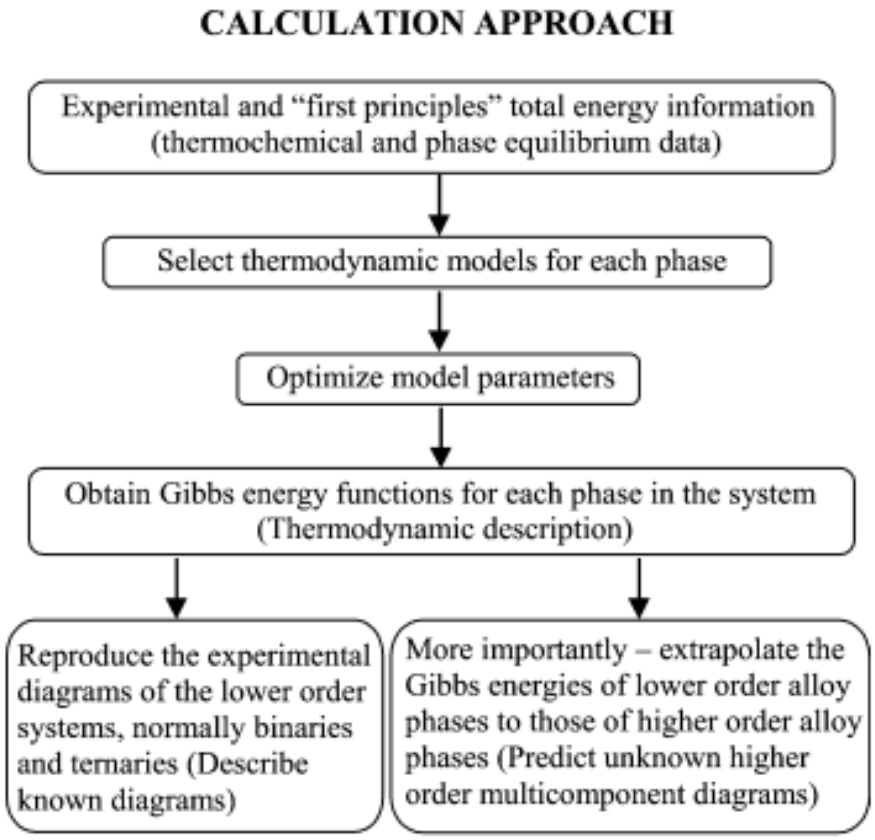

Fig.2.14: The Calphad or phenomenological approach used to obtain a thermodynamic description of a multicomponent system [35].

The CALPHAD approach can be summarized as follows [18]:

▪ A rigorous and complete literature search on the system of interest is conducted, acquiring all relevant experimental and theoretical information. Next, the experimental and theoretical information is scrutinized, with only the accurate data being considered in the evaluation process.

▪ Determine a weighted value for each piece of entered data. The weight of the data is contingent upon its relative importance and experimental accuracy as determined by the modeler.

▪ Assign a specific model and model parameters to each phase based upon their crystal structure and experimental description. One of the models described above should be able to accommodate any phase that will need to be entered into the system.

▪ Evaluate the model parameters via Pareto Chart to minimize the error of sum, while maintaining the best possible agreement with the relevant experimental data. A model can only be considered valid if it can accurately reproduce all of the accepted experimental and theoretical information.

2.7.2 Calculation of Phase Diagram

The basic principle of thermodynamic equilibrium calculation is the minimization of total Gibb's energy of the system (Figure 2.15) [19]. Calphad-type thermodynamic assessments produce parameters of semi-empirically modeled Gibbs energies for all phases present in a given system. These parameters are determined by least-squares fitting of thermodynamic functions to experimental data and are stored in computer databases which enable the calculation of Gibbs energy data as well as its derivatives, as a function of composition, temperature and pressure. The utilization of different, but nevertheless correlated experimental data, such as enthalpies, chemical potentials and phase diagram information, can provide thermodynamic descriptions having an extended validity, which is more reliable than a description obtained using a single type of experimental observation [20].

While considerable knowledge exists regarding two-phase systems and their corresponding binary phase diagram, most established and functional alloys are multicomponent. The experimental creation of multicomponent phase diagrams becomes increasingly more complicated as additional components are added to a system. For dealing with such multi-component systems, an accurate CALPHAD model is more powerful than interpretation of experimental phase diagrams. With an accurate thermodynamic database of a higher order system, one is able to produce phase diagrams tailored to their specific problems. Since all of the information is contained in a database form, it is possible to vary temperature, composition, and pressure, or to fix those values as constants, producing the desired isotherm, isopleth or isobar phase diagrams. Such a wealth of information is not possible from experimental extrapolations since it is too time consuming to produce phase diagrams for every subtle change occurring throughout a system. Additionally, when dealing with systems of four components and greater, the CALPHAD diagrams are of great use, since one can set additional composition constraints to produce diagrams that can be conceptualized using standard two-dimension form or the

Gibbs triangle [16, 21, 22].

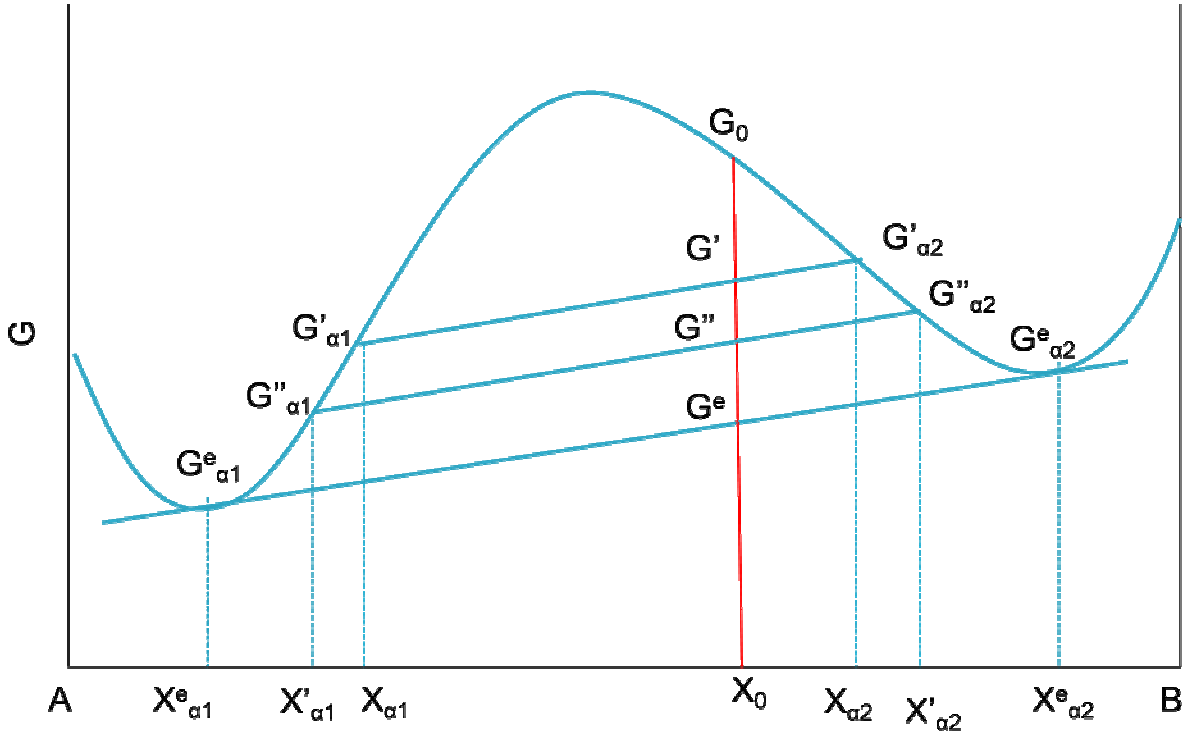

Figure 2.15: Thermodynamic Functions to Phase Diagram [19], where

$$G' = \left\{\frac{(X_o - X'_{\alpha 1})}{(X'_{\alpha 2} - X'_{\alpha 1})}\right\} G'_{\alpha 2} + \left\{\frac{(X'_{\alpha 1} - X_o)}{(X'_{\alpha 2} - X'_{\alpha 1})}\right\} G'_{\alpha 1}$$

Creating thermodynamic databases for such higher order systems can be a very costly process since the creation of a higher order system depends on the accurate creation of all lower order systems within it. For example, to fully model a quaternary database, one must have modeled the six binary systems and four ternary systems that are comprised of the components of the quaternary system. The fact that each database described using the CALPHAD model is done so using a standard form allows one to build upon existing lower order databases to create higher order ones.

It is through the creation and dissemination of the thermodynamic models for binary and ternary systems and their resultant phase diagrams that will allow an increase in efficiency and productivity when dealing with higher order systems. Because of this, one doesn't have to expend energy modeling the binary systems relevant to the higher order system of

interest if they have been published and are accurate. It is, however, of extreme importance to make sure the shared thermodynamic databases are of high quality and capable of being combined for the creation of a higher order system, else such advantages are lost [23].

The CALPHAD method is based on the fact that a phase diagram is a representation of the thermodynamic properties of a system. Thus, if the thermodynamic properties are known, it would be possible to calculate the multi-component phase diagrams. Thermodynamic descriptions of lower-order systems (e.g., the Gibbs energy of each phase) are combined to extrapolate higher-order systems.

The Gibbs energy of a phase is described by a model that contains a relatively small number of experimentally optimized variable coefficients. Examples of experimental information used include melting and other transformation temperatures, solubilities, as well as thermodynamic properties such as heat capacities, enthalpies of formation, and chemical potentials.

For pure elements and stoichiometric compounds, the following model is most commonly used [24]:

$$G_m - H_m^{SER} = a + b\cdot T + c\cdot T\cdot \ln(T) + \Sigma d_i \cdot T^i \qquad (2.2)$$

where, $G_m - H_m^{SER}$ is the Gibbs energy relative to a standard element reference state (SER), H_m^{SER} is the enthalpy of the element in its stable state at the temperature of 298.15 Kelvin and the pressure of 10^5 Pascal (1 bar), and a, b, c, and d_i are the model parameters.

For multi-component solution phases, the following expression for the Gibbs energy is used:

$$G = G^{\circ} + {}^{id}G_{mix} + {}^{xs}G_{mix} \qquad (2.3)$$

where, G° is the Gibbs energy due to the mechanical mixing of the constituents of the phase, ${}^{id}G_{mix}$is the ideal mixing contribution, and ${}^{xs}G_{mix}$ is the excess Gibbs energy of mixing (the non-ideal mixing contribution).

Thermodynamic calculations have often been perceived as rather theoretical and applicable only to simple systems. However, verification of CALPHAD predictions against multi-component alloys of many types has shown that they provide results that are very close to experimental observation [26]. It is only in recent years that attempts have been made to calculate phase equilibria for multi-component Al-alloys [27-29]. Previous work had tended to rely on modeling binary and ternary sub-systems, but this position has changed and predictions for complex Al-alloys can now be routinely performed.

Well established models have been developed that can be used to describe the thermodynamic properties of many different types of phase [26, 30-32]. All types of models require input of coefficients that uniquely describe the properties of the various phases and these coefficients are held in databases, which are either in the open literature or proprietary. These databases are then accessed by software that performs Gibbs energy minimization and complex multi-component calculations can be performed. There are now a variety of software packages for doing such calculations [33-34].

The roots of the CALPHAD approach lie in the mathematical description of the thermodynamic properties of the phases of interest. If they are stoichiometric compounds their composition is defined and a mathematical formula is then used to describe fundamental properties such as enthalpy and entropy. Where phases exist over a wide range of stoichiometries, which is the usual case for metallic materials, other mathematical models are used which account for the effect of composition changes on Gibbs energy.

The main solution phase models used for Al-alloys are the substitutional type model and the multiple sub lattice models [26].

The Gibbs energy of a substitutional phase in a many component system can be represented by the equation

$$G = \sum_i X_i \, G_i^\circ + RT \sum_i X_i \, lnX_i + \sum_i \sum_j X_i X_j \sum_v \Omega_v \left(X_i - X_j\right)^v \qquad (2.4)$$

where x is the mole fraction of component i, G_i^o is the Gibbs energy of the phase in the pure component i, T is the temperature and R is the gas constant. Ω_v is an interaction coefficient dependent on the value of v. When v is limited to a value of 0, this corresponds to the

regular solution model and when values for 0 and 1 are provided, this corresponds to a sub-regular type model. In practice values for v does not usually rise above 2.

Eqn. 2.4 assumes higher order interactions are small in comparison to those arising from the just the binary terms but this may not always be the case. Ternary interactions are often considered, but there is little evidence of the need for interaction terms of a higher order than this. Various other polynomial expressions for the excess term have been considered. However all are based on predicting the properties of the higher-order system from the lower-component systems.

The multi-sublattice model is substantially more complex and considers the phase to be made up of multiple interlocking sublattices. There are then interaction terms to be considered (i) between the sublattices and (ii) on the sublattices themselves. Full descriptions of such models, as well as further reading, can be found in elsewhere [25, 26, 35-37].

2.7.3 Thermodynamic Databases

To ease the task of modelling, different databases are available. These databases supply the necessary thermodynamic parameters for each phase, determined from low order (unary, binary & ternary) systems for calculation of higher order systems. Using these databases through computer software pakages, phase fractions as a function of temperature can be predicted. There are several databases for Al-Si alloys such as SGTE Database, SGSOL, MALT, Al-Data, EurAl, COST 507 Thermochemical Database for Light Alloys, etc. Details of these databases are discussed elsewhere [20, 26]. Al-Data, a database especially for aluminium alloys, is found to provide good results for commercial cast Al alloys and will be used in this project.

2.7.4 Modelling Software Packages

There are several commercial software packages available that implement CALPHAD methods to perform multi-component phase diagram calculations. These include MTDATA, Thermo-calc, FactSage and Pandat. Details of these software can be found elsewhere [33, 35]. These software packages have a long record in determining phase

diagrams of multi-component multiphase alloys. Recently, a new package, JMatPro, has also been developed. This software is designed not only to calculate phase diagrams, but also the physical and mechanical properties of materials, based on the predicted microstructures. For calculation this software relies on physical properties of the material rather than statistical methods. This software has been shown to be capable of giving close prediction to experimental results. Data for separate phases are calculated first and then combined to obtain the final prediction. JMatPro can be used to determine time-temperature-transformation (TTT) and continuous-cooling-transformation (CCT) curves with few input parameters. It can be used to determine the low temperature and high temperature mechanical properties. JMatPro can be used to determine optimum solution treatment temperature. But, JMatPro cannot plot phase diagrams directly and the database (Al-Data) still lacks data for scandium and lithium. In the current project, JMatPro will be used to determine phase fractions as a function of temperature. This Al-Data database is able to run simulation with the following elements: Al, B, C, Ca, Cr, Cu, Fe, H, La, Mg, Mn, Ni, Sc, Si, Sr, Ti, V, Zn and Zr. It includes all the elements present in the alloys considered in current work. Metallographic identification of phases in aluminium alloys are shown in Table 2.1. The phases this database can predict are as below.

Al (fcc)	Liquid	Si	$Al_5Cu_2Mg_8Si_6$	$Al_8FeMg_3Si_6$
Al_3Ni	Al_2Cu	Al_3(Fe,Mn,Ni..)	Al_3Mg_2	Al_6(Mn,Fe,CU..)
Mg_2Si	$Al_3(Ni,Cu)_2$	AlFeSi_Alpha	Al(Fe,Mn,..)Si _Alpha	AlFeSi_Beta
	Al_7Cu_4Ni	$Al_9(Fe,Ni)_2$	Al_7Cu_2Fe	Al_2CuMg

Table 2.1: Metallographic Identification of Phases in Aluminium Alloys.

Phase	Characteristics
Si	Primary Si has the shape of isometric polygons and eutectic morphology may script, blades or very fine lamellae. Natural colour is light bluish grey.
Mg_2Si	It forms scripts that coalesce on heating. Colour is darker bluish grey which is usually tarnishes to bright blue, black or vari-coloured.
$CrAl_7$	Iron and manganese can enter the solution as (Cr, Fe)AL_7 and (Cr, Mn)Al_7 respectively. Common morphology is elongated polygon. Natural colour is light metallic grey.
$CuAl_2$	The shape is rounded or irregular, except when precipitated from solid solution. It has a pale pinkish colour.
$FeAl_3$	Chromium and manganese can enter the solution as (Fe, Cr)Al_3 and (Fe, Mn)Al_3 respectively. The external eutectic shape is elongated blade or star shaped clusters. They do not usually coalesce. Colour is light metallic grey.
$FeAl_6$	Isomorphous with $MnAl_6$ and forms only under higher solidification rates. Shape is fine lamellar eutectic. Appearance can not be defined as it is too fine.
Mg_2Al_3, Mg_5Al_8	External shape is well rounded or irregular. Colour is white and lighter than aluminium. This colour may tarnish to yellow.
$MnAl_6$	Iron can enter the solution as (Fe, Mn)Al_6. Primary or course eutectic can form solid or hollow parallelogram and eutectic can form as fine script. Colour is light metallic grey.
Cu_2FeAl_7	Eutectic shape is elongated blade. This phase is capable of forming peritectically from iron rich phases. Colour is very light metallic grey (slightly darker than Cu_2Al)
$FeMg_3Si_6Al_8$	This is a quaternary phase having irregular shape. Sometimes it shows hexagonal symmetry. Colour is very light metallic grey.

$Cu_2Mg_8Si_6Al_5$	This is also a true quaternary phase having irregular shape. Natural colour is light metallic grey (darker than $CuAl_2$).
Mn_3SiAl_{12}, (Al-Mn-Si), $(Fe\text{-}Cu)_3SiAl_{12}$, (Al-Fe, Cr-Si), (Al-Fe, Mn-Si)	Eutectic shape is usually well-defined script. However, polyhedron, irregular shapes or Widmanstätten shapes are also possible. Natural colour is light metallic grey.
$Cr_4Si_4Al_{13}$	Same as Mn_3SiAl_{12}
$NiAl_3$	It has a needle or script like formation. The colour is pinkish-grey.
$TiAl_3$	It has a needle shape and grey in colour.

2.8 Solidification Technique

2.8.1 Equilibrium Solidification

Equilibrium solidification generally refers to the solidification of a metal or an alloy from liquid state at a very slow cooling rate. The very slow cooling, under equilibrium conditions, of a particular alloy M is described using Figure 2.16.

This alloy at temperature above T_L is a homogenous single phase liquid solution and remains so until temperature T_L is reached. Since T_L is on the liquidus line, freezing or solidification now begins. The first nuclei of solid solution to form N_1, will be very rich in the higher-melting point metal A and will be of composition C_1. Since the solid solution is forming takes material very rich in A from the liquid, the liquid must get richer in B. Just after the start of solidification, the composition of the liquid is approximated as C.

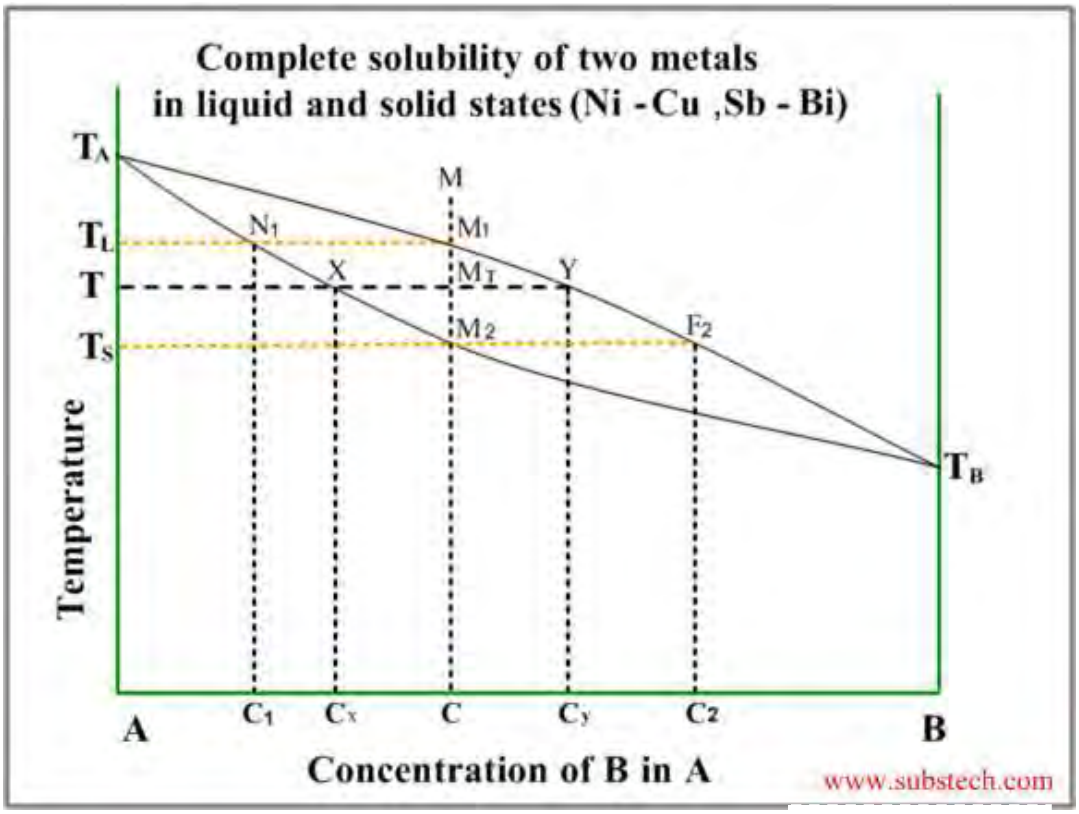

Figure 2.16: Equilibrium solidification of binary alloy.

As the temperature falls, the solid solution continues to grow at the expense of the liquid. The composition of solid solution follows the solidus line while the composition of liquid follows the liquidus line, and both phases are becoming richer in B. Finally, the solidus line is reached at T_S and the last liquid F_2 is very rich in B, solidifies primarily at the grain boundaries. However, diffusion will take place and all the solid solution will be of uniform composition M_2, which is the overall composition of the alloy. The microstructure of slow-cooled solid solution alloy contains only grains and grain boundaries; there is no evidence of any difference in chemical composition inside the grains, indicating that diffusion has made the grain homogeneous [11].

2.8.2 Non-equilibrium Solidification

In actual practice it is extremely difficult to cool under equilibrium conditions. Since diffusion in the solid state takes place at a very slow rate, it is expected that with ordinary cooling rates there will be some difference in the conditions as indicated by the equilibrium diagram. This can be shown by Figure 2.17.

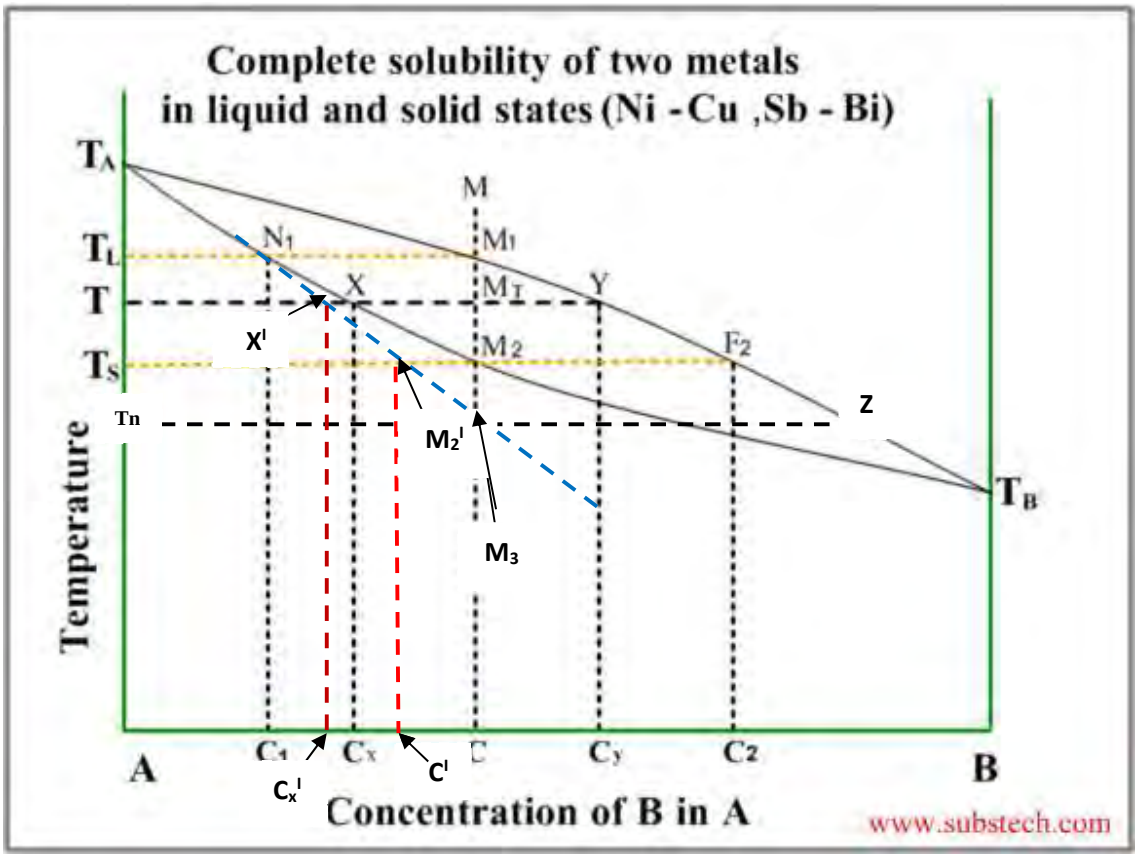

Figure 2.17: Nonequilibrium solidification of binary alloy.

Referring again to the alloy M, solidification starts at T_L, forming a solid solution of composition C_1. At T the liquid is at Y and the solid solution now forming is of composition X. Since diffusion is too slow to keep pace with crystal growth, not enough time will be allowed to achieve uniformity in the solid, and the average composition will be between C_1 and X i, e. X^I. As the temperature drops, the average composition of the solid solution will depart still further from the equilibrium conditions. It seems that the composition of the solid solution following a 'non-equilibrium' solidus line N_1M_3, shown blue colored dotted in Figure 2.17. The liquid on the other hand has essentially the composition given by the liquidus line, since diffusion is relatively rapid in liquid. Under equilibrium cooling, solidification should be complete at Ts; however, since the average composition of the solid solution C^l has not reached the composition of the alloy, some liquid must still remain. Solidification will therefore continue until T_n is reached. At this temperature the composition of the solid solution M_3 coincide with the alloy composition, and solidification is complete. The last liquid to solidify Z is richer in B than the last liquid to

solidify under equilibrium conditions. It is apparent from the study of Figure 2.17 that the more rapidly the alloy is cooled the greater will be the composition range in the solidified alloy. Since the rate of chemical attack varies with composition, proper etching will reveal the dendritic structure microscopically. The final solid consist of a cored structure with a higher-melting central portion surrounded by the lower-melting last-to-solidify shell. The above condition is referred to as coring or dendritic segregation. The faster the cooling rate, the greater will be the coring effect [11].

2.8.3 The Scheil-Gulliver (SG) Solidification Model

Recently the application of so-called 'Scheil-Gulliver' modelling via a thermodynamic calculation route has led to the ability to predict a number of critical thermo-physical properties for alloys [41-42]. Such calculations can be computationally very fast and used within solidification packages such as ProCAST5. The model assumes that solute diffusion in the solid phase is small enough to be considered negligible and that diffusion in the liquid is extremely fast, fast enough to assume that diffusion is complete. Such a process is quite simple to model using thermodynamic calculations based on CALPHAD method.

For equilibrium solidification described by the lever rule and with linear liquidus and solidus lines, the composition of the solid (*Cs*) as a function of the fraction solid transformed (f_s) is given by

$$C_s = \frac{k\,C_o}{f_s\,(k-1)+1} \tag{2.5}$$

Where k is the partition coefficient and C_o is the composition of the original liquid alloy. This can be re-arranged to give

$$f_s = \left(\frac{1}{1-k}\right)\left(\frac{T_L - T}{T_f - T}\right) \tag{2.6}$$

where T is the temperature below the liquidus and T_L and T_f are, respectively, the equilibrium liquidus and solidus temperatures. A complementary limiting case to equilibrium solidification is to assume that solute diffusion in the solid phase is small enough to be considered negligible

and that diffusion in the liquid is extremely fast, fast enough to assume that diffusion is complete. In this case eqn. 2.5 can be re-written as

$$C_s = kC_o(1 - f_s)^{(k-1)} \tag{2.7}$$

and eqn.2.6 as

$$f_s = 1 - \left(\frac{T_L - T}{T_f - T_L}\right)^{\left[\frac{1}{k-1}\right]} \tag{2.8}$$

The treatment above is the traditional derivation of the Scheil equation but it has quite severe restrictions when applied to multi-component alloys. It is not possible to derive this equation, using the same mathematical method, if the partition coefficient, k, is dependent on temperature and/or composition. The Scheil equation is applicable only to dendritic solidification and cannot, therefore, be applied to eutectic alloys which are commonplace for Ni-based alloys. Further, it cannot be used to predict the formation of intermetallics (e.g. the Laves phase) during solidification [41].

Using thermodynamic modeling all of the above disadvantages can be overcome. The process that physically occurs during 'Scheil' solidification can be envisaged as follows. A liquid of composition C_o is cooled to a small amount below its liquidus. It precipitates out solid with a composition $C_{S,1}$ and the liquid changes its composition to $C_{L,1}$. However, on further cooling the initial solid cannot change its composition due to lack of back diffusion and it is effectively 'isolated'. A local equilibrium is then set up where the liquid of composition $C_{L,1}$ transforms to a liquid of composition $C_{L,2}$ and a solid with composition $C_{S,2}$, which is precipitated onto the original solid with composition $C_{S,1}$. This process occurs continuously during cooling and, when $k<1$, leads to the solid phase becoming lean in solute in the center of the dendrite and the liquid becoming more and more enriched in solute as solidification proceeds. Eventually, the composition of the liquid will reach the eutectic composition and final solidification will occur via this reaction.

Any appearance of secondary phases can be easily taken into account in this approach with the assumption that no back diffusion occurs in them. Therefore, all transformations can be accounted for, including the final eutectic solidification. The approach described here is based on

an isothermal step process but as the temperature step size becomes small it provides results that are almost completely equivalent to that which would be obtained from continuous cooling. A further and very significant advantage of using a thermodynamic approach is that the heat evolution during solidification is a straightforward product of the calculation [42-43].

The solidification process is driven by the extraction of heat, whether the alloy is binary or muticomponent, whether it involves one solid or several solids, or whether it can be approximated by conditions of equilibrium, non-equilibrium or partial equilibrium. If the temperature is lowered successively for a small degree ΔT from the liquidus temperature and the phase equilibrium of a given system is calculated at each temperature step with a thermodynamic database, the equilibrium solidification path and fraction of solid as well as other interesting properties can be obtained readily. For the Scheil-Gulliver model, the assumption of local equilibrium at phase interface can be used with keeping change in the composition and the amount of liquid, the phase equilibrium calculation is performed.

2.9 Plastic Deformation and Work Hardening

Dislocations are another type of defect in crystals. Dislocations are areas were the atoms are out of position in the crystal structure. Dislocations are generated and move when a stress is applied. The motion of dislocations allows slip – plastic deformation to occur (Figure 2.18) [45].

The interaction of mobile dislocations with other dislocations during dislocation slip produce changes in the distribution and density of the dislocations. That is, dislocations themselves are obstacles to dislocation motion. Thus, the glide resistance for dislocations increases. This results in work hardening [45].

Plastic deformation occurs as a consequence of work being done on a material; energy is added to the material. In addition, the energy is almost always applied fast enough and in large enough magnitude to not only move existing dislocations, but also to produce a great number of new dislocations by jarring or working the material sufficiently enough. New dislocations are generated in proximity to a Frank-Read source [47].

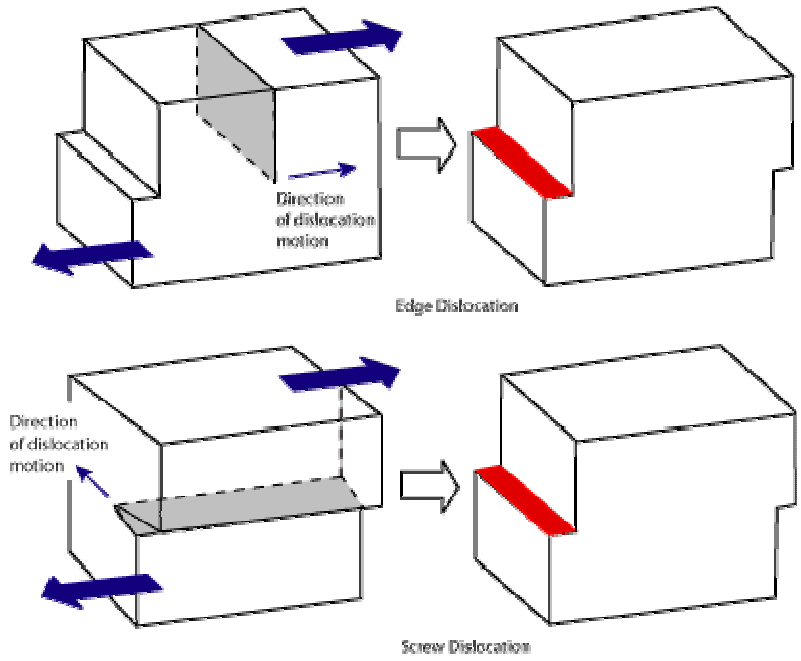

Figure 2.18: Direction of dislocation motion in edge and screw dislocation [44].

Yield strength is increased in a cold-worked material. Using lattice strain fields, it can be shown that an environment filled with dislocations will hinder the movement of any one dislocation. Because dislocation motion is hindered, plastic deformation cannot occur at normal stresses. Upon application of stresses just beyond the yield strength of the non-cold-worked material, a cold-worked material will continue to deform using the only mechanism available: elastic deformation, the regular scheme of stretching or compressing of electrical bonds (without dislocation motion) continues to occur, and the modulus of elasticity is unchanged. Eventually, the stress is great enough to overcome the strain-field interactions and plastic deformation resumes.

However, the processes of dislocation generation and recovery are much less understood, at least on a quantitative level, although the basic models are about 50 years old, already [45-46].

Since the homogeneous nucleation of dislocations requires stresses of about one tenth of the shear modulus, the generation of dislocations during plastic deformation occurs at much lower stresses as an elongation of the length of existing dislocations. The best-known mechanism of dislocation generation is the Frank–Read source [47], which may be characterized as a localized source. A dislocation segment lying on a slip plane is pinned at its ends, e.g. by nodes of the

dislocation network or simply by changing onto another plane where it is not mobile, as sketched in Figure 2.19. Under the applied stress, the mobile segment moves through different stages marked a to e. This localized source can operate repeatedly to emit a greater number of dislocations on the same slip plane.

The second mechanism is the double-cross slip mechanism suggested by Koehler [48] and Orowan [49], and experimentally first observed indirectly by Johnston and Gilman [8]. It is shown schematically in Figure 2.20. A screw dislocation (a) moves on its glide plane, which is identical with the image plane. Cross slip of a segment of length L results in two super jogs J acting as pinning agents. The segment then multiplies similarly to the Frank–Read source. Simple line tension arguments show that both sources can act only if the segment length L is larger than a critical value,

$$L_c = \mu b/\tau \tag{2.9}$$

Where μ is the shear modulus, b the absolute value of the Burgers vector and τ is the local component of the acting stress. Using characteristic values, Lc is in the range of about 100–200 nm. In stage (c) of the double-cross slip mechanism, the branches adjoining the jogs have to pass each other on their parallel planes. This is only possible if the height of the jogs, i.e. the distance between the parallel glide planes, is larger than a critical value (dipole opening criterion),

$$h_c = \mu b / [8\pi (1-\nu)\tau] \tag{2.10}$$

with ν being Poisson's ratio. It is obvious that hc is about 20 times smaller than L_c. Thus, both L_c and h_c are well below the foil thickness of about 500 nm in an HVEM in situ experiment, so that the mechanisms of dislocation generation can well be observed. If it is considered that the cross slip events show characteristic frequency distributions of L and h, it is reasonable to assume that the frequency of dislocation multiplication increases with increasing stress since sources with smaller values of L and h can be activated at higher stresses. In many cases, the intermediate configuration of stage (c) is metastable. It is characterized by the highlighted -like configuration in Fig. 2.20, which is frequently observed in dislocation structures under stress.

The double-cross slip mechanism usually emits only a single new dislocation loop. Since the generated dislocation moves on a plane parallel to the original one, slip may spread leading to a

growth of the width of the slip bands, in contrast to the Frank–Read source which emits many dislocations on the same plane. Cross slip events happen during the motion of the dislocations. Accordingly, the increase in the dislocation density dρ should be proportional to the area dA swept by all dislocations. Considering the dependence of the creation rate of dislocations on τ, the creation rate may be written as

$$d\rho = w\tau\, dA = w\tau\rho ds = (wb) / \tau\, d\varepsilon \tag{2.11}$$

where w is a constant, d is the displacement of all dislocations and dε is the increment in shear strain. If the cross slip height is smaller than h_c in Eq. (2.9), the dislocation trails a dipole at each jog as outlined in stage (d) of Fig. 2.20. These dipoles may be terminated by glide of the jogs along the dislocation line. If the stress increases later on, yielding a smaller value of hc, dipoles may open and emit additional new dislocations [47].

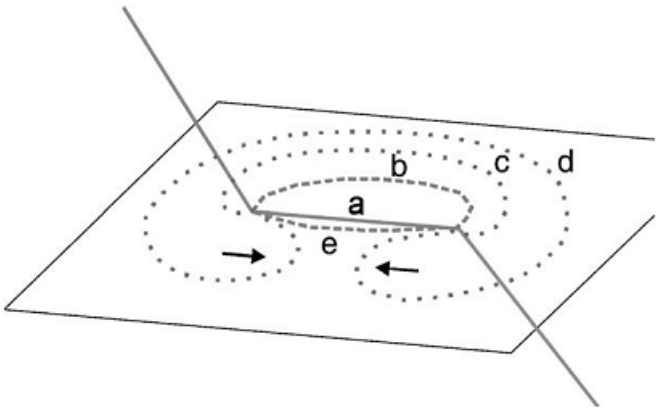

Figure 2.19: Dislocation generation in a Frank Read Source [47].

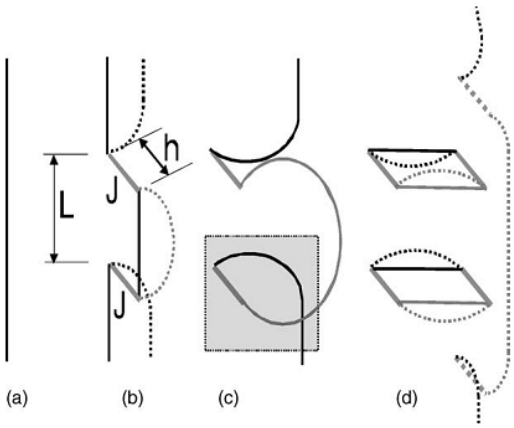

Figure 2.20: Double-cross slip mechanism of dislocation generation [47].

2.10 Recent Works on Aluminum Copper Alloys

Lots of works had been done on effects of alloying elements on microstructure and mechanical properties of aluminum by various researchers [50-56].

H.N. Girisha and K.V. Sharma [1] investigated the effect of magnesium on strength and microstructure of Al-Cu-Mg alloys which are widely used in aircraft, aerospace, ships and boat making, industrial and architectural applications for their good mechanical properties, high strength-to-weight ratio. They studied the influence of magnesium on microstructural changes and mechanical properties such as tensile strength and hardness of the Al-4Cu alloys with 0.5 to 2 % Mg addition in the interval of 0.5% and found that strength and hardness increases with increasing magnesium content.

Omotoyinbo and Oladele [8] determined the effect of plastic deformation and magnesium content on the mechanical properties of 6063 aluminum alloys. The effect of increased magnesium addition on the strengthening behavior during deformation was determined by adding, 0.451%Mg, 0.551%Mg, 0.651%Mg, and 0.751%Mg in addition to the other elements which are constant. Deformation was carried out at 20% and 40%. From the results, it was observed that the tensile properties of the aluminum alloys improved with increase in percentage deformation and magnesium content.

M. R. Khan et al [50] studied the beneficial effect of heat treatment on mechanical properties and microstructure of aluminum alloys, containing up to 4.5% copper and 1.5% magnesium, used in aerospace industry. They revealed that measured mechanical properties were related to microstructures present in these alloys. Variation of microstructure was created by heat treatment of these alloys at different temperatures and by using different quenching media. The mechanical test data gave information about their Yield Strength, Tensile Strength, Elongation, Ductility and hardness. Microstructures measured gave information of their grain size and were determined by using scanning electron microscope equipped with EDX.

The effect of Mg addition on the microstructural evolution and mechanical properties of high-purity aluminum was studied by J. Gubicza et al [51] over a wide range of strain, up to ~8. The high strains were achieved by applying the equal-channel angular pressing technique. It was found that in the early stages of plastic deformation the interaction between the dislocations and the Mg solute atoms results in an increase of the flow stress with temperature. The stable microstructure is developed at higher strains owing to the Mg addition resulting in the saturation of the proof stress at higher strains in Al–Mg alloys.

R.S. Rana and R. Purohit [52] studied the effect of magnesium enhancement on mechanical property and wear behavior of LM6 aluminum alloy. They came to a conclusion that microstructure can be modified and mechanical properties, wear resistance can be improved by alloying, cold working and heat treatment. Hardness was found to increase with increase in Mg content while the yield strength and ductility was found to decrease with increase in Mg content due to brittleness of the material. Wear rate was also found to decrease with increase in Mg content. This is due to softening of the material at the warm surfaces due to higher temperature at the contact surface.

2.10 Scope of the Current Work

The current research emphasizes establishment of relationship between microstructure and cold deformation behavior of few aluminum alloys using thermodynamic modeling method and phase quantification techniques. The specific objectives include microstructural and quantitative analysis of phases and particles, formed by the addition of different alloying elements in aluminum alloys, using image processing techniques and finally to correlate the microstructural changes caused by alloying elements and deformation.

From this research it will be possible to fabricate aluminum alloys using different alloying elements. Homogenization temperatures of these alloys will also be possible to determine using thermodynamic modeling. These might provide important information regarding the influence of alloying elements on microstructure and mechanical properties.

CHAPTER 3
EXPERIMENTAL PROCEDURES

Different aluminum alloys were being prototyped by varying composition and by developing suitable microstructure with different heat treatment schedules. The current study includes the microstructural effects on deformation of aluminum alloys. Aluminum alloys of pre-determined composition was casted and homogenized at 400 ^{o}C for four hours. Then microstructures of as-cast and homogenized alloys were observed. Compression tests involving 10%, 20% and 50% deformations were performed on the homogenized samples using ASTM standards. The effects of alloying elements on mechanical properties were observed by measuring the hardness of as cast, homogenized and deformed alloys. The changes in microstructure due to deformation of aluminum alloys were studied using optical micrographs, Scanning Electron Microscopy (SEM). Phases present in those alloys were determined using Energy Dispersive X-ray (EDX) and solidus and liquidus temperatures of alloys were determined by Differential Thermal Analysis (DTA). Finally, relationship between microstructure and cold deformation behavior of few aluminum alloys were established using thermodynamic modeling method and phase quantification techniques.

3.1 Material

The base material aluminum was bought from local market as aluminum ingot manufactured by a Canadian company. Chemical composition of the ingot was verified by Optical Emission Spectroscopy (OES) and found 99.75% pure. Main alloying elements copper and magnesium were bought from local market as ribbons with 99% purity. Total nine different alloys were prepared by casting containing copper and magnesium with varying percentages. Table 3.1 shows the alloy designation of Al-Cu-Mg alloys.

Table 3.1: Alloy designation of Al-Cu-Mg alloys used in the current work

Alloy	%Aluminum	% Copper	% Magnesium
A0	98	2	0
A1	97	2	1
A2	96	2	2
B0	96	4	0
B1	95	4	1
B2	94	4	2
C0	94	6	0
C1	93	6	1
C2	92	6	2

3.2 Alloy Preparation

At first a certain amount of aluminum was cut from the ingot and melted inside a crucible in a furnace. Then pre-defined percentages of copper wire were added into it. The mixture was manually stirred using a stirrer. When the metal melted completely magnesium of pre-determined percentage was added (when required) which created silver lightening and also stirred uniformly. In order to remove the gaseous products from the liquid melt and to reduce after-cast porosity, ammonium chloride (NH_4Cl) was used as degasser (0.2% per kg). The melt was again stirred and temperature of the entire melt was measured using a thermocouple. Then the melt was poured from the crucible to a metal mold made of mild steel of dimension 20 cm length, 8 cm wide and 5 cm height. After casting the as cast alloy was cooled and cut into pieces for testing. As cast samples were cut to measure the chemical composition, determine microstructure and hardness.

3.3 Determination of Chemical Composition of As Cast Alloys

3.3.1 Optical Emission Spectroscopy (OES)

Chemical analysis was carried out using Optical Emission Spectroscopy (Shimadzu PDA-7000) in aluminum-copper group. The range of copper in this group is 1-6% and for magnesium 0.3-1.7%. As cast sample was polished to flat surfaces for OES. For each alloy, at least four sparks were made in different locations of the casting section and average composition was determined.

3.3.2 Wet Chemical Analysis of As Cast Alloys

Wet chemical analysis was also carried out to measure the actual percentage of copper in as cast alloys.

3.4 Homogenization Treatment of As-Cast Aluminum Alloys

As cast alloys were homogenized to get uniform structure in a BLUE M furnace. Each sample was heated to 400 ^{o}C for 4 hours. After holding for 4 hours at 400 ^{o}C, the sample was quenched in water. Figure 3.1 shows the heat treatment cycle of aluminum alloys.

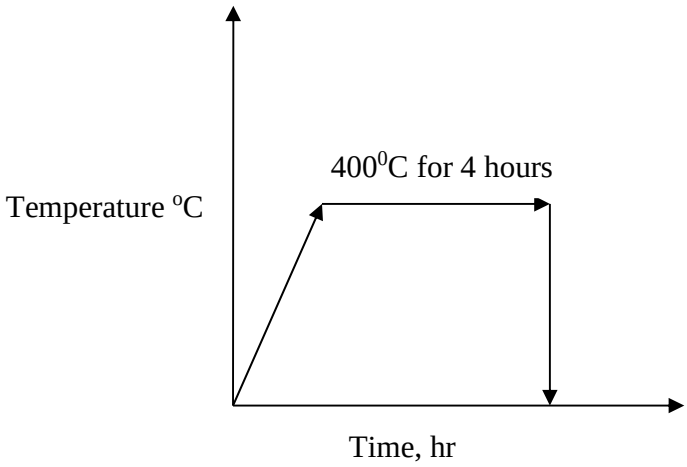

Figure 3.1: Heat treatment cycle.

3.5 Deformation of Homogenized Alloys

Homogenized alloys were cut into cylindrical shapes of diameter 25 mm and height of 20 mm. For each alloy, three specimens were prepared and deformed by compression using Universal

Testing Machine (UTM) model UH-5000kNA, SHIMADZU. Each alloy was deformed to 10%, 20% and 50% of its original height. Maximum load required to deform to a certain percentage was recorded and percentage of deformation was calculated using the following equations:

Initial diameter = D

Initial height = H_1

Final height = H_2

$$\% \text{ Deformation} = \frac{(H_1 - H_2)}{H_1} \times 100\ \%$$

3.6 Sample Preparation for Optical Microscopy

In order to reveal the microstructure of as cast, homogenized and deformed alloys, optical microscopy was performed using standard procedure.

For each alloys total five specimens were prepared for optical micrographs such as, as cast specimen, homogenized specimen, deformed specimens to 10%, 20% and 50%. In case of each specimen, almost 50 images were captured, 25 images of 200X magnification and 25 images of 500X magnification. These images will be shown in result and discussion section.

The prepared specimens were analysed at first by optical microscope. For this purpose, Olympus BH2 microscope was used. Digital greyscale images were acquired using the camera attached to it using the software Leica DC View at a resolution of 1798x1438.

3.7 Determination of Phases Present in the Microstructure

Presence of phases and particles in the alloys due the alloying elements i.e., copper and magnesium was determined by Scanning Electron Microscope (SEM), Energy Dispersive X-Ray (EDX) and Image analysis software.

3.7.1 Scanning Electron Micrographs (SEM)

Scanning electron microscopy (SEM) was carried out on SEM with energy dispersive X-ray analysis (EDX) system. The operating voltage was 25 kV. Images were acquired both in

secondary and backscattered mode because in backscattered mode some phases gave better contrast.

3.7.2 Energy Dispersive X-Ray (EDX)

For EDX, the measuring time was 100 seconds in all cases. Quantax QX2 1.6 and EDAX software packages were used for EDX analysis.

To identify the images optically, at first, some spots were marked on the specimen surface using a pen and then in SEM those spots were identified and a nearby area was analysed by EDX. Then, in the optical microscope, the same area was found out and from the spot analysis of SEM EDX, phases were identified optically.

3.7.3 Differential Thermal Analysis (DTA)

Differential thermal analysis (or DTA) is a thermo-analytic technique, similar to differential scanning calorimetry. In DTA, the material under study and an inert reference are made to undergo identical thermal cycles, while recording any temperature difference between sample and reference. This differential temperature is then plotted against time, or against temperature (DTA curve or thermogram). Changes in the sample, either exothermic or endothermic, can be detected relative to the inert reference. Thus, a DTA curve provides data on the transformations that have occurred, such as glass transitions, crystallization, melting and sublimation. The area under a DTA peak is the enthalpy change and is not affected by the heat capacity of the sample. In this research heating rate was maintained 20°C/min.

3.7.4 Image Analysis

For image analysis, ImageJ software package was used. Shading correction was necessary during collection of the images from optical microscope; otherwise image analysis would not give accurate results. This was done for every single image using a graticule. After placing the graticule in the microscope, it was focused in a scratch free zone and proper brightness was adjusted and was acquired. Then shading correction was done by using this image. Shading

correction was done in every sessions of image collection. All the images were converted to 8 bit grey scale images.

The size of each pixel is necessary information before analyzing the images. This was done using ImageJ software. An image of the graticule at 200X magnification was taken in the same microscope. Then in ImageJ, a straight line of 100 µm was drawn on the scale in the image. Then using the 'Set Scale' command, it was found that 1 µm contained 2.240 pixels. This scale was used for all the analyses which were done at 200X magnification. For different magnification, a different scale was measured.

Shading correction alone could not solve the problem of shadow in the images. Some shadows were found in the left top corner of the images. So, the images were cropped to 1200x950 pixel dimensions to get rid of any shading problem.

In ImageJ, a pre-written macro file was used to analyse the images. Two types of measurements were made: field measurements for the whole image and region measurements for the individual particles. The whole area of the image (1200x950 pixels) was considered. So, frame was not used to exclude the edges where some incomplete phases may exist. The reason is that excluding the edges may cause some large particles being not considered. Before starting the measurements, upper threshold was set for the first image of the specimen. Since the images were converted to gray values, the different regions can be distinguished using different gray value ranges. For example, a range of 0 to 20 should be enough to identify regions of black colour. Therefore the phases having black colour were identified using this range of gray values. The selected regions were eroded and dilated using open and close binary operations. Using the similar principles, different phases were identified and analyzed. For intermetallic measurements, a slightly different approach was applied. Because if there was any relief surrounding the selected phases, it would result in shadows which would have similar grey level to the intermetallics (Figure 3.2); this would lead to incorrect measurements. So, matrix was discriminated from all the phases. Then slightly dilated (to include some shading) total black phases were subtracted from the segmented phases. Phase fractions and feret diameter of black

phases, light gray phases and total intermetallics were calculated. All the results were saved in MS Excel format.

In short, threshold command helped to set lower and upper threshold values, segmenting the image into black phase and background. This software shows the pixels having brightness values greater than or equal to the lower threshold and less than or equal to the upper threshold in red. All the loaded images were checked. If it was found that most of the images were not discriminated well, threshold value was changed to match most of the images. Then thresholded pixels were set to black and all other pixels to white. Then ‘open’ command was used which performed an erosion operation followed by dilation. Erosion operation removes pixels from the edge of the black object; it simply means the size of the objects darker than the background (e.g. black phases after threshold) is reduced. On the other hand, dilation adds pixels to the edges of the black objects (so that size of the objects darker than background is increased). The final effect of these two commands is to smooth the image and remove the isolated pixels. Then another condition (‘limit to threshold’) was applied to measure only the thresholded segment. Then using ‘analyze particles’ command, thresholded particles were analyzed. Before starting the measurement, an option was selected so that calculation would include edges of the image. Area fractions and feret diameters for all the images were measured and data was saved. In the histogram, it is clear that the difference in grey scale is not sufficient to properly segment intermetallics and black phases. So, all the phases including black phases were discriminated against the matrix (aluminium) so that later the results can be subtracted from the black phases measured to give the total intermetallics data. An ‘Open’ operation was not run for intermetallics as it was desired to select all the pixels that were different from the matrix. Area fractions and feret diameter data were saved. The area fraction data of black phases were then subtracted to get the total intermetallic area fraction. A flowchart for ImageJ is also shown in Figure 3.3.

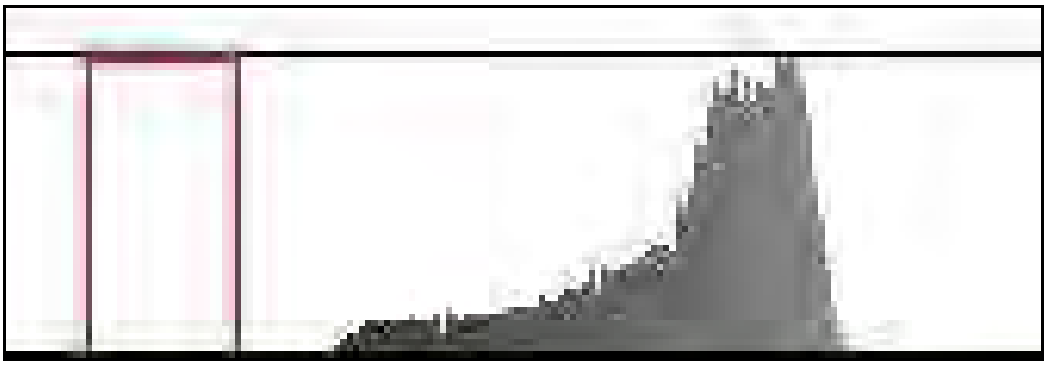

Figure 3.2 Histogram shows very little difference in grey colour.

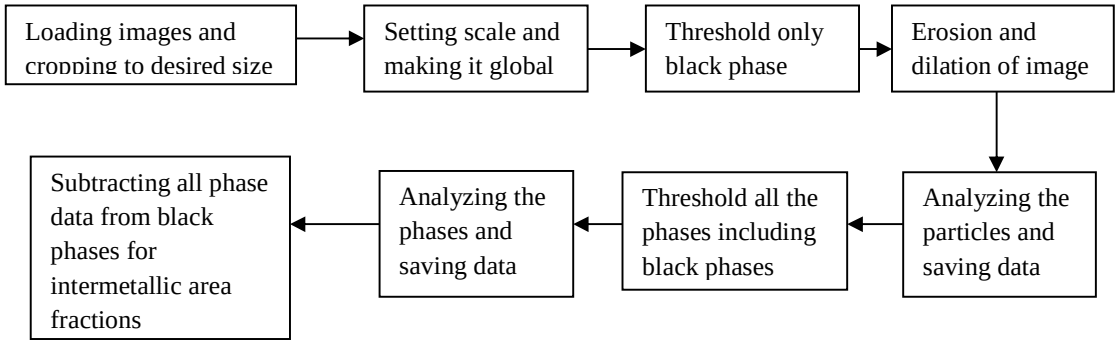

Figure 3.3: Flowchart of image analysis using ImageJ software.

ImageJ was also used to measure area fractions of the individual phases. Segmenting only a particular phase is mainly impossible because most of the phases have similar colour and shape. To get around this, each phase was manually identified and given a different colour. Thresholding was done only that grey level. At first, a particular phase was given white or black colour (any other colour could not be given as the images were in grey scale) using MS Paint software. It was decided to give only white colour to any phase because there were some phases which were already black and also the porosity appeared black in colour. Then during segmenting only that phase, lower and upper threshold value was selected to be 255 and 255 so that only white portions of the image would be thresholded. As there was not anything pure white in any image, this was thought likely to give the most accurate results.

3.8 Thermodynamic Modelling

JMatPro v4.0 was used to predict phase fractions of all the alloys. The temperature range used was 700-100^{0}C for both equilibrium and Scheil-Gulliver conditions. A 5^{o}C step temperature was used for the equilibrium condition and 4^{o}C was used for the Scheil-Gulliver condition. Simulations were saved in graphical and tabular form to interpret the results in different format. Stability information of all the phases during cooling was observed. Also, variations in composition of a particular phase were extracted. The most important information taken from the simulations was phase fractions at a pre-defined temperature (400^{o}C). The composition of each phase for every alloy was taken as both at % and wt %. Al-data database (v 5.0) was used in JMatPro.

3.9 Mechanical Property Determination

The effects of alloying elements on mechanical properties were also determined by taking the hardness in a Rockwell Hardness Tester. The Rockwell scale is a hardness scale based on the indentation hardness of a material. Depending on materials softness different measuring scales are used in this hardness testing machine. Since aluminum alloys are comparatively softer they are usually tested in F scale which shows hardness values in HRF scale with a load 60 kg using 1/16” steel ball indenter. For each alloy hardness of as cast and homogenized condition and also under 10%, 20% and 50% deformed state were measured in HRF scale in different locations of the sample.

CHAPTER 4
RESULTS AND DISCUSSION

4.1 Chemical Analysis

After casting, composition of each alloy was assured by chemical analysis using OES and for magnesium containing alloys, manual wet analysis techniques were performed to determine the exact %Cu. This is due to the fact that when magnesium is added due to higher and lower limit of % element in OES alloy groups, %Cu values may not be accurate.

Table 4.1 shows actual chemical composition of as cast aluminum alloys determined using OES.

Table 4.1: Chemical composition of as-cast aluminum alloys (balance Al).

Alloy	Cu	Mg	Fe	Si	Mn	Ni
A0 (Al-2%Cu)	1.96	0.09	0.26	0.00	-	0.19
A1 (Al-2%Cu-1%Mg)	2.21	0.57	0.17	0.11	0.04	-
A2 (Al-2%Cu-2%Mg)	2.76	0.69	0.30	0.12	0.07	-
B0 (Al-4%Cu)	3.69	0.06	0.07	0.08	-	-
B1 (Al-4%Cu-1%Mg)	3.51	0.30	0.10	0.05	0.003	-
B2 (Al-4%Cu-2%Mg)	4.03	0.59	0.08	0.13	0.002	-
C0 (Al-6%Cu)	6.16	0.06	0.06	0.12	0.001	0.003
C1 (Al-6%Cu-1%Mg)	5.45	0.55	0.01	0.09	-	0.06
C2 (Al-6%Cu-2%Mg)	6.45	0.76	0.09	0.12	0.007	-

4. 2 Thermodynamic Modeling: CALPHAD

CALPHAD modeling software package was used to determine the weight fractions of phases formed during solidification and homogenization. Weight fractions of phases with temperature were predicted all alloys in both equilibrium (EQM) and non equilibrium Scheil-Gulliver (SG) condition.

4.2.1 Significant Phases of Al-Cu-Mg Alloys

4.2.1.1 Phases Predicted

Alloy A0: Equilibrium Solidification

During equilibrium solidification, significant phases formed are Al_9M_2, Al_7Cu_2M, Al_7Cu_4Ni and Al_2Cu as shown in Figure 4.1. First phase Al_9M_2 started to form at 625 °C and retained up to 336 °C. It reached to a maximum 1.19 wt%. Al_7Cu_2M formed at 544 °C reached a maximum of 1.75 wt % and was stable till room temperature. Another Al-Cu phase Al_7Cu_4Ni started to form at 440 °C with maximum 1.58 wt % and was stable at room temperature. The most important phase that provides hardness in Al-Cu alloys is Al_2Cu and it began to form at 310 ^oC, this phase reached a maximum of 0.82 wt % and retained up to room temperature.

Alloy A0: Non-equilibrium Solidification

During non-equilibrium cooling, since there is no solid state diffusion, once the solidification process is complete, a solid phase remains stable. From Figure 4.2, it is clear that in non-equilibrium cooling condition, few additional phases were formed compared to equilibrium cooling for the same composition, alloy A0. Total seven phases were predicted. First Al_3Fe formed at 626 °C and reached to 0.1%. Then Al_9M_2 nucleated at 621^oC and reached 0.89%. Then at 597 °C Al_6Mn nucleated and reached 0.02%. The next phase formed is Al_7Cu_2M at 586 °C and increased to 0.3%. Also, two nickel containing phases, Al_3Ni_2 and Al_7Cu_4Ni formed at the same temperature of 558.37 °C. Finally, at 540 °C Al_2Cu started to solidify and reached to a maximum of 1.38%.

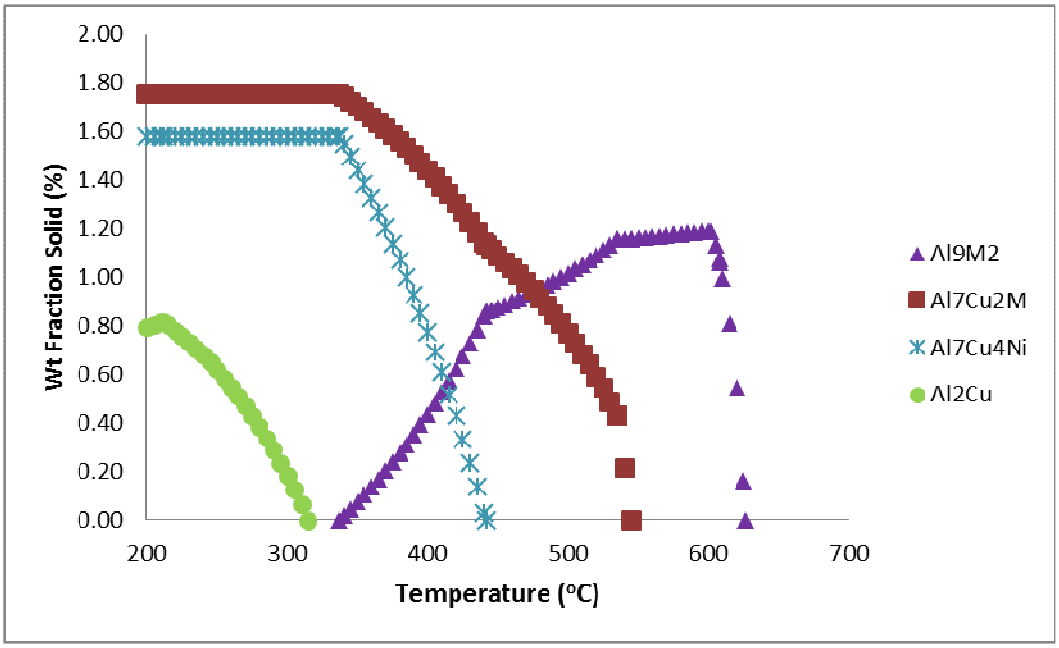

Figure 4.1: Change in fraction solid wt % with temperature of alloy A0 (EQM).

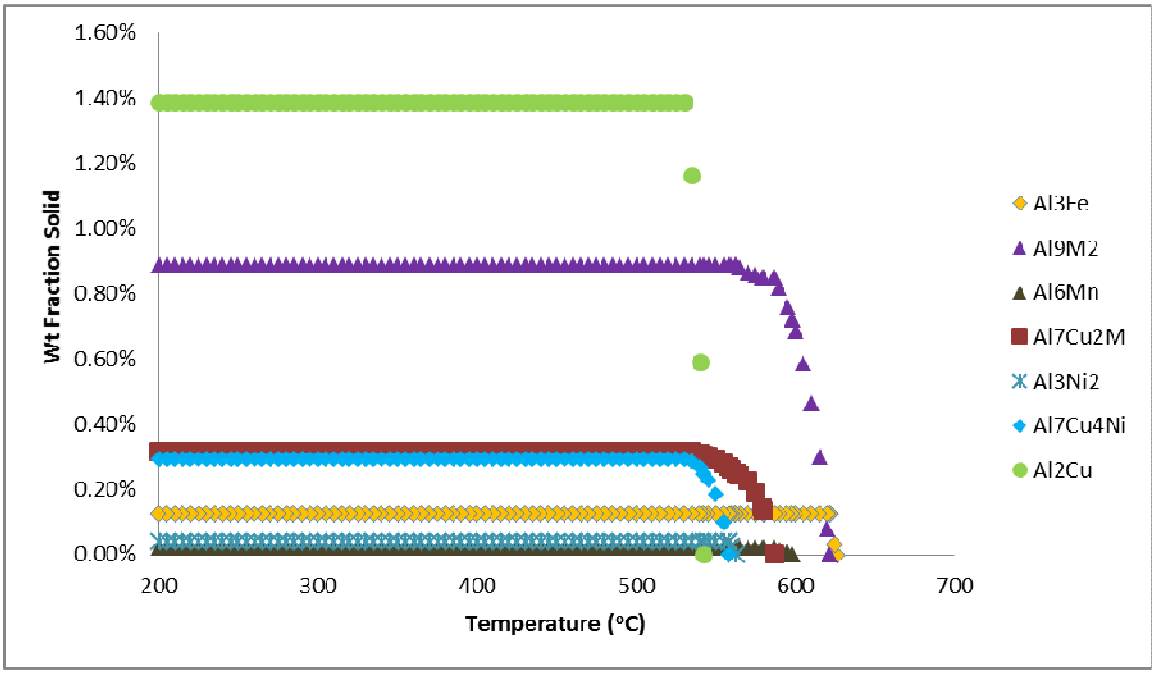

Figure 4.2: Change in fraction solid wt % with temperature of alloy A0 (SG).

Alloy A1: Equilibrium Solidification

During equilibrium solidification, significant phases formed are Al_6Mn, Al_7Cu_2M, Silicon and Al_2Cu as shown in Figure 4.3. First phase Al_6Mn started to form at 619 °C and reached to a maximum 0.78 wt%. This phase completely dissolved in aluminum matrix at 536 °C. Al_7Cu_2M formed at 558 °C reached a maximum of 1.15 wt % and retained 200 °C. Al_2Cu began to form at 420 °C, reached a maximum of 3.9 wt % at 200 °C. Another phase Silicon started to form at 330 °C with maximum 0.1 wt % and found at 200 °C. At 223°C there is a sharp increase in Al_2Cu phase and a sharp decrease in Al_7Cu_2M phase because at that temperature Al_2Cu phase is thermodynamically more stable than Al_7Cu_2M phase.

Alloy A1: Non-equilibrium Solidification

During non-equilibrium cooling, no additional phases were formed compared to equilibrium cooling condition for the same composition of alloy A1. The phase silicon that was very negligible in the equilibrium cooling condition is completely disappeared in non-equilibrium cooling. Total three phases were predicted as shown in Figure 4. 4. First Al_6Mn formed at 610 ^oC and reached to 0.45%. Then Al_7Cu_2M solidified at 585 ^oC and reached 0.47%. Then at 540 ^oC Al_2Cu nucleated and reached to a maximum of 2.0%.

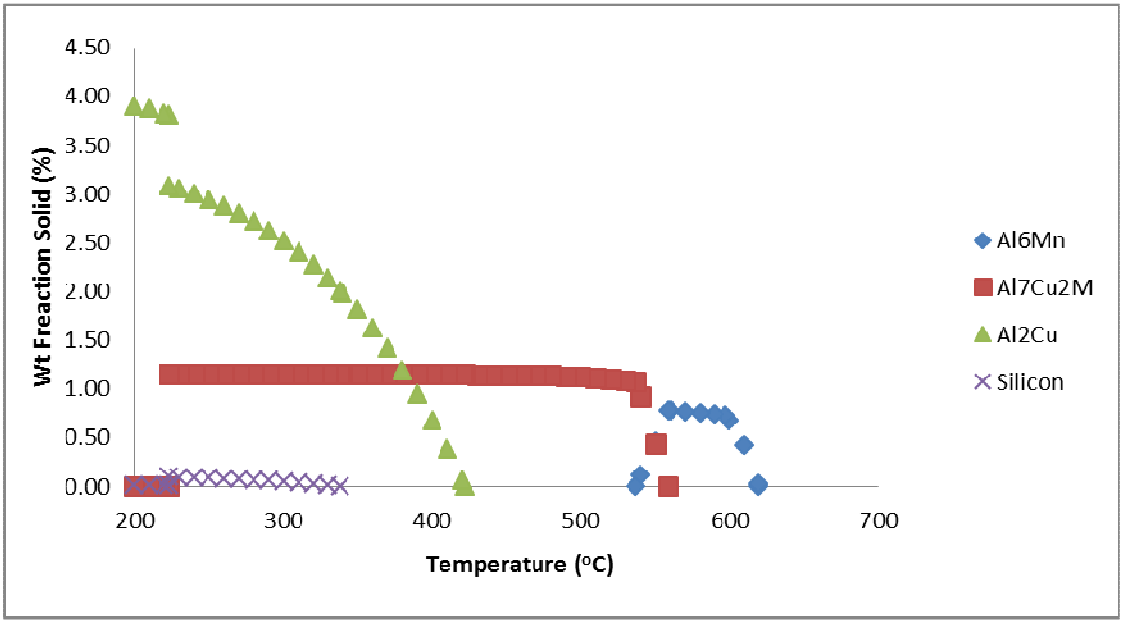

Fig. 4.3: Change in fraction solid wt % with temperature of alloy A1 (EQM).

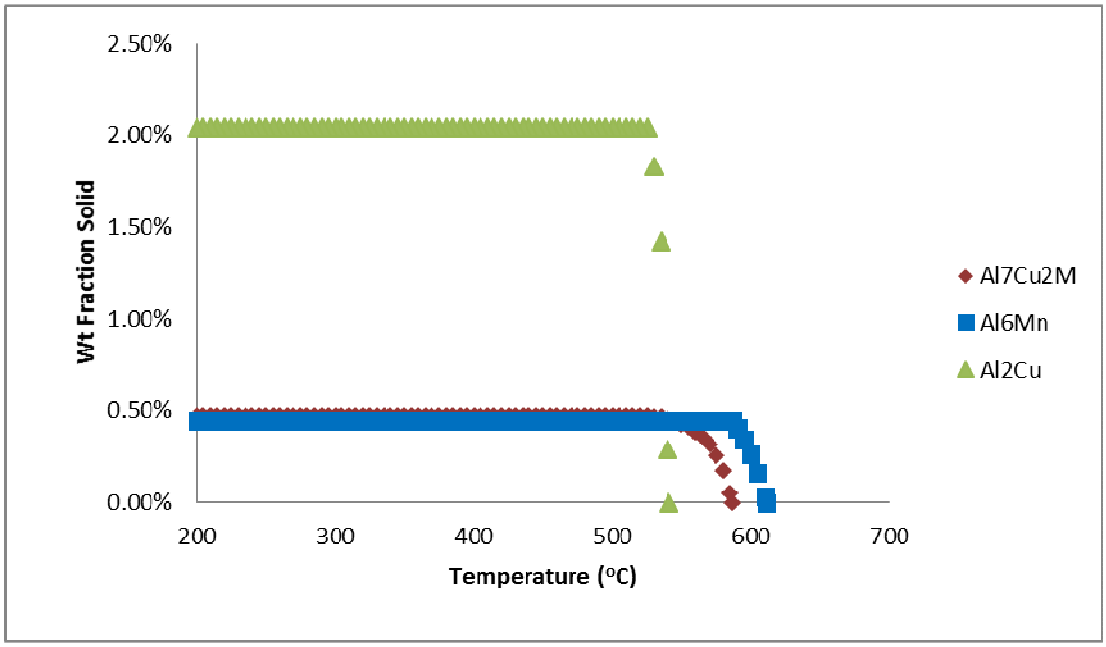

Fig. 4.4: Change in fraction solid wt % with temperature of alloy A1 (SG).

Alloy A2: Equilibrium Solidification

During equilibrium solidification, significant phases formed are Al_7Cu_2M, Silicon and Al_2Cu. First phase Al_7Cu_2M was predicted to form at 587 °C and reached to a maximum 2.01 wt%. This phase started to dissolve in aluminum matrix at 220 °C. The most important phase that provides hardness in Al-Cu alloys, Al_2Cu began to form at 437 °C, reached a maximum of 4.6 wt % at 200 °C. Another phase Silicon started to form at 320 °C with maximum 0.1 wt % and dissolved completely in matrix at 200 °C as shown in Figure 4.5. At 230°C there is a sharp increase in Al_2Cu phase and a sharp decrease in Al_7Cu_2M phase because at that temperature Al_2Cu phase is thermodynamically more stable than Al_7Cu_2M phase.

Alloy A2: Non-equilibrium Solidification

During non-equilibrium cooling, an additional phase Al_6Mn was formed for the same composition of alloy A2. The phase silicon that was very negligible in equilibrium cooling is totally disappeared in non-equilibrium cooling. Total three phases were predicted from Figure 4.6. First Al_6Mn formed at 619 °C and reached to 0.97%. Then Al_7Cu_2M solidified at 585 °C and reached 0.59%. Then at 541 °C Al_2Cu nucleated and reached to a maximum of 2.71%.

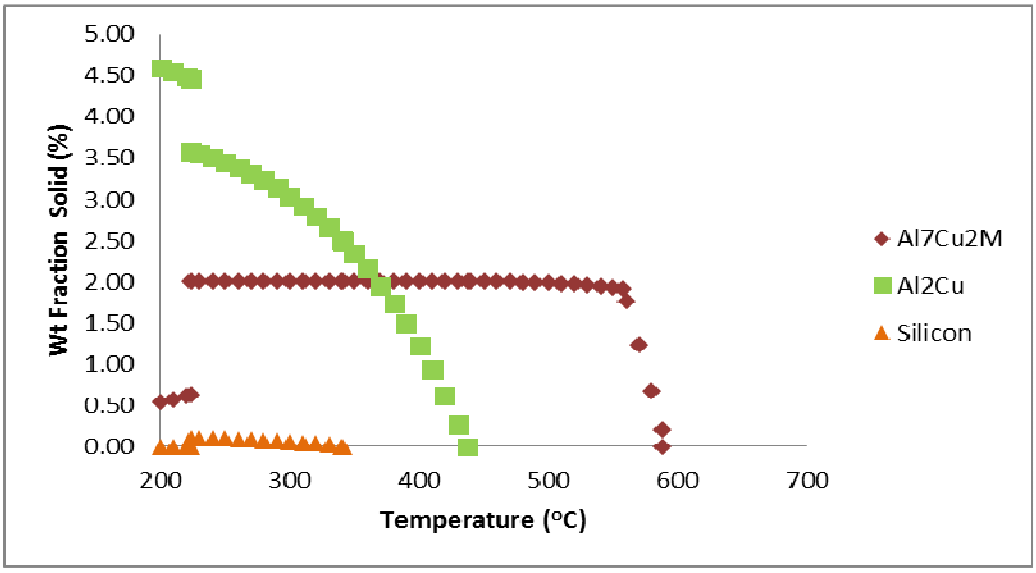

Fig. 4.5: Change in fraction solid wt % with temperature of alloy A2 (EQM).

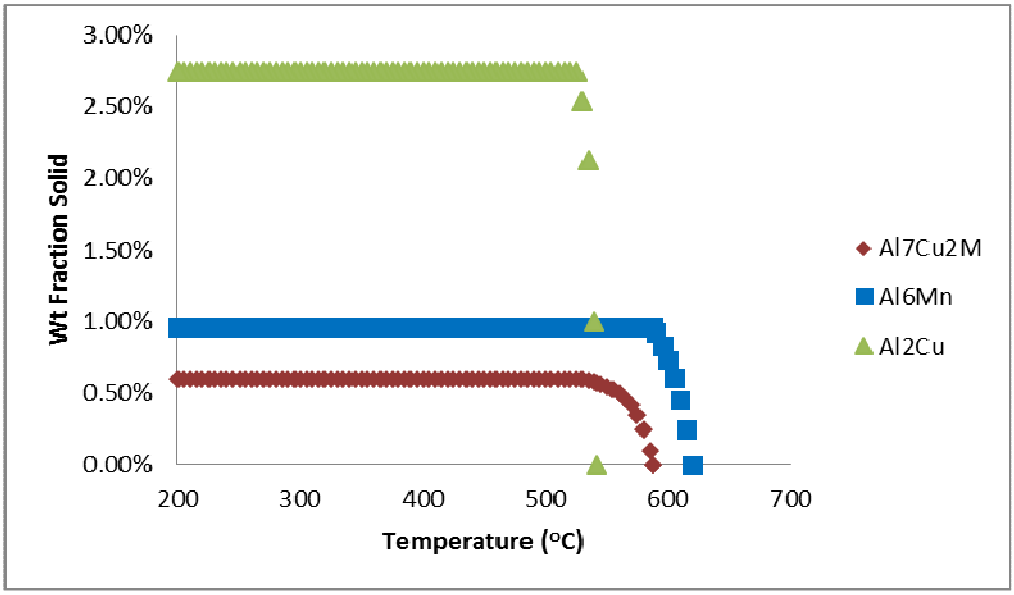

Fig. 4.6: Change in fraction solid wt % with temperature of alloy A2 (SG).

Alloy B0: Equilibrium Solidification

During equilibrium solidification, significant phases formed are Al_7Cu_2M, $Al_5Cu_2Mg_8Si_6$ Silicon and Al_2Cu (Figure 4.7). First phase Al_7Cu_2M formed at 588 ^oC and reached to a maximum 0.46 wt%. This phase started to dissolve in aluminum matrix at 200 ^oC. Al_2Cu started to form at 490

°C, reached a maximum of 6.5 wt % at 200 °C. $Al_5Cu_2Mg_8Si_6$ nucleated at 330 °C and their content increased to a maximum of 0.18 wt%. Another phase Silicon started to form at 270 °C with maximum 0.02 wt % and dissolved completely in matrix at 200 °C.

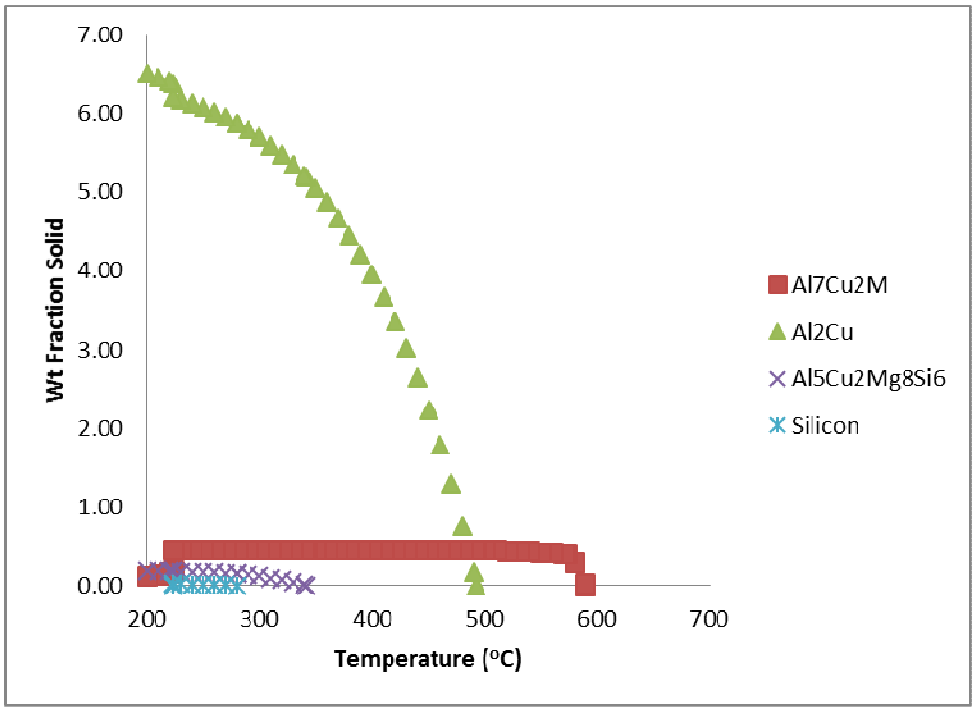

Fig. 4.7: Change in fraction solid wt % with temperature of alloy Bo (EQM).

Alloy B0: Non-equilibrium Solidification

During non-equilibrium cooling only two significant phases were formed. The phases silicon and $Al_5Cu_2Mg_8Si_6$ were very negligible in equilibrium cooling is totally disappeared in non-equilibrium cooling. First phase to be solidified was Al_7Cu_2M at 575 °C and reached 0.30 wt%. Then, at 543 °C, Al_2Cu nucleated and reached to a maximum of 2.88% (figure 4.8).

Alloy B1: Equilibrium Solidification

During equilibrium solidification, significant phases formed are Al_7Cu_2M, Al_2CuMg, Mg_2Si and Al_2Cu as shown in Figure 4.9. First phase Al_7Cu_2M formed at 584 °C and reached to a maximum 0.68wt%. The most important phase that provides hardness in Al-Cu alloy, Al_2Cu began to form

at 479 °C, reached a maximum of 5.33 wt % at 200 °C. Mg_2Si nucleated at 380 °C and their content increased to a maximum of 0.13 wt%. Another phase Al_2CuMg started to form at 280 °C with maximum 0.87 wt % and retained up to 200 °C.

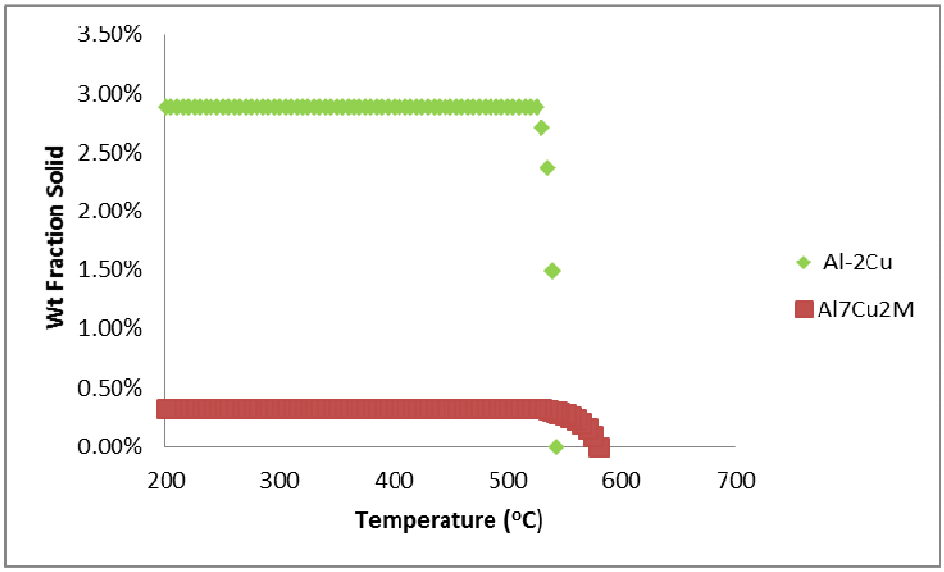

Fig. 4.8: Change in fraction solid wt % with temperature of alloy B0 (SG).

Alloy B1:Non-equilibrium Solidification

For non-equilibrium cooling, an additional phase Al_6Mn was present than equilibrium cooling for the same alloy B1. Total five phases were predicted as can be seen in Figure 4.10. First Al_6Mn formed at 575 °C and reached to 0.1%. Then Al_7Cu_2M solidified at 570 °C and reached 0.60 wt%. Then, at 535 °C, Al_2Cu nucleated and reached a maximum of 3.97 wt%. The next phase formed is Al_2CuMg at 503 °C and increased to 0.42 wt%. Finally, at 470 °C, Mg_2Si started to solidify and reached to a maximum of 0.07%.

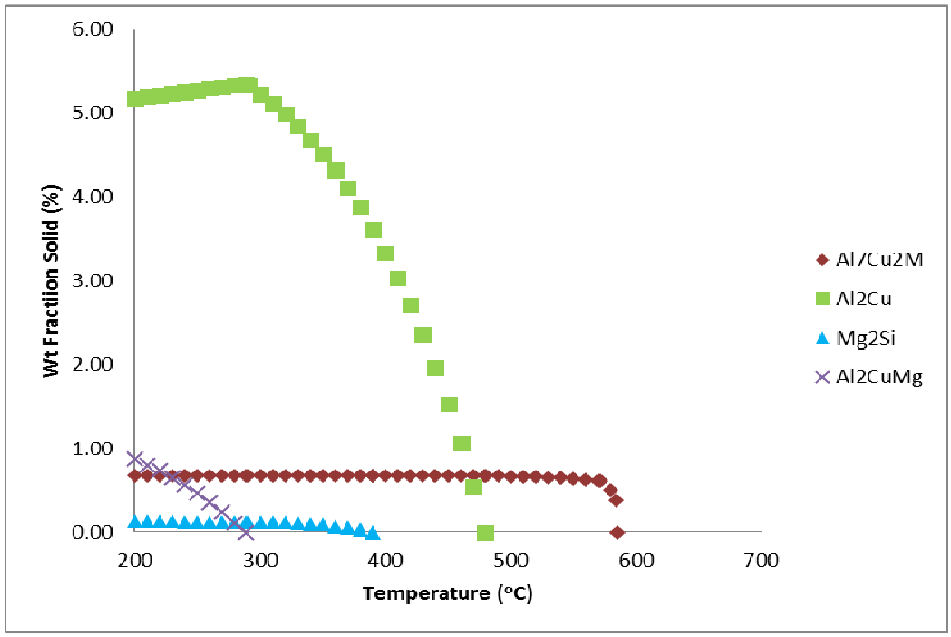

Fig. 4.9: Change in fraction solid wt % with temperature of alloy B1 (EQM).

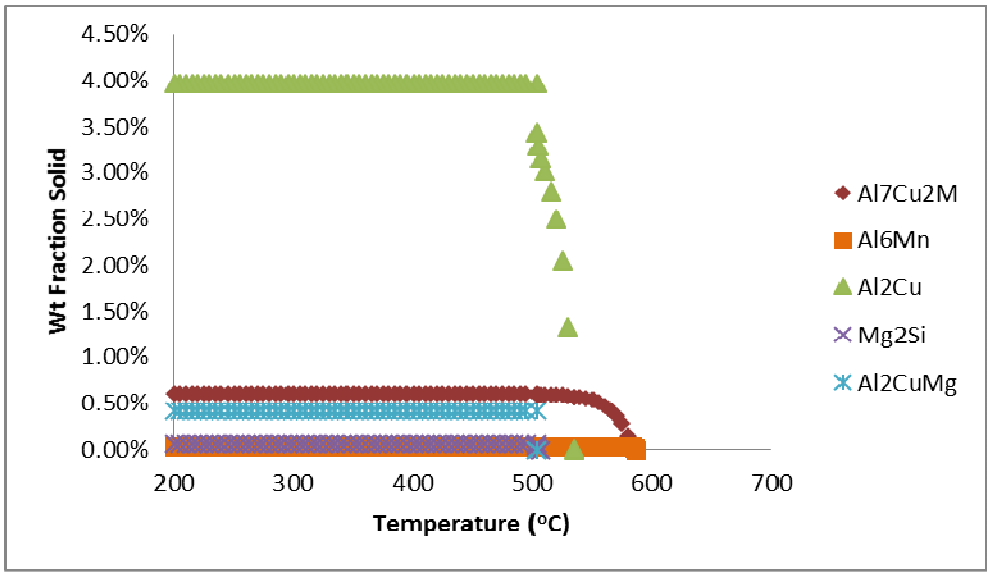

Fig. 4.10: Change in fraction solid wt % with temperature of alloy B1 (SG).

Alloy B2: Equilibrium Solidification

During equilibrium solidification, significant phases formed are Al_7Cu_2M, Al_2CuMg, Mg_2Si and Al_2Cu (Figure 4.11). First phase Al_7Cu_2M formed at 578 °C and reached to a maximum 0.51 wt%. Al_2Cu started to form at 490 °C, reached a maximum of 5.77 wt % at 310 °C. Mg_2Si nucleated at 454 °C and their content increased to a maximum of 0.36 wt%. Another phase Al_2CuMg started to form at 337 °C with maximum 1.69 wt % and retained up to 200 °C.

Alloy B2:Non-equilibrium Solidification

For alloy B2 number of phases present in case of non-equilibrium solidification matches with that of equilibrium solidification as observed from Figure 4.12. First Al_7Cu_2M formed at 574 °C and reached to 0.5%. Then at 524 °C Al_2Cu nucleated and reached a maximum of 4.70 wt%. The next phase formed is Mg_2Si at 505 °C and increased to 0.22 wt%. Finally at 503 °C Al_2CuMg started to solidify and reached to a maximum of 0.67%.

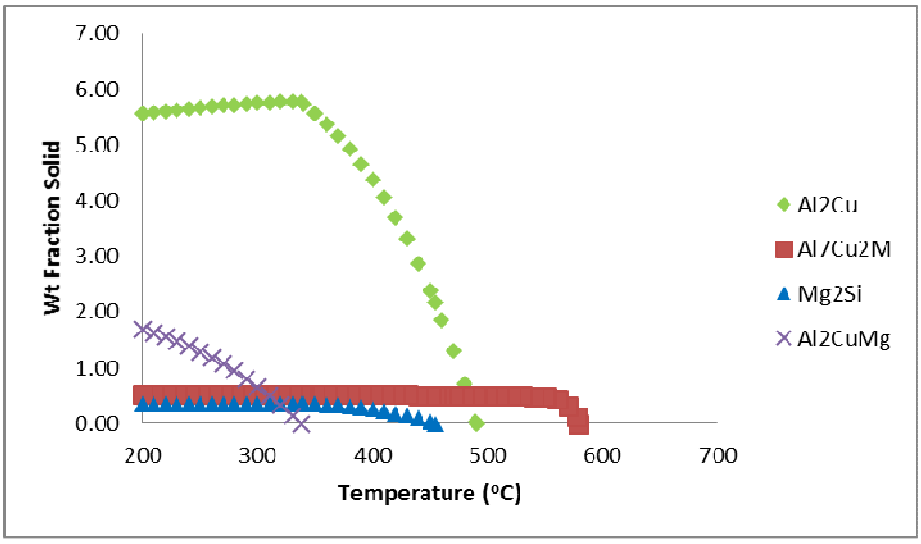

Fig. 4.11: Change in fraction solid wt % with temperature of alloy B2 (EQM).

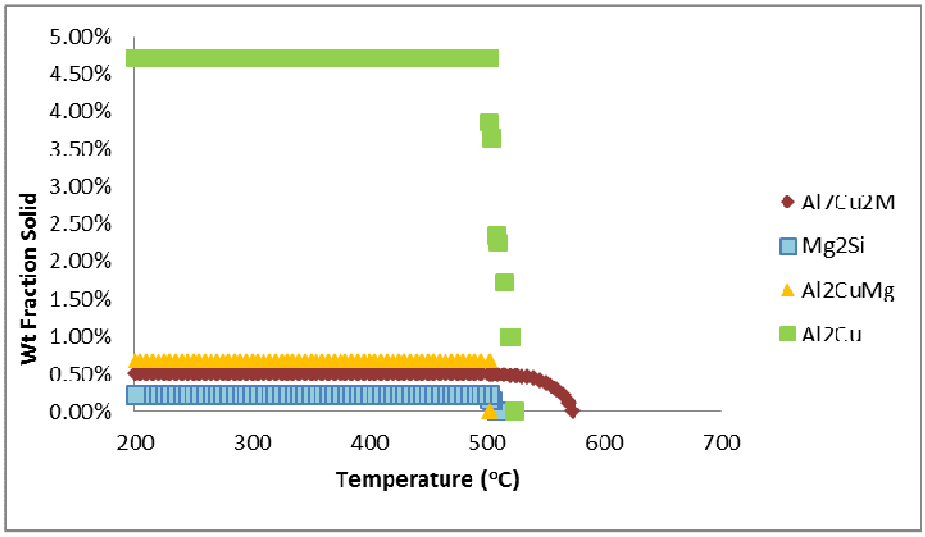

Fig. 4.12: Change in fraction solid wt % with temperature of alloy B2 (SG).

Alloy C0: Equilibrium Solidification

During equilibrium solidification, significant phases formed are Al_7Cu_2M, AlFeSi, Silicon and Al_2Cu (Figure 4.13). First phase Al_7Cu_2M formed at 575 °C and reached to a maximum 0.38 wt%. The most important phase that provides hardness in Al-Cu alloy, Al_2Cu started to form at 545 °C, reached a maximum of 11.3 wt % at 200 °C. Silicon nucleated at 337 °C and their content increased to a maximum of 0.1 wt%. Another phase AlFeSi started to form at 223 °C with maximum 0.21 wt % at 200 °C.

Alloy C0: Non-equilibrium Solidification

During non-equilibrium cooling only two significant phases were formed for the same alloy C0 (Figure 4.14). The phase silicon and AlFeSi those were very negligible in equilibrium cooling are totally disappeared in non-equilibrium cooling. First phase to be solidified was Al_2Cu at 545.3 °C and reached 8.06 wt% and remained stable till 200 °C. Then at 568 °C Al_7Cu_2M nucleated and reached to a maximum of 0.36%.

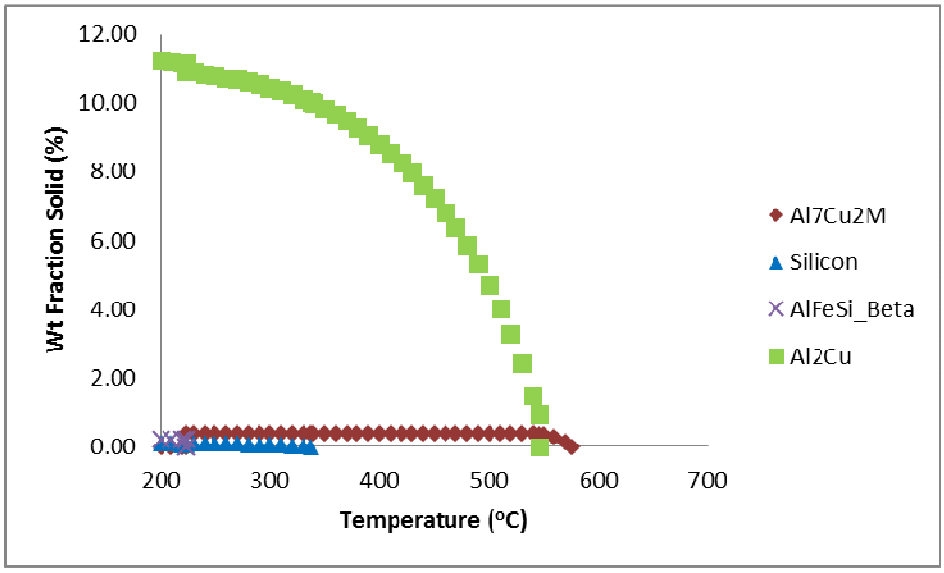

Fig. 4.13: Change in fraction solid wt % with temperature of alloy C0 (EQM).

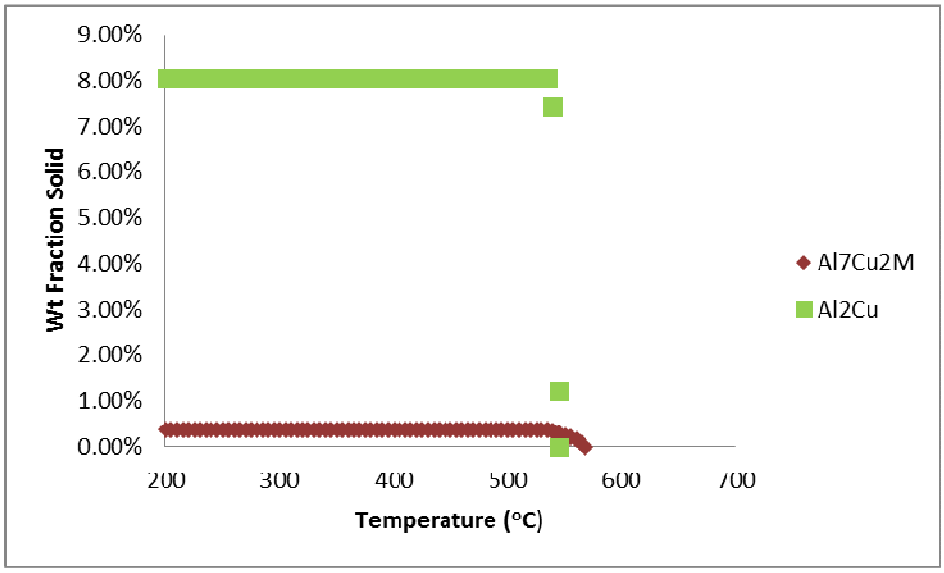

Fig. 4.14: Change in fraction solid wt % with temperature of alloy C0 (SG).

Alloy C1: Equilibrium Solidification

During equilibrium solidification, significant phases formed are Al_7Cu_2M, AlFeSi, Silicon and Al_2Cu (Figure 4.15). First phase Al_7Cu_2M formed at 562 °C and reached to a maximum 0.1 wt%. Al_2Cu started to form at 540 °C, reached a maximum of 9.93 wt % at 200 °C. Silicon nucleated at 321 °C and their content increased to a maximum of 0.05 wt%. Another phase AlFeSi started to form at 223 °C with maximum 0.05 wt % at 200 °C.

Alloy C1: Non-equilibrium Solidification

During non-equilibrium cooling condition, only two significant phases were formed for the same composition of alloy C1. The phase silicon and AlFeSi those were very negligible in equilibrium cooling are totally disappeared in non-equilibrium cooling. First phase to be solidified was Al_7Cu_2M at 547 ºC and reached 0.08 wt% and remained stable till 200 °C. Then at 545 °C Al_2Cu nucleated and reached to a maximum of 7.20% (Figure 4.16).

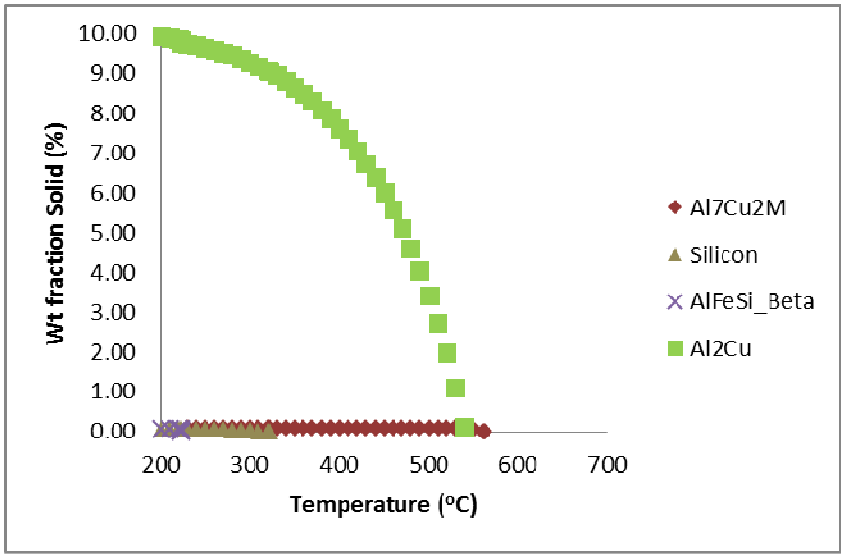

Fig. 4.15: Change in fraction solid wt % with temperature of alloy C1 EQM).

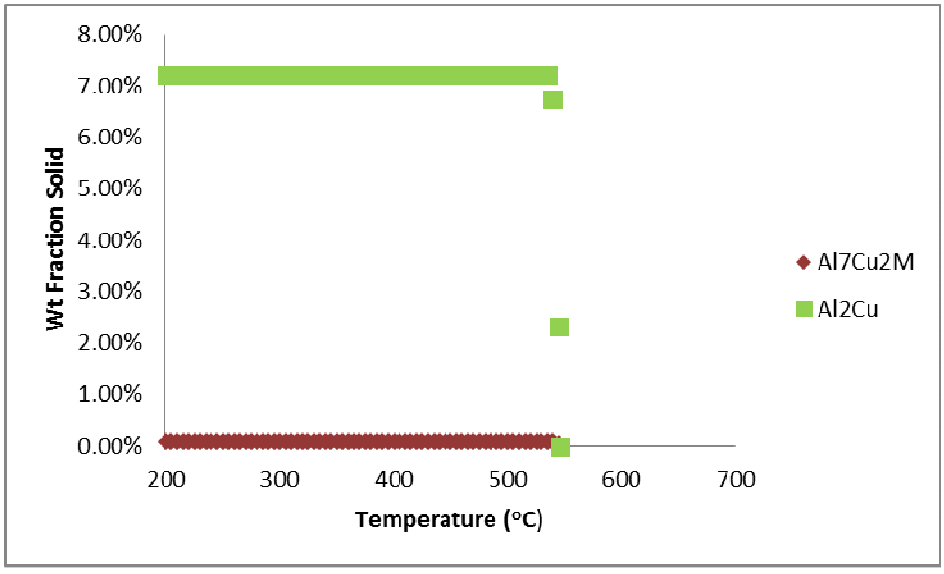

Fig. 4.16: Change in fraction solid wt % with temperature of alloy C1 (SG).

Alloy C2: Equilibrium Solidification

During equilibrium solidification, significant phases formed are Al_7Cu_2M, Al_2CuMg, Mg_2Si and Al_2Cu (Figure 4.17). First phase Al_7Cu_2M formed at 573 °C and reached to a maximum 0.6 wt%. The most important phase that provides hardness in Al-Cu alloys, Al_2Cu, started to form at 526 °C, reached a maximum of 9.26 wt % and at 200 °C it became 9.05 wt %. Mg_2Si nucleated at 468 °C and their content increased to a maximum of 0.33 wt%. Another phase Al_2CuMg started to form at 391 °C with maximum 2.83 wt % at 200 °C.

Alloy C2: Non-equilibrium Solidification

For alloy C2 number of phases present in case of non-equilibrium solidification matches with that of equilibrium solidification. First Al_7Cu_2M formed at 570 °C and reached to 0.6 wt%. Then at 528 °C Al_2Cu nucleated and reached a maximum of 8.08 wt%. The next phase formed is Mg_2Si at 505 °C and increased to 0.22 wt%. Finally at 503 °C Al_2CuMg started to solidify and reached to a maximum of 1.58 wt% (Figure 4.18).

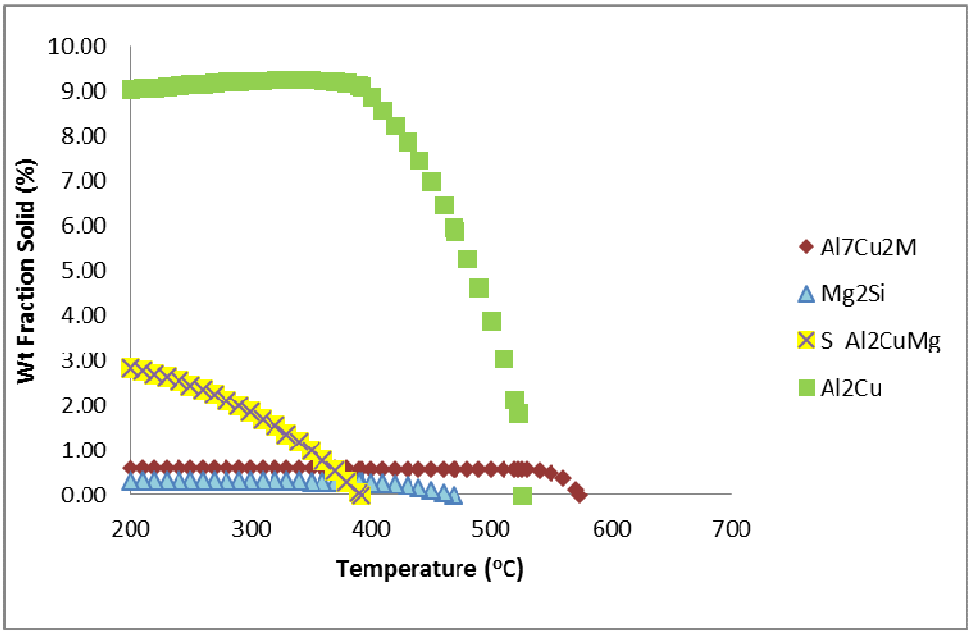

Fig. 4.17 Change in fraction solid wt % with temperature of alloy C2 (EQM).

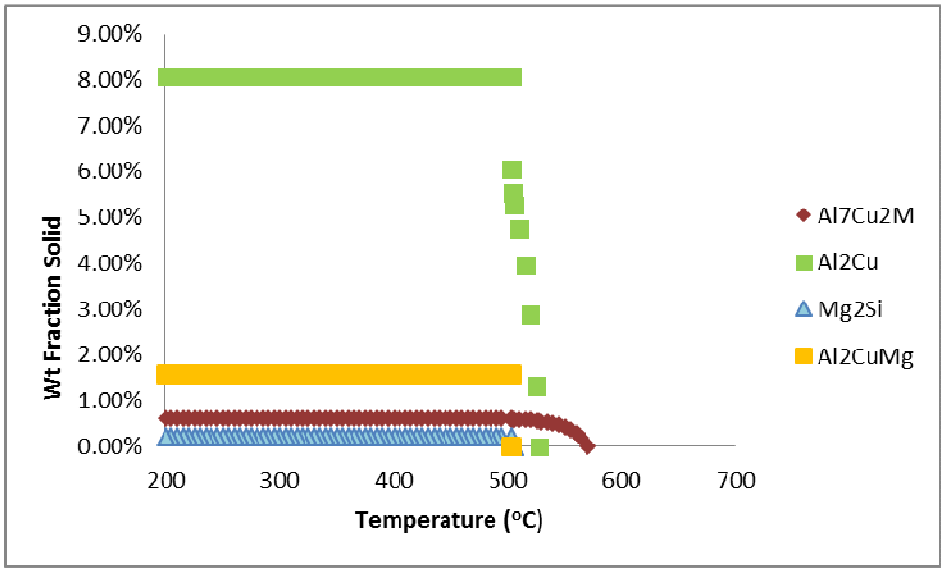

Figure 4.18: Change in fraction solid wt % with temperature of alloy C2 (SG).

Summary of the phases predicted from CALPHAD modeling method is shown in Table 4.2. From this table, it is clear that the major phase formed is Al_2Cu in almost all alloys (except A0 EQM). Apart from this phase, magnesium bearing phase contributed to the microstructure. Similar effects were observed experimentally in previous works [57-58].

Table 4.2: Significant phases of investigated alloys (s= significant; ns = not significant; vs= very significant).

		Phase>0.2 wt%						
Alloy	Condition	Al_9M_2	Al_7Cu_2M	Al_7Cu_4Ni	Al_2Cu	Al_6Mn	Al_2CuMg	Mg_2Si
Ao	EQM	S	vs	s	s	-	-	-
	SG	S	ns	ns	vs	ns	-	-
A1	EQM	-	s	-	vs	s	-	-
	SG	-	s	-	vs	s	-	-
A2	EQM	-	s	-	vs	-	-	-
	SG	-	s	-	vs	s	-	-
Bo	EQM	-	s	-	vs	-	-	-
	SG	-	ns	-	vs	-	-	-
B1	EQM	-	s	-	vs	-	s	ns
	SG	-	s	-	vs	ns	s	ns

		Phase>0.2 wt%						
Alloy	Condition	Al_9M_2	Al_7Cu_2M	Al_7Cu_4Ni	Al_2Cu	Al_6Mn	Al_2CuMg	Mg_2Si
B2	EQM	-	s	-	vs	-	s	ns
	SG	-	s	-	vs	-	s	ns
Co	EQM	-	s	-	vs	-	-	-
	SG	-	s	-	vs	-	-	-
C1	EQM	-	ns	-	vs	-	-	-
	SG	-	ns	-	vs	-	-	-
C2	EQM	-	s	-	vs	-	vs	s
	SG	-	s	-	vs	-	s	ns

Table 4.3: Prediction of the alloys investigated [Here, T1 denoted phase formation start temperature and T2 denotes the lowest stable temperature, st disl = starting temperature of dissolving and c disl = complete dissolving temperature].

Alloy	Condition	Phase	T1 (°C)	T2 (°C)	Max wt %
Ao	EQM	Al_9M_2	625	336	1.19
		Al_7Cu_2M	544	200	1.75
		Al_7Cu_4Ni	440	200	1.58
		Al_2Cu	**310**	**200**	**0.82**
	SG	Al_3Fe	626	200	0.1
		Al_9M_2	621	200	0.89
		Al_6Mn	597	200	0.02
		Al_7Cu_2M	586	200	0.3
		Al_3Ni	558	200	0.04
		Al_7Cu_4Ni	558	200	0.29
		Al_2Cu	**540**	**200**	**1.38**
A1	EQM	Al_6Mn	619	536 (c disl)	0.78
		Al_7Cu_2M	558	200	1.15
		Silicon	330	200	0.1
		Al_2Cu	**420**	**200**	**3.9**
	SG	Al_6Mn	610	200	0.45
		Al_7Cu_2M	585	200	0.47
		Al_2Cu	**540**	**200**	**2.0**
A2	EQM	Al_7Cu_2M	587	220 (st disl)	2.01
		Silicon	320	200	0.1
		Al_2Cu	**437**	**200**	**4.6**
	SG	Al_6Mn	619	200	0.97
		Al_7Cu_2M	585	200	0.59
		Al_2Cu	**541**	**200**	**2.71**

Alloy	Condition	Phase	T1 (^oC)	T2 (^oC)	Max wt %
Bo	EQM	Al_7Cu_2M	588	200(st disl)	0.46
		$Al_5Cu_2Mg_8Si_6$	330	200	0.18
		Silicon	270	200(c disl)	0.02
		Al_2Cu	**490**	**200**	**6.5**
	SG	Al_7Cu_2M	575	200	0.3
		Al_2Cu	**543**	**200**	**2.88**
B1	EQM	Al_7Cu_2M	584	200	0.68
		Al_2CuMg	**280**	**200**	**0.87**
		Mg_2Si	380	200	0.13
		Al_2Cu	**479**	**200**	**5.33**
	SG	Al_6Mn	575	200	0.1
		Al_7Cu_2M	570	200	0.6
		Al_2Cu	**535**	**200**	**3.97**
		Al_2CuMg	**503**	**200**	**0.42**
		Mg_2Si	470	200	0.07
B2	EQM	Al_7Cu_2M	578	200	0.51
		Al_2CuMg	**337**	**200**	**1.69**
		Mg_2Si	454	200	0.36
		Al_2Cu	**490**	**310 (max)**	**5.77**
	SG	Al_7Cu_2M	574	200	0.5
		Al_2Cu	**524**	**200**	**4.7**
		Mg_2Si	505	200	0.22
		Al_2CuMg	**503**	**200**	**0.67**
Co	EQM	Al_7Cu_2M	575	200	0.38
		AlFeSi	180	100	0.21
		Silicon	337	200	0.1
		Al_2Cu	**545**	**200**	**11.3**
	SG	**Al_2Cu**	**545**	**200**	**8.06**
		Al_7Cu_2M	568	200	0.36
C1	EQM	Al_7Cu_2M	562	200	0.1
		AlFeSi	223	100	0.05
		Silicon	321	200	0.05
		Al_2Cu	**540**	**200**	**9.93**
	SG	Al_7Cu_2M	547	200	0.08
		Al_2Cu	**545**	**200**	**7.20**
C2	EQM	Al_7Cu_2M	573	200	0.6
		Al_2CuMg	**391**	**100**	**3.16**
		Mg_2Si	468	200	0.33
		Al_2Cu	**526**	**200 (9.05%)**	**9.26**
	SG	Al_7Cu_2M	570	200	0.6
		Al_2Cu	**528**	**200**	**8.08**
		Mg_2Si	505	200	0.22
		Al_2CuMg	**503**	**200**	**1.58**

4.2.1.2 Phase Characteristics

Aluminum Phase

Aluminum phase decreased slightly during equilibrium cooling due to reduce solubility at lower temperature. In Scheil-Gulliver condition more aluminum is retained due to diffusion-less transformation characteristics. Aluminum content decreases with increasing copper and magnesium in alloys as shown in Table 4.4.

Table 4.4: Weight fraction of Al phase at 200°C.

Alloy	Phase	Wt % at 200°C EQM	Wt % at 200°C SG
Ao	Al	95.79	96.93
A1		95.44	97.04
A2		94.05	95.7
Bo		92.99	96.79
B1		93.15	96.45
B2		91.88	96.35
Co		88.46	91.57
C1		89.94	92.71
C2		87.19	95.31

Al_2Cu Phase

The most dominating phase in Al-Cu alloy is Al_2Cu. Addition of copper results the formation of this phase which provides necessary hardness in Al-Cu alloys. This phase is predominating, both in equilibrium and non-equilibrium cooling condition, in all alloys (except A0 EQM) considered in this study. Analysis of this phase from CALPHAD modeling results a slight decrease in content in case of non-equilibrium solidification as shown in Table 4.5. This is due to the fact that solubility of copper in aluminum decreases with decreasing temperature and copper diffuse out of solution to form more Al_2Cu phase in equilibrium solidification. On the other hand, non-equilibrium solidification is a diffusionless solidification process and once the alloy solidified, no further diffusion occurs.

However, there is one exception for alloy A0, where Al_2Cu content in equilibrium solidification is lower than that of Scheil-Gulliver condition. This may be due to the fact that, in alloy A0 few Ni is present which forms another copper containing phase Al_7Cu_4Ni of about 1.58 wt% and

solidification of Al_2Cu starts at a temperature (310 °C**)** much lower than that of Al_7Cu_4Ni about 544 °C.

Table 4.5: Weight fraction of Al_2Cu phase at 200°C.

Alloy	Phase	Wt % at 200°C EQM	Wt % at 200°C SG
Ao	Al_2Cu	0.82	1.38
A1		3.9	2.0
A2		4.6	2.71
Bo		6.5	2.88
B1		5.33	3.97
B2		5.77	4.70
Co		11.3	8.06
C1		9.93	7.20
C2		9.26	8.08

Al_7Cu_2M Phase

Another copper containing phase present in Al-Cu alloys in Al_7Cu_2M. It was also found that there is a slight decrease in Al_7Cu_2M content in case of non-equilibrium solidification. This is due to the same reason that solubility of copper in aluminum decreases with temperature and copper diffuse out of solution to form more Al_7Cu_2M phase in equilibrium solidification.

It was also observed from comparing the phase fraction of two copper bearing phases Al_2Cu and Al_7Cu_2M that, with increasing copper content (2, 4, and 6 %) Al_2Cu phase content increases but Al_7Cu_2M phase content decreases as evident from Table 4.6. This may be due to higher attraction of copper with aluminum and thermodynamically more stable for copper to form Al_2Cu rather than forming Al_7Cu_2M.

Table 4.6: Weight fraction of Al_7Cu_2M phase at 200°C.

Alloy	Phase	Wt % at 200°C EQM	Wt % at 200°C SG
Ao	Al_7Cu_2M	1.75	0.3
A1		1.15	0.47
A2		2.01	0.59
Bo		0.46	0.3
B1		0.68	0.60
B2		0.51	0.50
Co		0.38	0.36
C1		0.10	0.08
C2		0.60	0.60

Al_6Mn Phase

This phase is very negligible in Al-Cu alloys. It was found mostly in Scheil-Gulliver condition, since there is no diffusion once it forms retain up to room temperature. It is also found from Table 4.7 that this phase forms only in low copper containing alloys.

Table 4.7: Weight fraction of Al_6Mn phase at 200°C.

Alloy	Phase	Wt % at 200°C EQM	Wt % at 200°C SG
Ao	Al_6Mn	-	0.02
A1		-	0.45
A2		-	0.97
Bo		-	-
B1		-	0.10
B2		-	-
Co		-	-
C1		-	-
C2		-	-

Al_2CuMg Phase

Al-Cu alloys those contain high copper and magnesium as alloying element have this phase. With increasing magnesium content, %Al_2CuMg increases in both equilibrium and non-equilibrium condition as shown in Table 4.8.

Table 4.8: Weight fraction of Al_2CuMg phase at 200°C.

Alloy	Phase	Wt % at 200°C EQM	Wt % at 200°C SG
Ao	Al_2CuMg	-	-
A1		-	-
A2		-	-
Bo		-	-
B1		0.87	0.42
B2		1.69	0.67
Co		-	-
C1		-	-
C2		3.16	1.58

Mg_2Si Phase

Another magnesium containing phase Mg_2Si was found in high Al-Cu-Mg alloys. Their content also increases with increasing magnesium for both equilibrium and non-equilibrium condition as shown in Table 4.9.

Table 4.9: Weight fraction of Mg_2Si phase at 200°C.

Alloy	Phase	Wt % at 200°C EQM	Wt % at 200°C SG
Ao	Mg_2Si	-	-
A1		-	-
A2		-	-
Bo		-	-
B1		0.13	0.07
B2		0.36	0.22
Co		-	-
C1		-	-
C2		0.33	0.22

Minor Phases

Apart from these significant Al-Cu-Mg containing phases some inferior phases were found in Al-Cu alloys such as, Al_9M_2, Al_3Fe, Al_3Ni, $Al_5Cu_2Mg_8Si_6$, Silicon and AlFeSi.

4.2.1.3 Effect of Copper on Phase Fraction

In Al-Cu-Mg alloys addition of copper increases copper containing phase Al_2Cu in both solidification mechanisms. From thermodynamic modeling method, it was found that as copper content increased in aluminum alloy (A0<B0<C0) the weight fraction of Al_2Cu increased from 0.82% to 6.5% to 11.3%. Not only from those alloys, aluminum alloys, containing 1% Mg and 2% Mg, also contained higher percentage of Al_2Cu phase with increased copper content in alloys (A1<B1<C1) and (A2<B2<C2) as shown in Table 4.3.

4.2.1.4 Effect of Magnesium on Phase Fraction

Similar to copper addition in Al-Cu-Mg alloys, addition of magnesium increases magnesium containing phase Al_2CuMg and Mg_2Si, in both solidification mechanisms. From thermodynamic modeling method, it was found that, with increasing magnesium in Al-Cu alloys (B0<B1<B2)

the weight fraction of Al_2CuMg increased from 0.00% to 0.87% to 1.69%. Similar trend was observed for other alloys (A0<A1<A2) and (C0<C1<C2) as shown in Table 4.3.

4.2.1.5 Effect of Alloy Addition in Solidus and Liquidus Temperature

From Table 4.10, it is clear that with increasing alloy content, liquidus and solidus temperature continues to decrease. Addition of impurities lowers the melting point of any material. Melting point of pure aluminum is 660.3°C, which decreases with increasing copper and magnesium content. However, copper appears to affect liquidus temperature more significantly than magnesium.

Table 4.10: Prediction of liquidus and solidus temperatures of the alloys investigated.

Alloy	Equilibrium Condition		Non-Equilibrium Condition	
	Liquidus Temp. (°C)	Solidus Temp. (°C)	Liquidus Temp. (°C)	Solidus Temp. (°C)
Ao	**653.35**	**601.50**	**650**	**530**
A1	**650**	**590**	**650**	**525**
A2	**650**	**587.91**	**650**	**525**
Bo	**640**	**570**	**645**	**525**
B1	**649.08**	**570**	**645**	**503**
B2	**645.97**	**550**	**645**	**503**
Co	**640**	**540**	**640**	**535**
C1	**640**	**541.40**	**645**	**535**
C2	**638.74**	**520**	**635**	**503**

From DTA, similar results were found for alloy C0-C2. Solidus and liquidus temperatures of these alloys are shown in Figures 4.19-4.21.

The addition of Cu decreased the liquidus temperature by around 13°C and decreased the equilibrium solidus temperature by around 30°C. According to the binary Al-Cu diagram, the liquidus temperature should be lowered with additions of copper. This anomaly may be due to the influence of other alloying elements. The equilibrium freezing range was increased by 20°C and the Scheil freezing range was not raised significantly. Formation temperature of Al2Cu phase was also detected from DTA plots which closely matches with that obtained from Figure 4.13, 4.15 and 4.17.

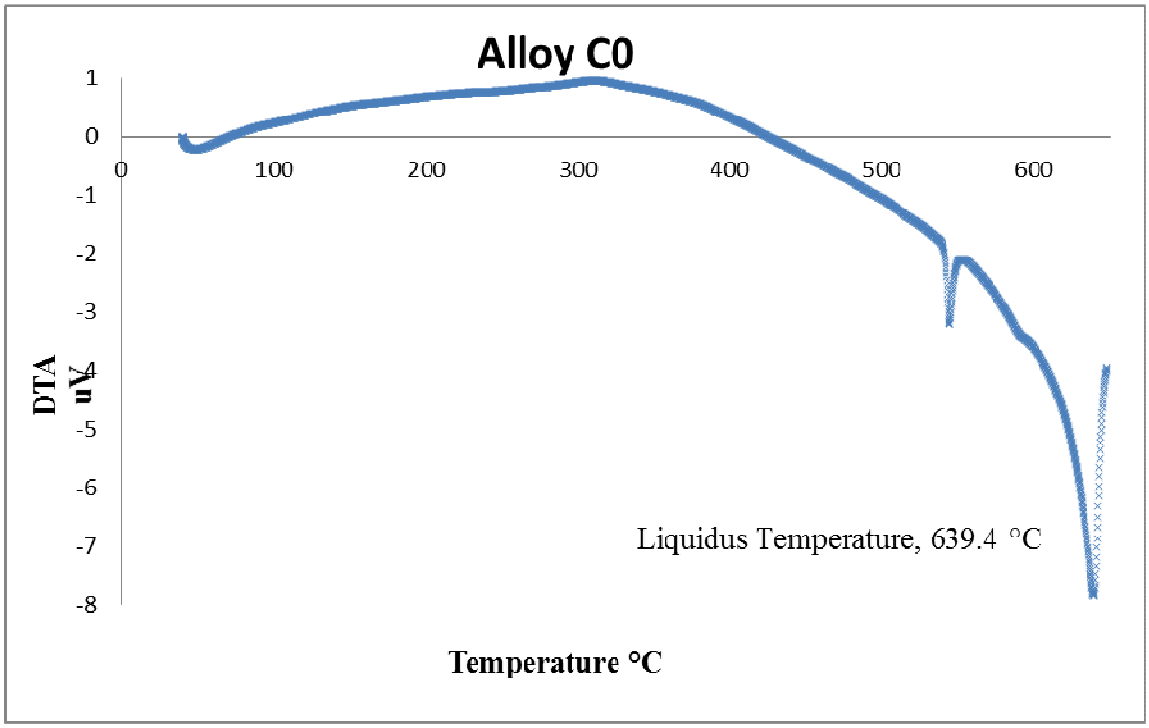

Figure 4.19: DTA curve for alloy C0.

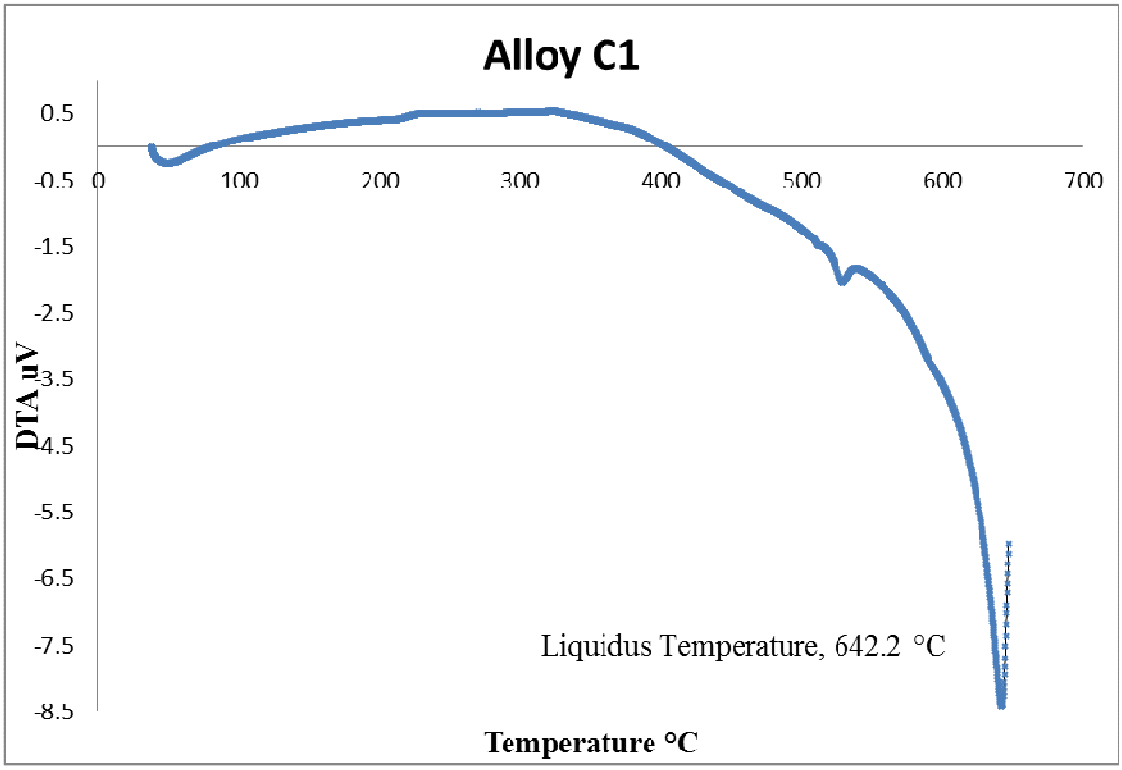

Figure 4.20: DTA curve for alloy C1.

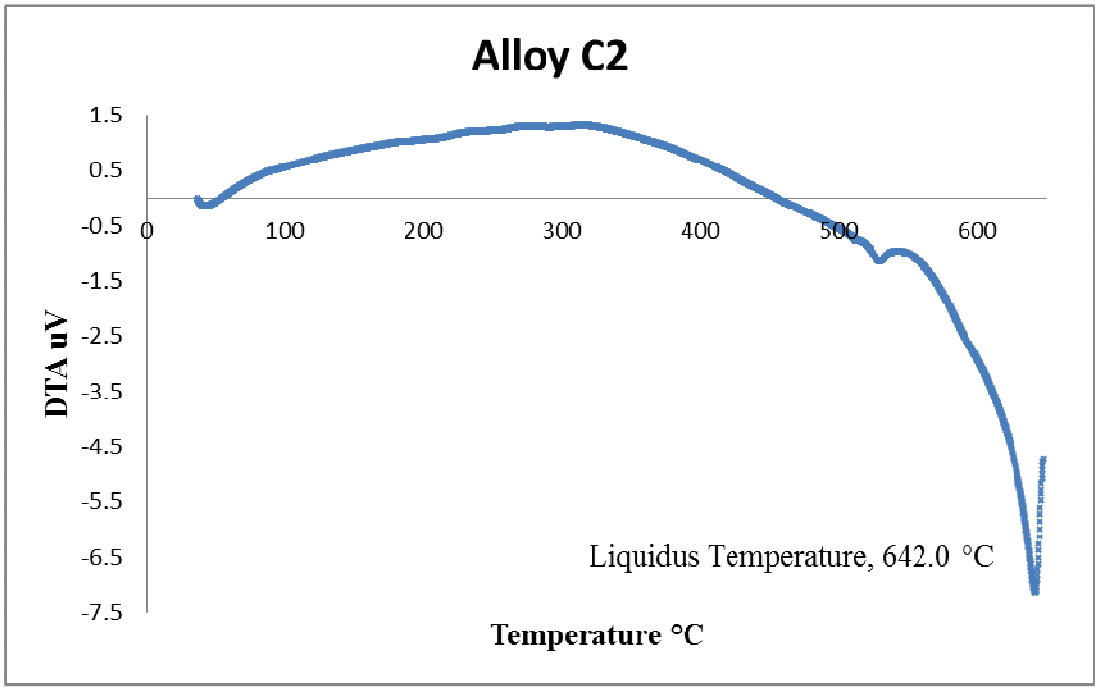

Figure 4.21: DTA curve for alloy C2.

4.2.2 Determination of Homogenization Temperature

In order to minimize microstructural non-uniformity of casting each alloy was homogenized at a specified temperature for a certain time. For this treatment, 400°C temperature was chosen. Since from CALPHAD analyses, (Figures 4.1-4.18) it was predicted that at this temperature most significant phases (Al_2Cu, Al_2CuMg and Al_7Cu_2M) were stable and minor phases such as silicon, Mg_2Si, Al_6Mn, Al_7Cu_4Ni, Al_9M_2 etc got dissolved in to aluminum matrix. Therefore, it became easier to find out the effects of these major significant phases on microstructure and hardness. Another reason is that at a higher temperature (>400°C), these significant phases would dissolve in matrix and that might make it difficult to determine the phases responsible for a change in hardness in those alloys. Together these reasons, all alloys were homogenized at 400 °C for 4 hours to maintain similar temperature effect.

4.2.3 Phase Fractions at 400 °C

After homogenizing at 400 °C significant phases present in the microstructure are shown in Figures 4.22-4.30 for alloys A0-C2. It was predicted from CALPHAD analysis that mainly Al_2Cu and Al_7Cu_2M phases were stable at 400 °C in most Al-Cu alloys. Al-Cu-Mg alloys with high %Mg (alloy B2 and C2) contained another phase Mg_2Si which provided hardness in those alloys.

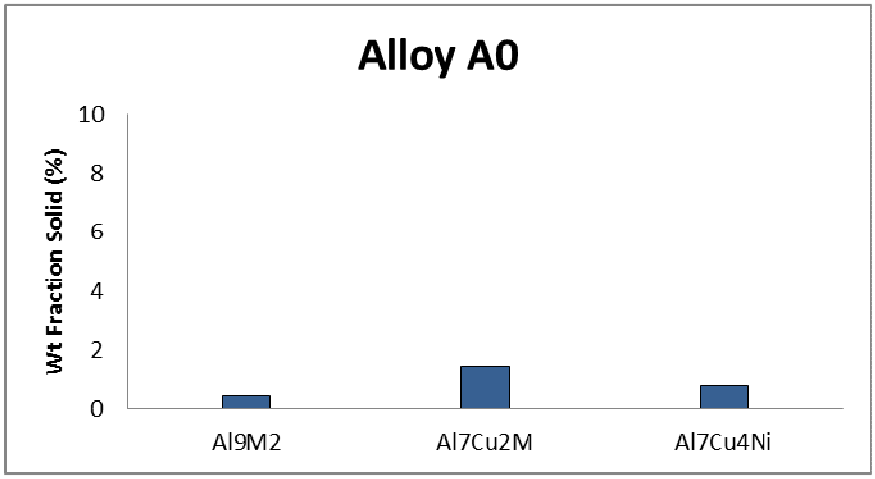

Figure 4.22: Weight fraction of phases at 400°C for alloy A0.

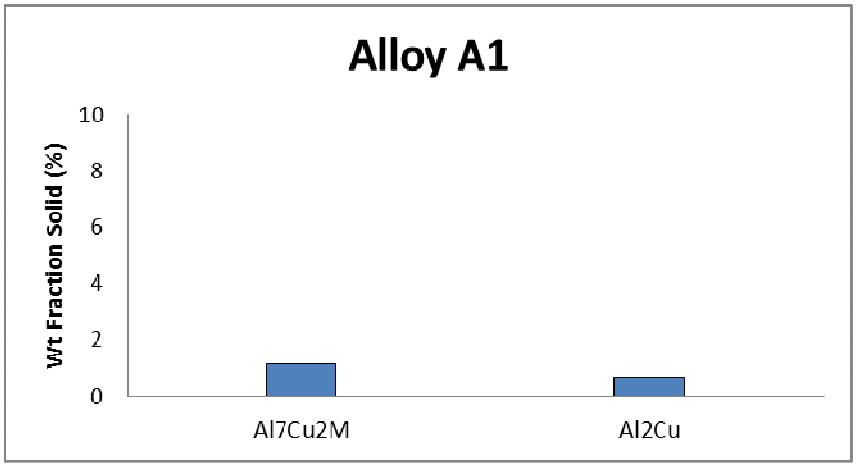

Figure 4.23: Weight fraction of phases at 400°C for alloy A1.

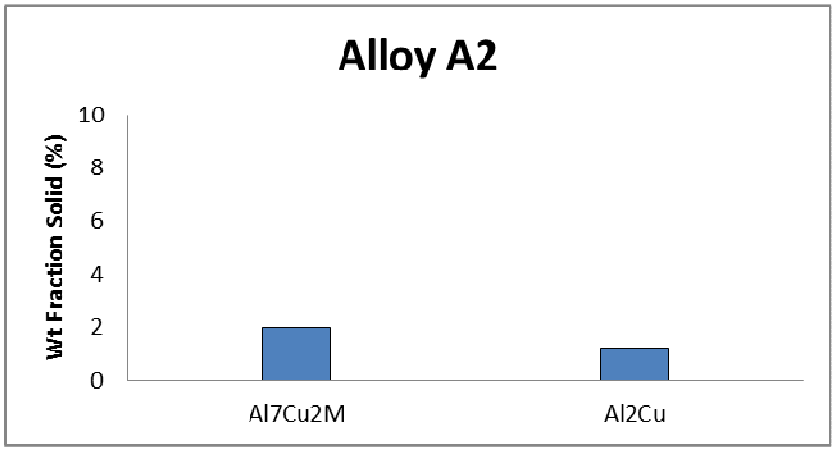

Figure 4.24: Weight fraction of phases at 400°C for alloy A2.

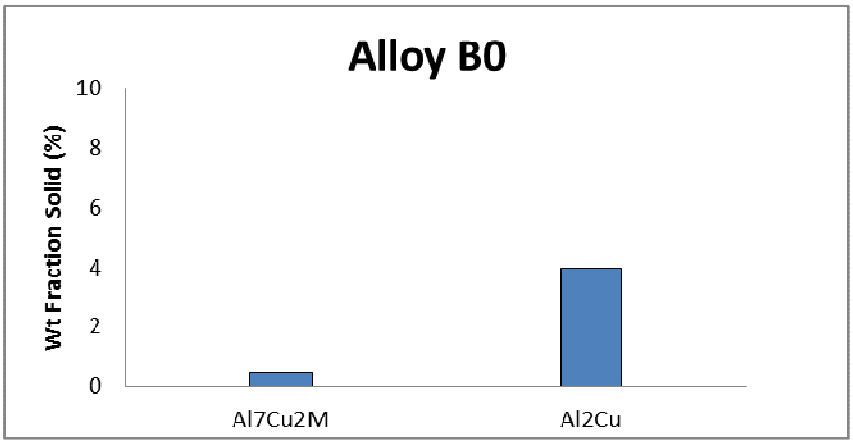

Figure 4.25: Weight fraction of phases at 400°C for alloy B0.

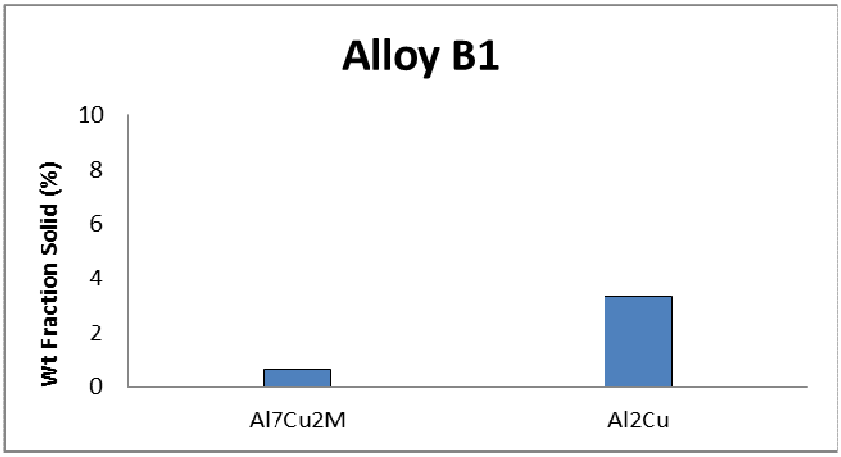

Figure 4.26: Weight fraction of phases at 400°C for alloy B1.

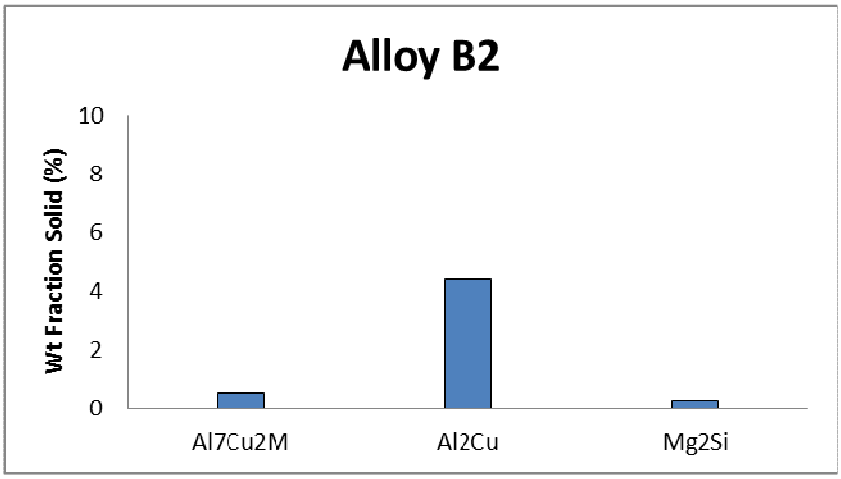

Figure 4.27: Weight fraction of phases at 400°C for alloy B2.

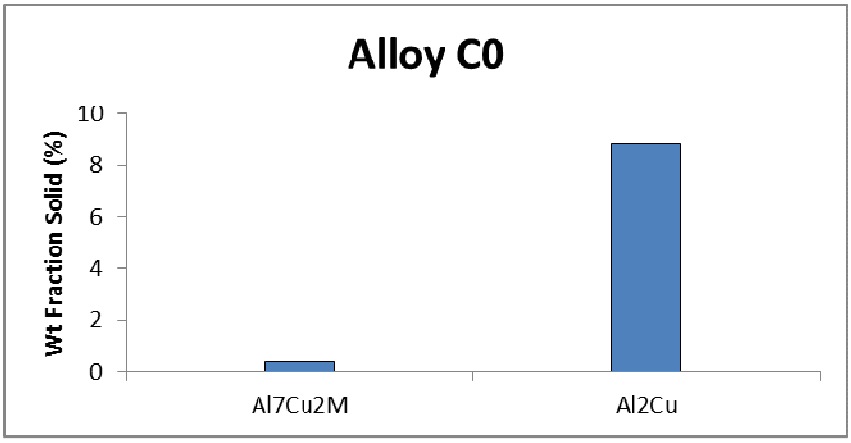

Figure 4.28: Weight fraction of phases at 400°C for alloy C0.

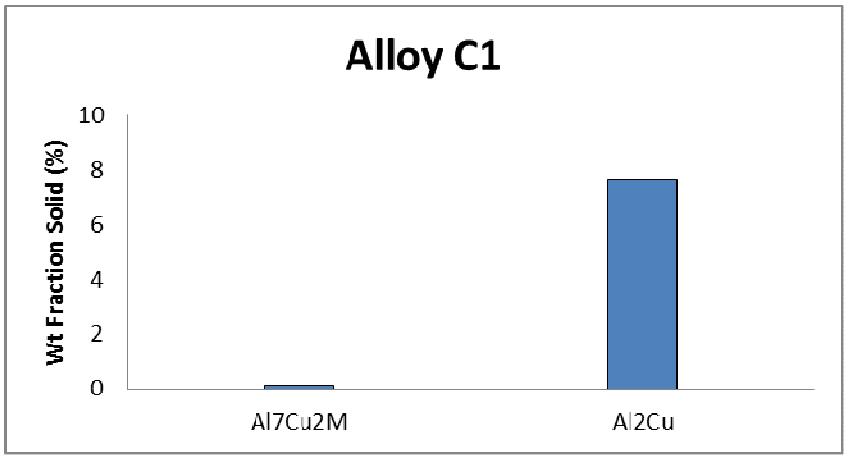

Figure 4.29: Weight fraction of phases at 400°C for alloy C1.

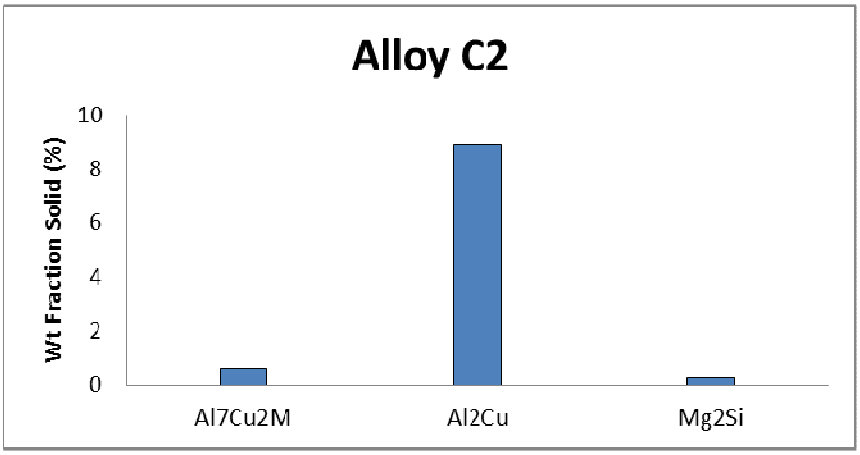

Figure 4.30: Weight fraction of phases at 400°C for alloy C2.

4.3 Microstructure

4.3.1 Effects of Homogenization Treatment

In order to homogenize the microstructure each casted alloy was heat treated at 400°C temperature for 4 hours and then quenched in water. Such treatment causes a change in microstructure as well as in mechanical properties (hardness). Among these effects, effects on hardness will be discussed later but effects on microstructure are explained below.

Homogenization treatment causes dissolution of some phases in the aluminum matrix. Since heat treatment was done at 400°C, some low melting point phases went into the solution in aluminum. This effect is supported by CALPHAD analysis as shown later. For each alloy, CALPHAD method was used to predict the variation of weight% of phases with temperature. It was found that, at that temperature Al-Cu-M (M=metal) phases disappears which results a change in microstructure from as cast condition. Also with increasing copper and magnesium content, phase fraction continues to increase as indicated by Figures 4.31-4.39.

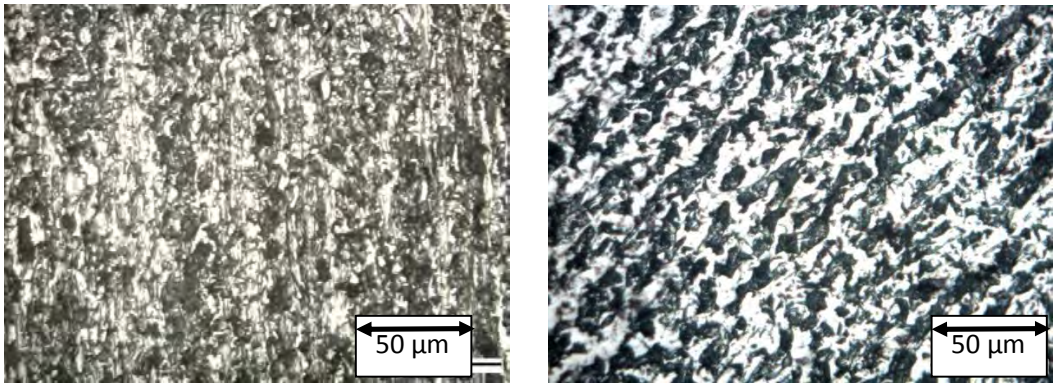

(a) (b)

Figure 4.31: Microstructure of Al-2% Cu (a) As Cast and (b) Homogenized.

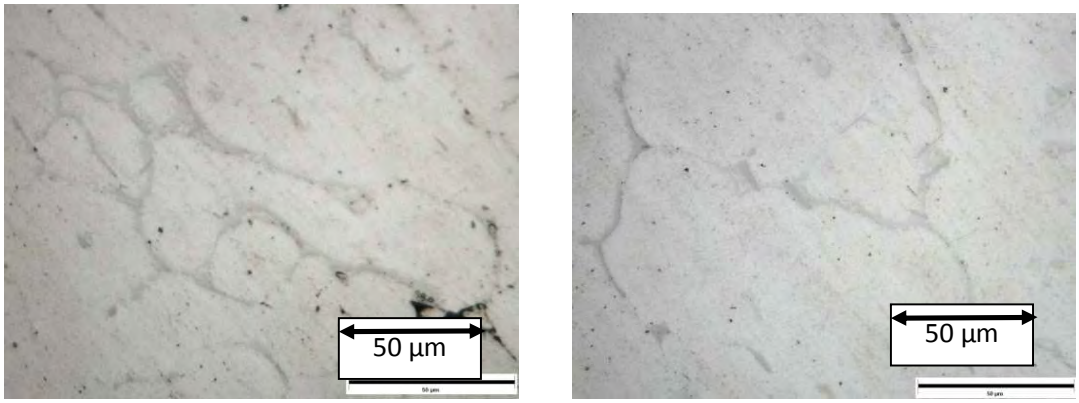

(a) (b)

Figure 4.32: Microstructure of Al-4% Cu (a) As Cast and (b) Homogenized.

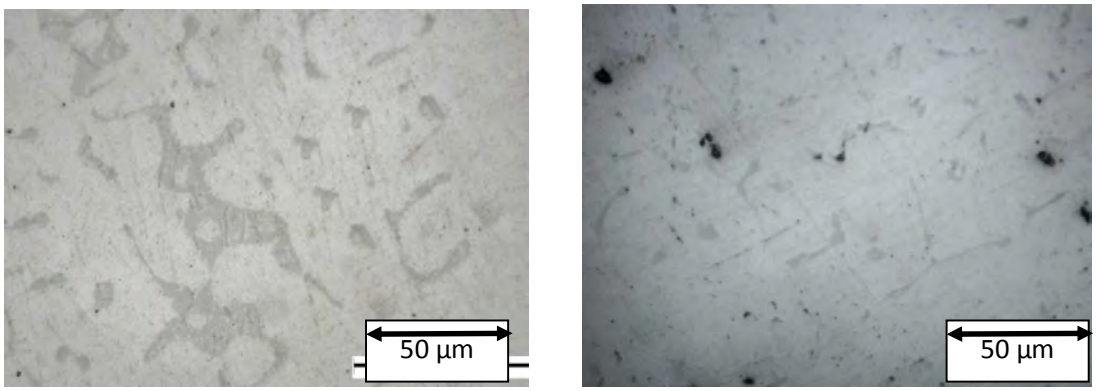

(a) (b)

Figure 4.33: Microstructure of Al-6% Cu (a) As Cast and (b) Homogenized.

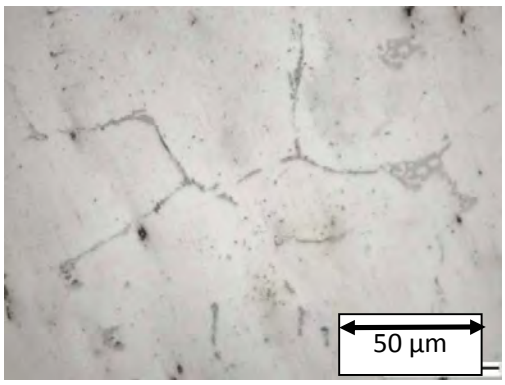

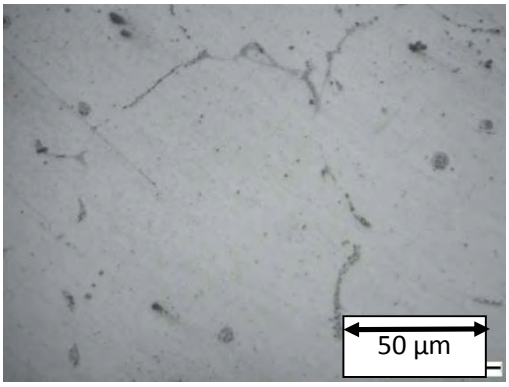

(a) (b)

Figure 4.34: Microstructure of Al-2% Cu-1%Mg (a) As Cast and (b) Homogenized.

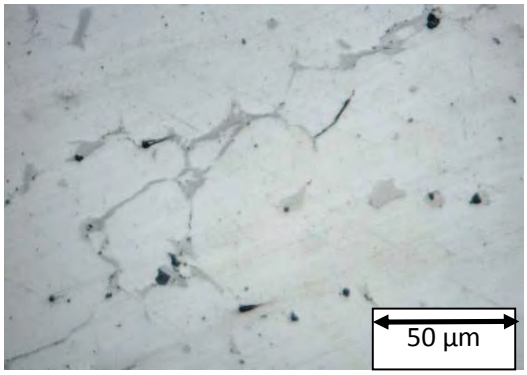

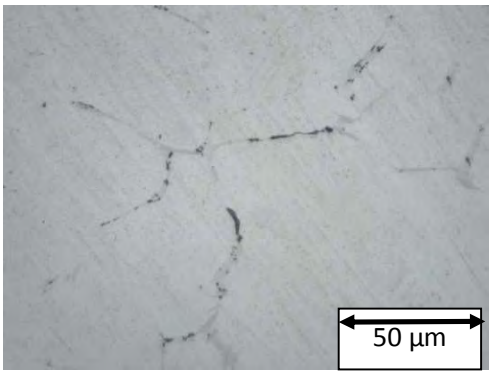

(a) (b)

Figure 4.35: Microstructure of Al-2% Cu-2%Mg (a) As Cast and (b) Homogenized.

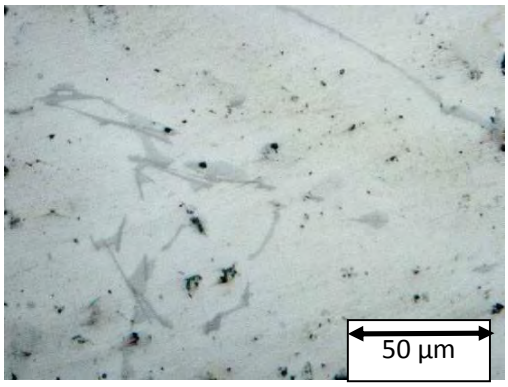

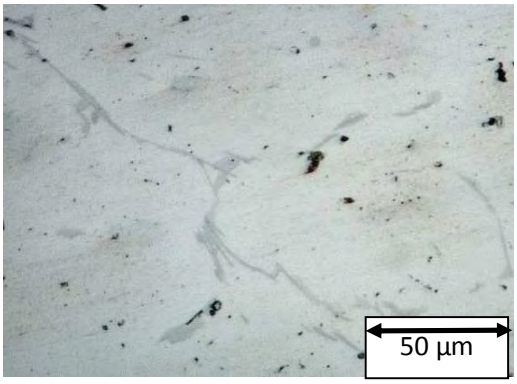

(a) (b)

Figure 4.36: Microstructure of Al-4% Cu-1%Mg (a) As Cast and (b) Homogenized.

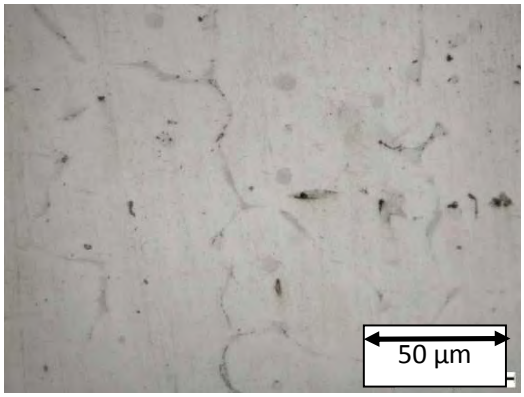

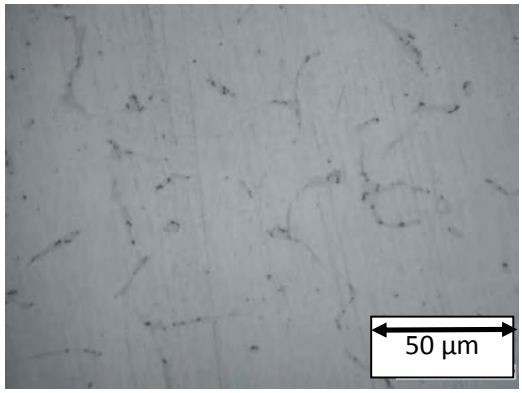

(a) (b)

Figure 4.37: Microstructure of Al-4% Cu-2%Mg (a) As Cast and (b) Homogenized.

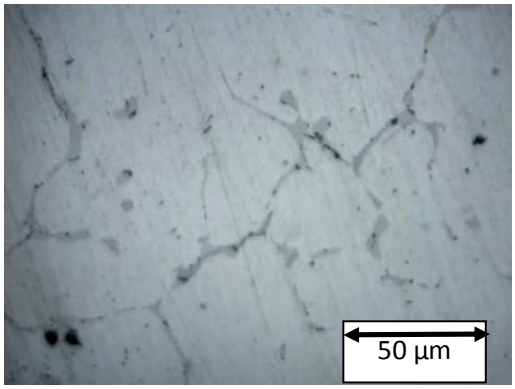

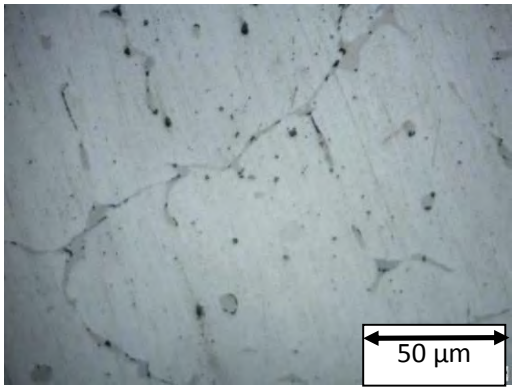

(a) (b)

Figure 4.38: Microstructure of Al-6% Cu-1%Mg (a) As Cast and (b) Homogenized.

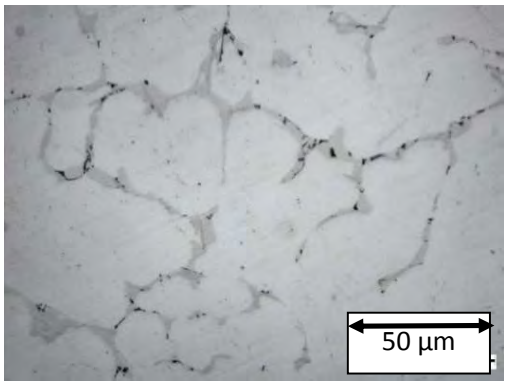

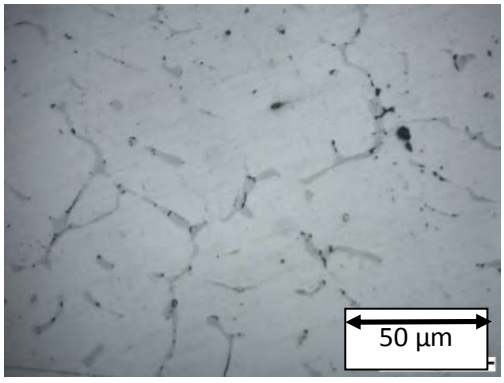

(a) (b)

Figure 4.39: Microstructure of Al-6% Cu-2%Mg (a) As Cast and (b) Homogenized.

4.4 Image Analysis

For conveniences in image analysis, the phases are denoted as ‘grey phases’ and ‘black phases’. It was shown earlier that grey phases were actually the phases containing aluminium and copper, and black phases are magnesium containing remaining phases. The phase fractions of magnesium containing phases were summed and shown as black phases in Table 4.11.

Table 4.11: Comparison of phase fractions of gray and black phases from image analysis and thermodynamic modelling.

Alloy	Image Analysis		Modelling Predictions	
	Gray Phases	Black Phases	Gray Phases	Black Phases
A0	-	40.67 ± 3.41		2.65
A1	5.98	1.10 ± 0.48	1.15	0.68
A2	4.10	0.97 ± 0.49	1.22	2.01
B0	5.10 ± 1.40	1.38 ± 0.35	3.95	0.46
B1	5.34 ± 2.12	0.54 ± 0.31	3.34	0.68
B2	6.01 ± 0.98	0.32 ± 0.58	4.38	0.77
C0	9.07 ± 0.98	0.93 ± 0.20	8.83	0.38
C1	5.53 ± 1.50	0.35 ± 0.17	7.63	0.1
C2	7.29 ± 1.33	0.45 ± 0.19	8.9	0.87

In alloy A0, accurate results were not obtained since the microstructure obtained was quite different.

Some errors are evident from the images. This is due to techniques of image analysis and acquired images. Most significant one is the pixels boundary errors in which pixels at the edge of a phase are not completely saturated with that phase. This results a decrease in gray value with increasing distance from the center of pixel.

In short, in an 8-bit image, contrast is obtained through different gray values ranging from 0 to 255. Since a phase is consisted of hundreds of pixels, pixels of same gray value is distinguishable and is visible as a different phase. However, near the edges/boundaries of a phase, the pixels may

not be completely filled with parent gray values. A slightly different gray value may be obtained. It is known that intensity of gray values is largest at the center pixel and it is reduced towards the boundary. Therefore, in segmentation, few errors may occur in selection. In medical imaging, such as cancer cell size determination, different algorithms are sometimes used to re-assign gray values of a certain area so that the intensity becomes similar. Such approach is beyond the scope of this current work.

4.5 Phases Observed

From CALPHAD modeling it was predicted that addition of copper and magnesium resulted formation of certain phases in aluminum matrix. Those phases remained on the matrix even after homogenization treatment at 400 °C. Figures 4.23-4.30 show the major phases present at that temperature. These phases were mainly Al_2Cu, Al_7Cu_2M and Mg_2Si. Presences of these phases in Al-Cu-Mg alloys were confirmed by EDX analysis. In order to perform EDX, alloy with maximum alloy content (C2) was selected, as it possessed maximum phase fractions and made easier to detect these phases from matrix. From SEM images (Figures 4.40-4.41) it was observed that, mainly two phases were present, one is the white phase and the other is black phase. Using spot EDX analysis it was possible to determine the atomic fractions of those phases. Several spots were analyzed and their average atomic fractions were measured. EDX results are shown in Table 4.12-4.13. From these tables it was assured that, the white phases are composed of aluminum and copper with 68.57 atomic % and 31.43 atomic% respectively i.e., this phase is none other than Al_2Cu. The black phase is composed of Al, Si, Cu and Mg with atom fraction of about 64.8%, 18.66%, 3.56% and 12.97% respectively. This indicates the presence of Al-Cu-Mg phase or Mg-Si phases. The spectrums of both phases are shown in Figures 4.42-4.43.

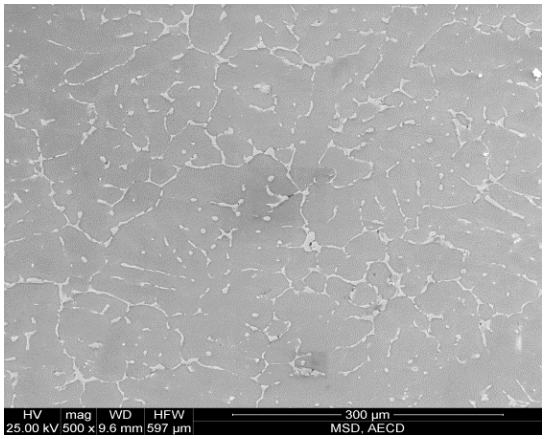

Figure 4.40: SEM image of alloy C2.

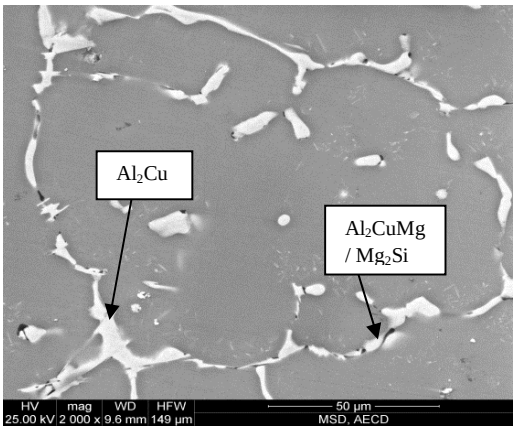

Figure 4.41: SEM image of alloy C2.

Table 4.12: Composition white phase.

Element	Wt %	At%
Al	48.09	68.57
Cu	51.91	31.43

Table 4.13: Composition black phase.

Element	Wt %	At%
Al	64.01	64.8
Si	20.57	18.66
Cu	3.05	3.56
Mg	12.37	12.97

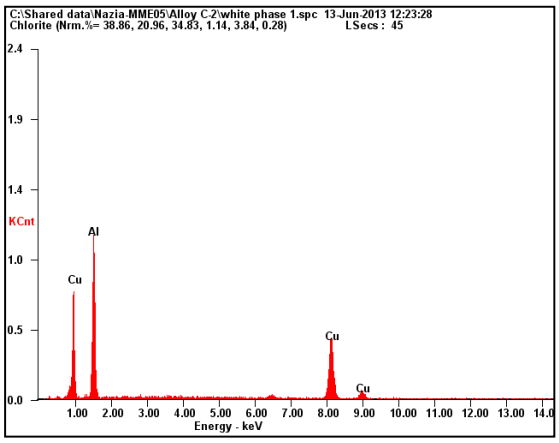

Figure 4.42: Spectrum of white phase.

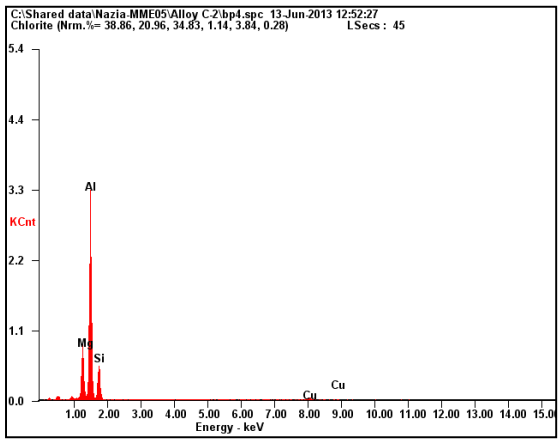

Figure 4.43: Spectrum of black phase.

4.6 Deformation of Homogenized Aluminum-Copper-Magnesium Alloys

After homogenizing the structure each alloy was deformed to 10%, 20% and 50% using UTM. It was found that with increasing the alloy content load required to attain as specified level of deformation continues to increase. This effect is shown in Table 4.13. From this table it is clear that with increasing alloy content load required to deform a significant amount increase due to an increase in certain phase fractions in microstructure.

In most crystalline materials, the dislocation density increases drastically during plastic deformation leading to work-hardening. This process may be described by an evolution law of the dislocation density containing a rate of dislocation generation minus an annihilation rate. The dependences of the dislocation density itself on the experimental parameters like strain, strain rate and temperature are well studied in many materials. Such an increase in dislocation density is the reason of requiring higher amount of load during deformation as shown in Table 4.13. It was found that for alloy A1, loads required to deform to 10%, 20% and 50% were 158.36 KN, 221.07 KN and 420.29 KN respectively. Similarly for alloy C2 loads required were 189.65 KN (10%), 276.70 KN (20%) and 435.35 KN (50%). Presence of strengthening element (Mg) also increases the required load for deformation. However this effect is significant only when we compare alloy without Mg and with Mg addition. For example, in order to deform 10% in alloy

C0 and alloy C1, there was a sharp increase in load requirement from 71.45 KN to 185.98 KN respectively. On the other hand, for alloy C1 and C2 increase in load with Mg addition is very low, 185.98 KN to 189.65 KN for 10% deformation.

Table 4.13: Loads required for deforming aluminum-copper-magnesium alloys.

Alloy	10%Deformation Load (KN)	20%Deformation Load (KN)	50%Deformation Load (KN)
Al-2%Cu	51.29	72.23	163.21
Al-2%Cu-1%Mg	158.36	221.07	420.29
Al-2%Cu-2%Mg	159.15	217.79	392.81
Al-4%Cu	78.78	88.99	214.91
Al-4%Cu-1%Mg	115.30	144.49	272.12
Al-4%Cu-2%Mg	166.74	240.31	424.88
Al-6%Cu	71.45	104.83	235.46
Al-6%Cu-1%Mg	185.98	245.54	442.29
Al-6%Cu-2%Mg	189.65	276.70	435.35

4.6.1 Effect of Deformation on Microstructure

Deformation has a surprising effect on microstructure. Figures 4.44-4.46 clearly show the effect of deformation on microstructure of alloy A1, B1 and C1. It was observed that for each alloy that the initial necklaces like phases were broken and form small segments instead of continuous network with the extent of deformation.

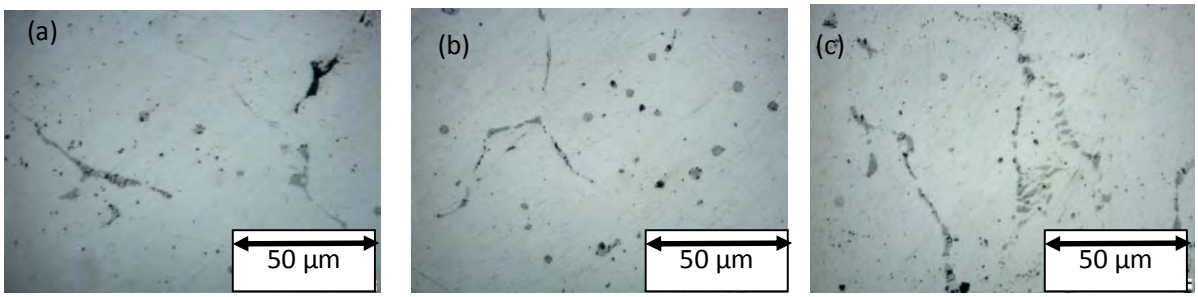

Figure 4.44: Microstructure of alloy A1 with deformation of (a) 10% (b) 20% (c) 50%.

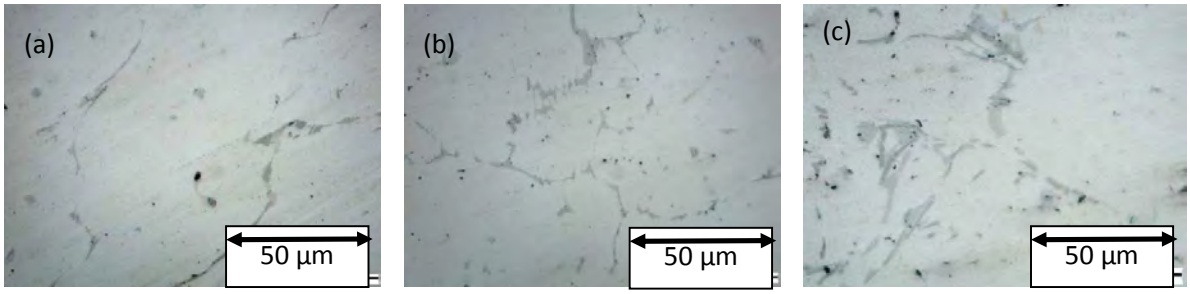

Figure 4.45: Microstructure of alloy B1 with deformation of (a) 10% (b) 20% (c) 50%.

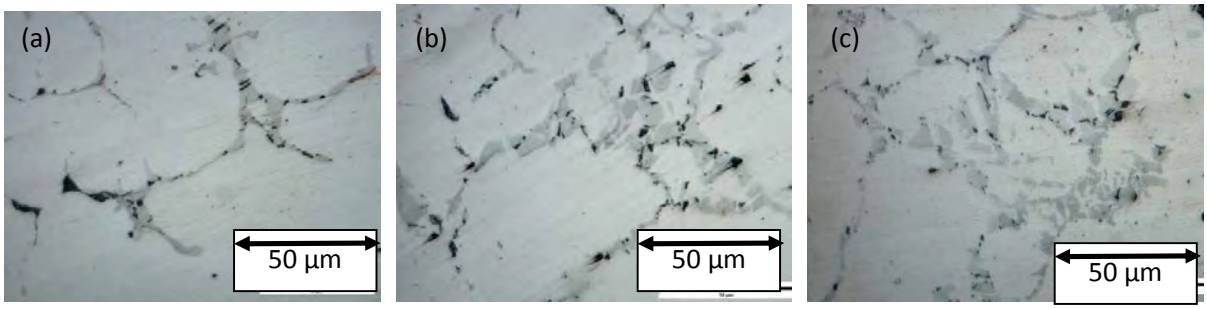

Figure 4.46: Microstructure of alloy C1 with deformation of (a) 10% (b) 20% (c) 50%.

4.7 Effect of Chemical Composition on Microstructure

This increase in magnesium content results formation of new phases in microstructure. Figure 4.47 reveals some black phases present on copper bearing phase in Al-6% Cu alloys with increasing magnesium content. These black phases are mainly magnesium containing phases as predicted from CALPHAD analysis. From Figures 4.13, 4.15 and 4.17, it was observed that with increasing %Mg, fractions of Al_2CuMg and Mg_2Si phases continues to increase.

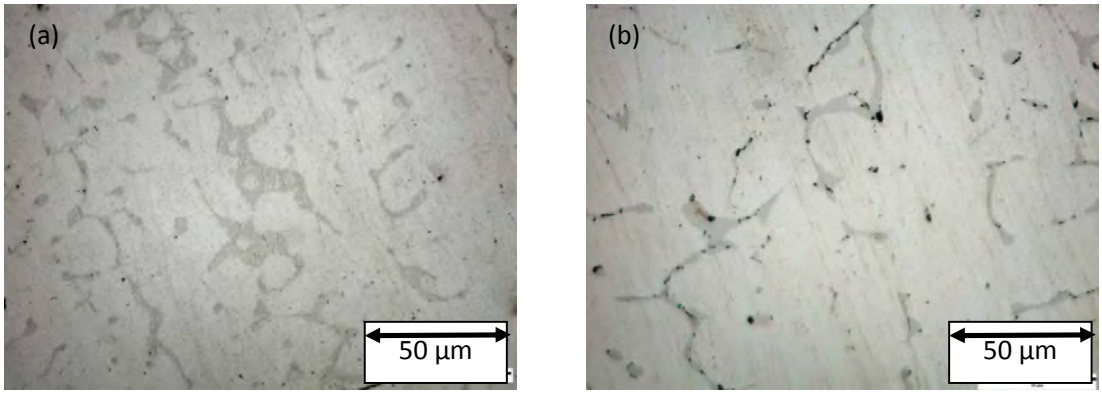

Figure 4.47: Microstructure of Al-6%Cu with (a) 0%Mg (b) 1%Mg (c) 2%Mg.

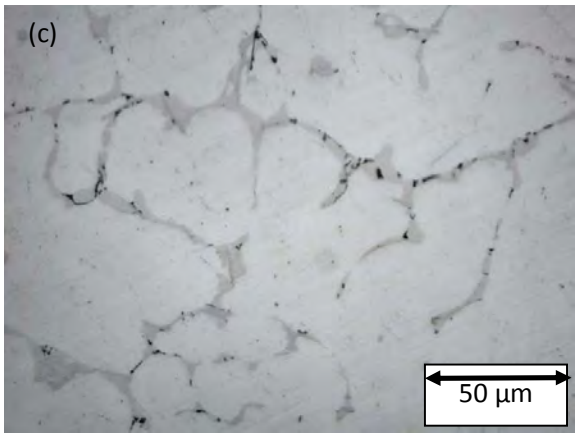

Figure 4.47: Microstructure of Al-6%Cu with (a) 0%Mg (b) 1%Mg (c) 2%Mg.

4.8 Effect of Solution Treatment

In order to understand what happen if these alloys are heated to a higher temperature, solution treatment was applied to the homogenized and deformed alloys with minimum and maximum composition at 500 ^{o}C for 30 minutes and then quenched in water.

This treatment affects both microstructure and mechanical properties.

4.8.1 Effect of Solution Treatment on Microstructure

Since the alloys were held at 500 ^{o}C for 30 minutes, within that time some Al-Cu-Mg phases got dissolved into the aluminum matrix and results a decrease in phases in the microstructure compared to that without any solution treatment, as shown in Figure 4.48. These micrographs reveal that the total % of phases in (a) is no longer visible in (b) of C2 alloy. From Figure 4.17, it was predicted that at 500 °C, fraction of major phase Al_2Cu decreases approximately half of that at 400 °C.

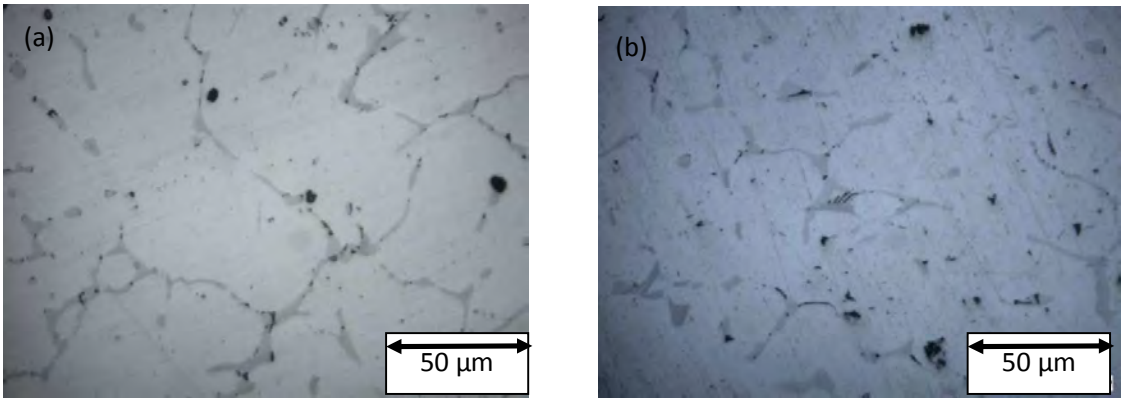

Figure 4.48: Microstructure of C2 alloy (a) homogenized and (b) solution treated.

Such a decrease in phase can also be explained with the help of CALPHAD analysis. It was found that, with increase in temperature the low melting point phases Al_2CuMg and Mg_2Si get dissolved in aluminum (Figure 4.17). This is the reason of microstructural changes after solution treatment. This type of behavior is also observed for alloys after deformation. Figure 4.49 shows that phases present in homogenized and 50% deformed C2 alloy were dissolved in matrix after solution treatment at 500 °C.

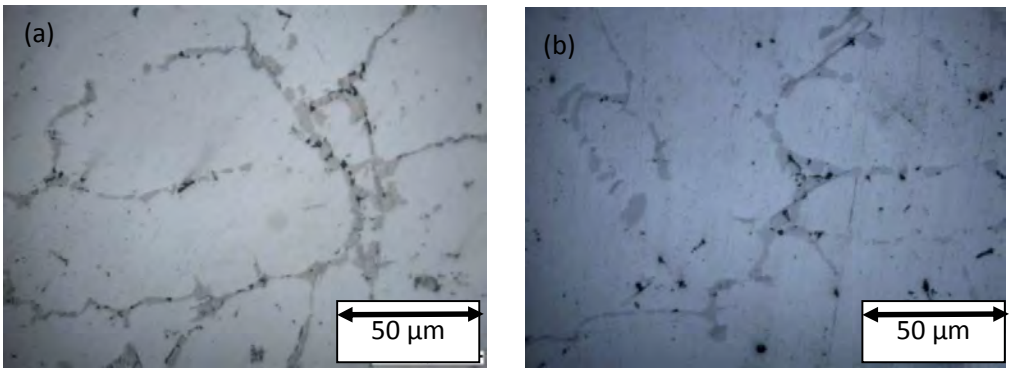

Figure 4.49: Microstructure of C2 alloy (a) homogenized and 50% deformed
(b) homogenized, 50% deformed and solution treated.

However, a little different effect was observer for alloy A0. There was a drastic change in microstructure after solution treatment. Figures 4.50-4.51 illustrate this effect. In Figure 4.50, before solution treatment microstructure contained large fraction of black colored phases which were completely disappeared after solution treatment. This effect can be explained with the help of CALPHAD analysis. From Figure 4.1, it was predicted that at 400 °C, stable phases are

Al_9M_2, Al_7Cu_2M and Al_7Cu_4Ni. After solution treatment, the nickel containing phase Al_7Cu_4Ni was completely absent. Thus those black colored phases are due to mainly of Al_7Cu_4Ni phase.

Experimentally some of the stoichiometric phases were found to have some solubility for other elements. When a stoichiometric phase showed a range of composition experimentally, this could be expected to affect phase stability. A phase like Al_7Cu_4Ni can accommodate different amounts of nickel or copper because these two elements have atomic similarity. For example, if more copper is substituted, it will tend to reduce the stability of other copper containing phases such as Al_2Cu.

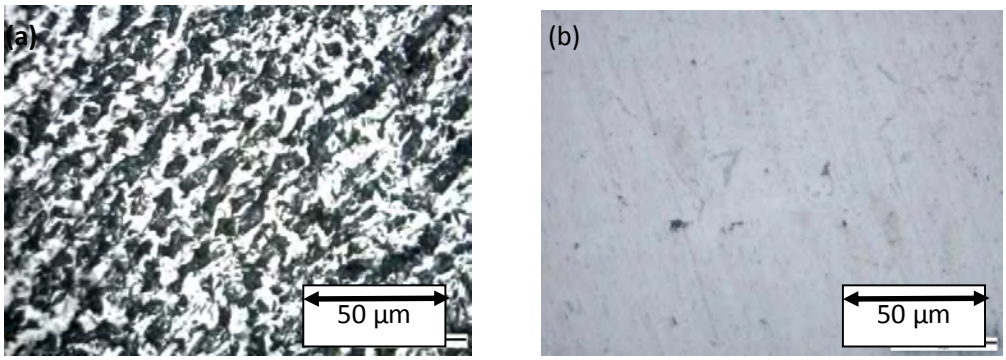

Figure 4.50: Microstructure of A0 alloy (a) homogenized and (b) solution treated.

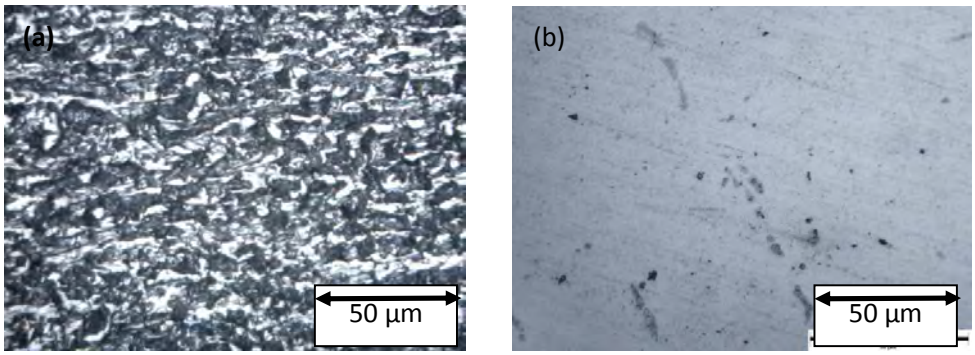

Figure 4.51: Microstructure of A0 alloy (a) homogenized and 50% deformed
(b) homogenized, 50% deformed and solution treated.

Similar effect was observed for deformed A0 alloys. Figure 4.49 shows that phases present in homogenized and 50% deformed A0 alloy were completely dissolved in matrix after solution treatment at 500°C. The effect of deformation was also revealed from Figure 4.51 (b) by broken phases on aluminum matrix.

4.9 Hardness of the Alloys Investigated

Any change in microstructure also causes a change in mechanical properties. In this present study, effects of chemical composition, homogenization, deformation and solution treatment were observed by measuring the hardness of all alloys. Following sections will explain how these factors affect hardness.

4.9.1 Effect of Chemical Composition on Hardness

Aluminum-copper alloys containing 2 to 10% Cu, generally with other additions, form important families of alloys. Both cast and wrought aluminum-copper alloys respond to solution heat treatment and subsequent aging with an increase in strength and hardness and a decrease in elongation. The strengthening is maximum between 4 and 6% Cu, depending upon the influence of other constituents present.

The main benefit of adding magnesium to aluminum-copper alloys is the increased strength possible following solution heat treatment and quenching. In wrought material of certain alloys of this type, an increase in strength accompanied by high ductility occurs on aging at room temperature. On artificial aging, a further increase in strength, especially in yield strength can be obtained, but at a substantial sacrifice in tensile elongation.

From previous research [8] it was found that addition of copper and magnesium in aluminum increases hardness and strength of aluminum as described in Chapter 2. Such effect was also observed in the present study. An increase in copper and magnesium tends to raise the hardness of homogenized aluminum alloys as shown in Figures 4.52 and 4.53.

Figure 4.52 shows an increase in hardness with increasing %Cu, there is an increase in Cu bearing phase Al_2Cu (obtained from CALPHAD analysis) in the microstructure as shown in figure 4.54.

On the other hand, as magnesium content increases magnesium containing phases continues to increase (from CALPHAD analysis) and results a change in microstructure and hardness as shown in Figures 4.13, 4.15 and 4.17.

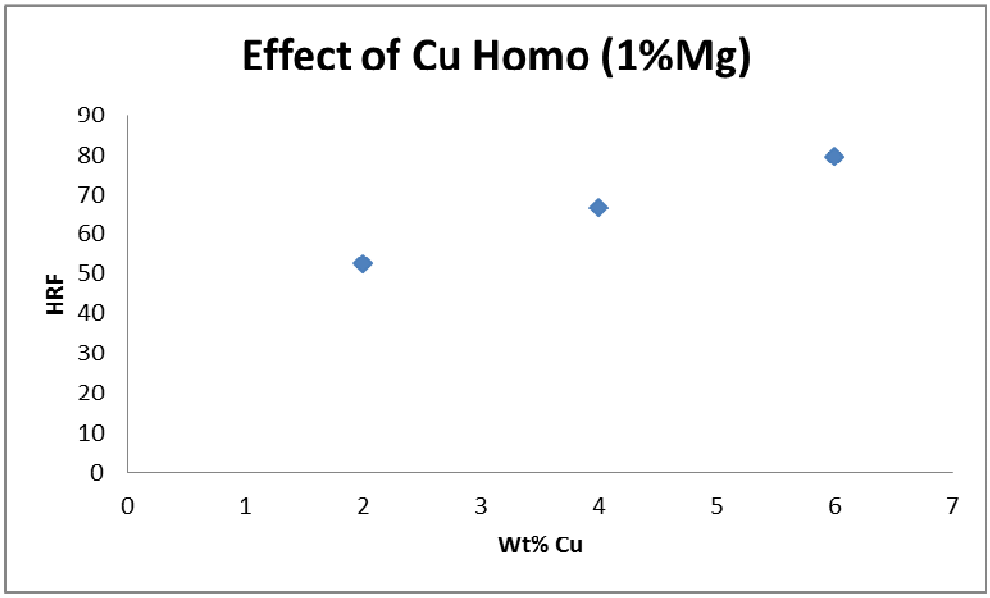

Figure 4.52: Variation of hardness with copper content in homogenized Al-Cu-1%Mg alloy.

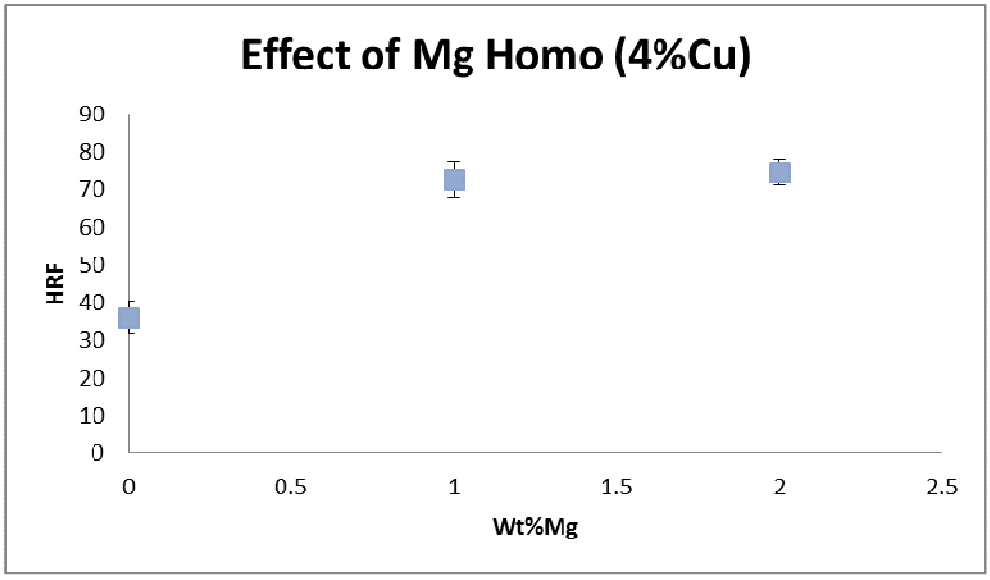

Figure 4.53: Variation of hardness with magnesium content in homogenized Al-4%Cu-Mg alloy.

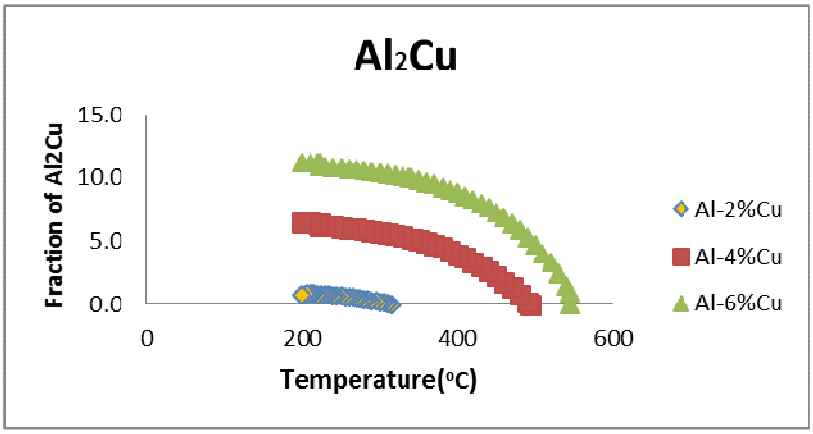

Figure 4.54: Fraction of Al_2Cu in aluminum copper alloy with varying copper content.

4.9.2 Effects of Homogenization Treatment on Hardness

After homogenization treatment hardness tends to reduce from as cast condition. This is again due the same reason that homogenization results some low melting point phases to dissolve into the matrix as described in Section 4.3.1.1. Effect of heat treatment on hardness is shown in Figures 4.55 and 4.56. From these figures it was evident that for both cases, i.e. with increasing copper and magnesium content, hardness of homogenized condition is less than that of as cast condition as a result of dissolution of strengthening phases (Al_2Cu, Al_7Cu_2M, Mg_2Si and Al_2CuMg) as shown in Figures 4.54 and 4.57.

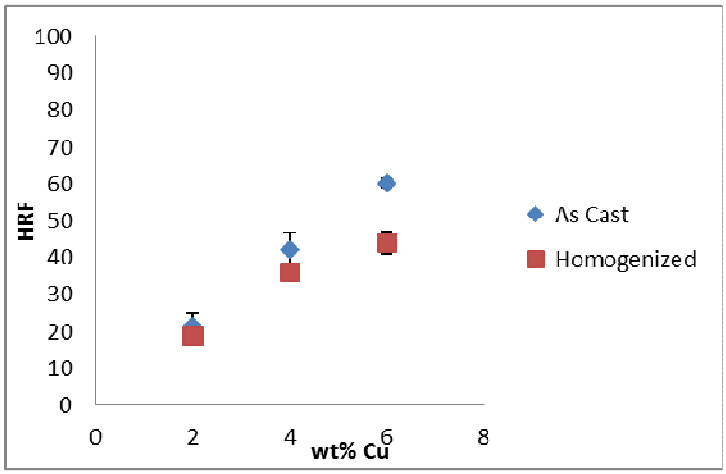

Figure 4.55: Effect of heat treatment on hardness of Al-Cu alloy with 0%Mg.

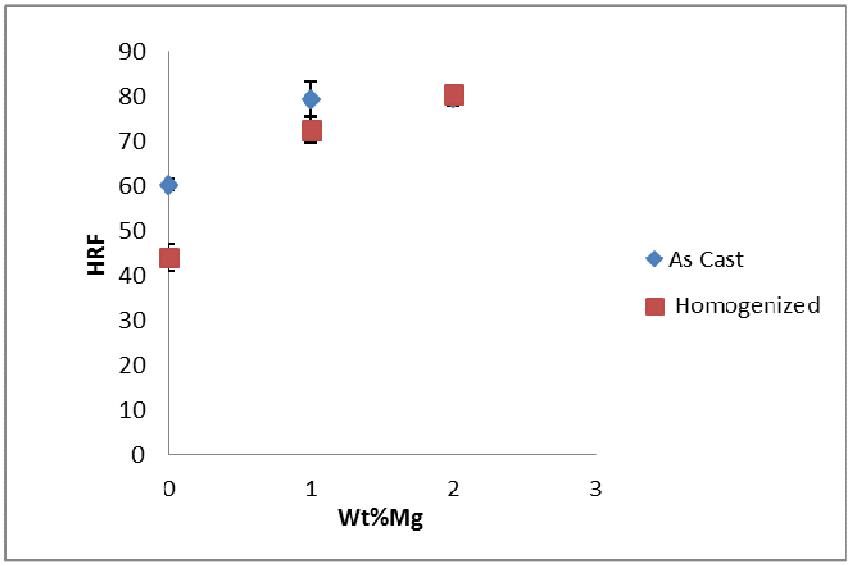

Figure 4.56: Effect of heat treatment on hardness of Al-Mg alloy with 6%Cu.

Such a decrease in hardness after homogenization can be explained by CALPHAD analysis as shown in Figure 4.57, where variation of phase fractions with temperature was predicted. For each alloy (C0, C1 and C2), there was a decrease in phase fraction at 400 °C which causes lowering of hardness values.

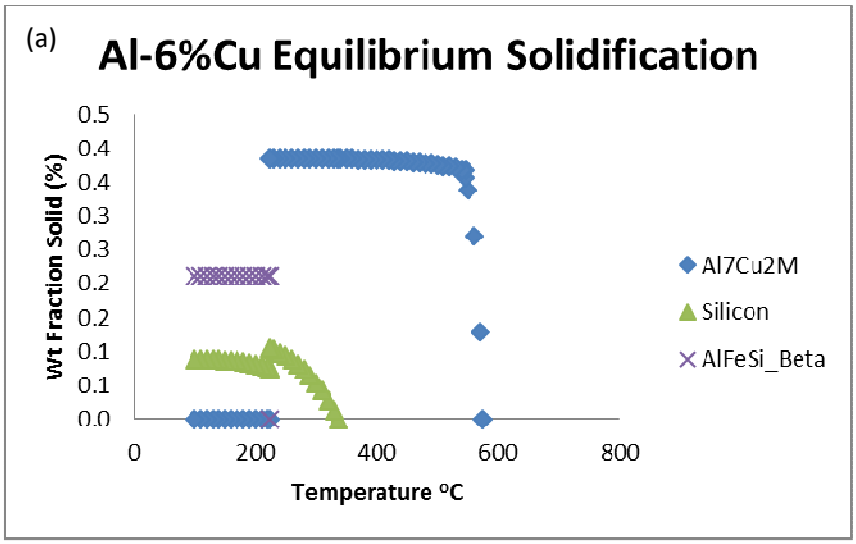

Figure 4.57: Formation of Mg containing phases with increasing Mg content in (a) Al-6%Cu (b) Al-6%Cu-1%Mg (c) Al-6%Cu-2%Mg.

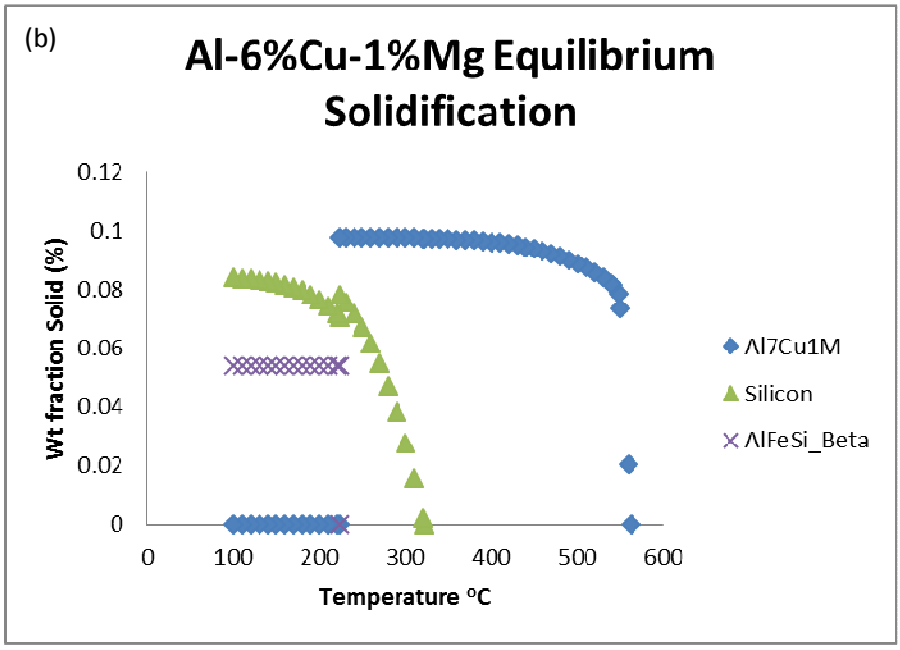

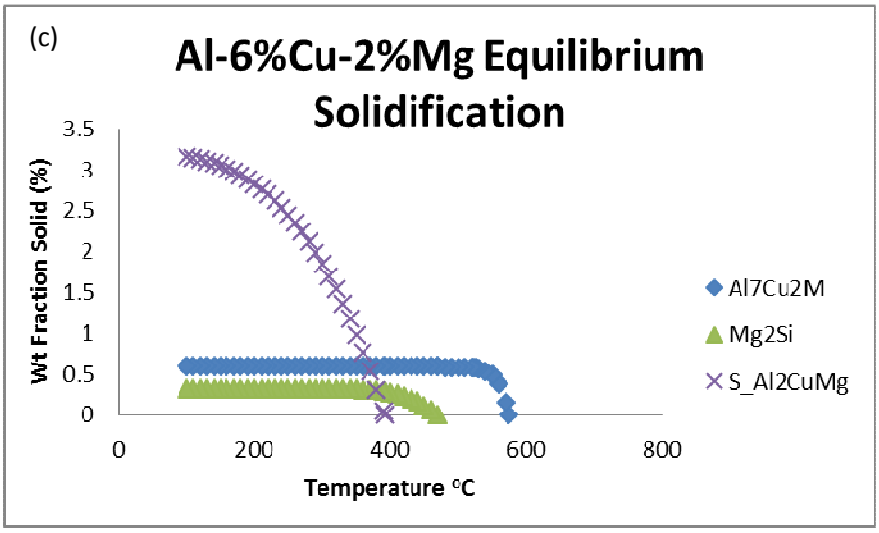

Figure 4.57: Formation of Mg containing phases with increasing Mg content in (a) Al-6%Cu (b) Al-6%Cu-1%Mg (c) Al-6%Cu-2%Mg.

4.9.3 Effect of Deformation on Hardness

Deformation increases the number of dislocations by interactions of dislocation during deformation and other defects, which cause an enhancement of hardness values. This increase in hardness is due to the increase of stored energy in the microstructure due to increase of

dislocation density. High dislocation density results in a large number of dislocation interactions which results in high strength and hardness [59-63]. Figures 4.58-4.63 clearly show the effects of deformation on hardness of aluminum-copper-magnesium alloys. It is to be noted that since the alloys were only cold deformed, any change of phase fractions should not occur (Figure 4.40-4.42). Therefore, the effect of deformation in this study is purely due to changes in dislocation structure.

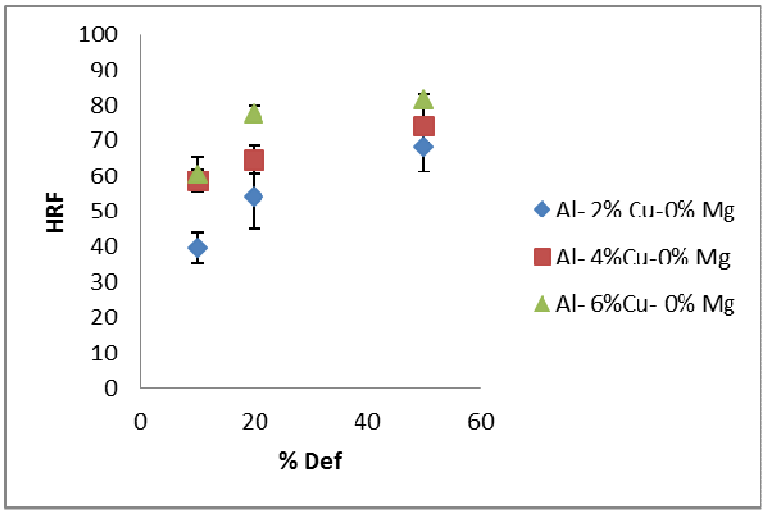

Figure 4.58: Effect of deformation on hardness of Al-Cu-0%Mg alloys.

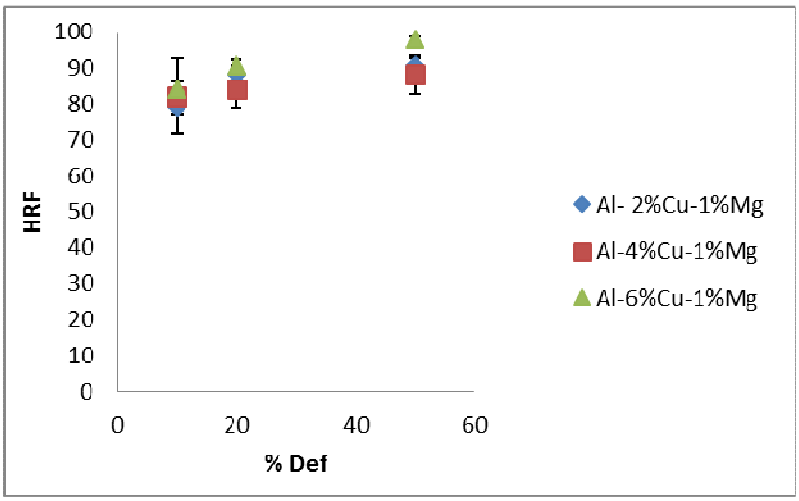

Figure 4.59: Effect of deformation on hardness of Al-Cu-1%Mg alloys.

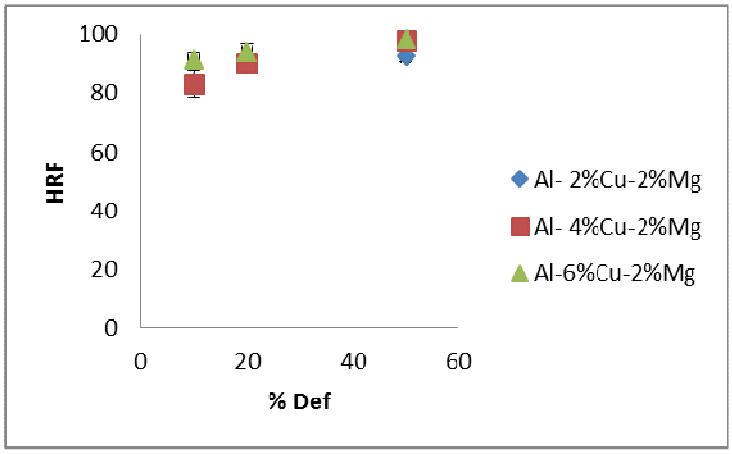

Figure 4.60: Effect of deformation on hardness of Al-Cu-2%Mg alloys.

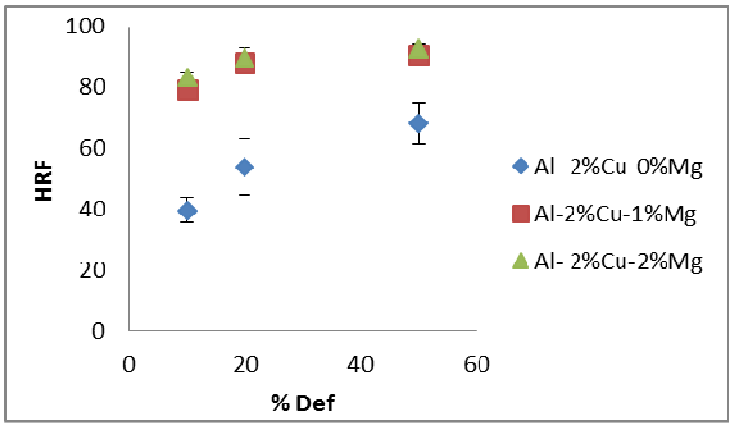

Figure 4.61: Effect of deformation on hardness of Al-2%Cu-Mg alloys.

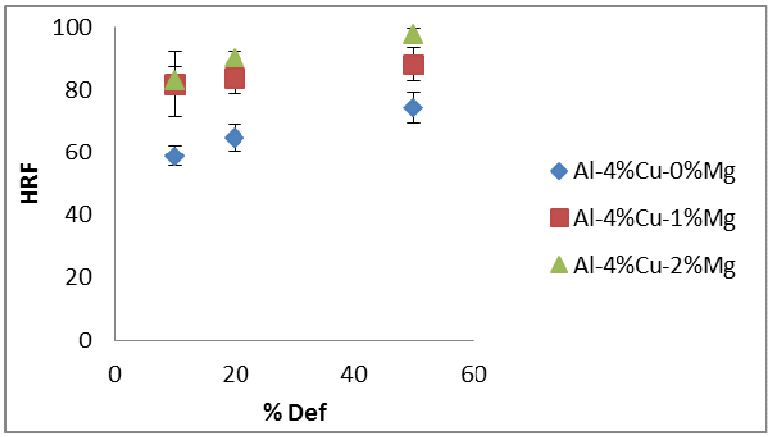

Figure 4.62: Effect of deformation on hardness of Al-4%Cu-Mg alloys.

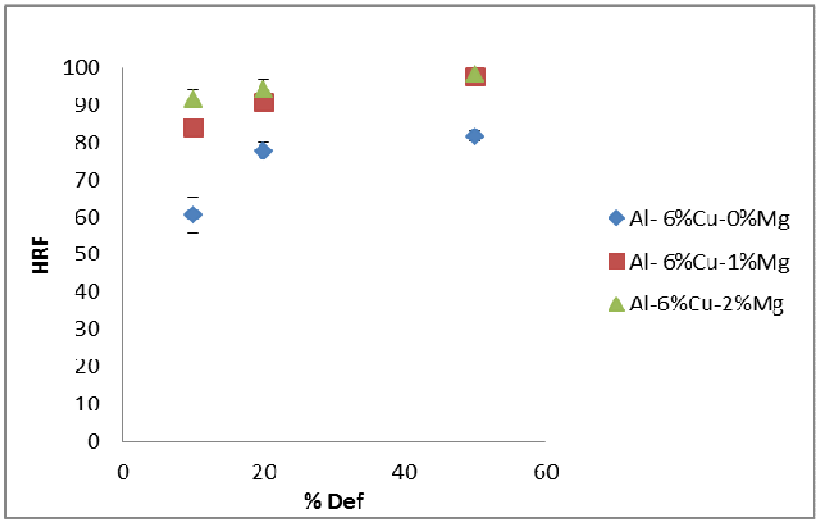

Figure 4.63: Effect of deformation on hardness of Al-6%Cu-Mg alloys.

4.9.4 Effect of Solution Treatment on Hardness

Solution treatment also decreases the hardness of aluminum alloys due to a change in microstructure as described in Section 4.6.1. Figure 4.26 reveled that at 400 °C fraction of Al_2Cu phase was 8.89% which got dissolved in aluminum matrix at 500 °C to 3.88%. Such a decrease in major copper containing phase results a reduction in hardness after solution treatment. Similarly 0.28 % of Mg_2Si, at 400 °C, completely dissolved at 500 °C. For alloy A0, copper containing phase Al_7Cu_2M, reduced from 1.44% (at 400°C) to 0.77% (at 500 °C), as predicted from CALPHAD analysis (Figure 4.10). The effect solution treatment on hardness is shown in Figures 4.64 and 4.65.

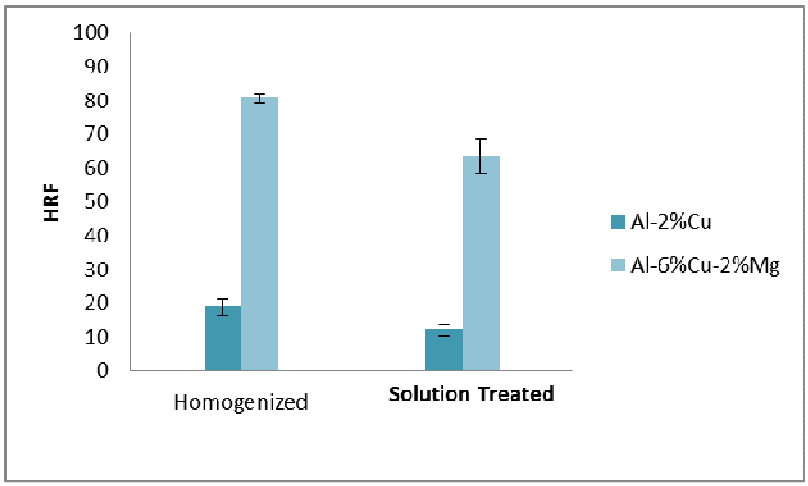

Figure 4.64: Effect of solution treatment on hardness.

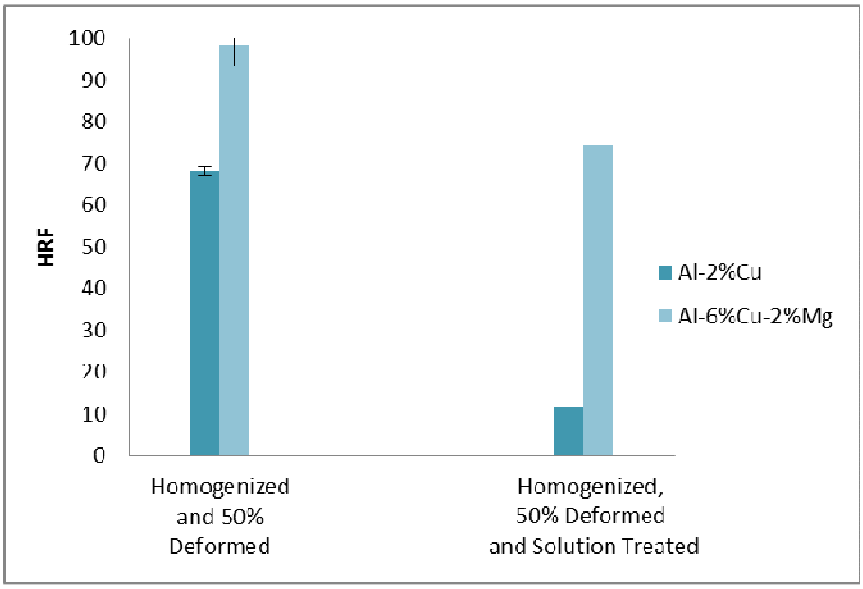

Figure 4.65: Effect of solution treatment on hardness.

4.10 Processing Parameters that Dominates Hardness in Aluminum Copper Magnesium Alloys

In the present work, effects of chemical composition, heat treatment and extent of deformation on microstructure and hardness were studied. All of these parameters individually and in combine form influenced microstructure, or in other sense, hardness, since any change in microstructure is reflected by its mechanical properties such as hardness. In order to understand the dominating parameter in changing hardness, statistical analysis method, ANOVA (Analysis of Variance Modeling) was performed. The reason for doing an ANOVA is to see if there is any difference between groups on some variables [64]. ANOVA is a particular form of statistical hypothesis testing heavily used in the analysis of experimental data. A statistical hypothesis test is a method of making decision using data. A test result (calculated from the null hypothesis and the sample) is called statistically significant if it is deemed unlikely to have occurred by chance, assuming the truth of the null hypothesis. A statistically significant result (when a probability (p-value) is less than a threshold (significance level)) justifies the rejection of the null hypothesis [65].

The current study consists of four variables: copper content, magnesium content, heat treatment condition and extent of deformation. Since it is a very complex process to use four variables at a

time, three of them were considered to form “Pareto Chart”. In one type of chart, copper content (A), magnesium content (B) and heat treatment condition (C) was considered as three variables and in other type, copper content (A), magnesium content (B) and extent of deformation (C) were taken. Two types of responses were considered at a time. That means, A can be 2% and 4% Cu, or 4% and 6% Cu. In the similar way, B can be 1% and 2%Mg or 0% and 1%Mg or 0% and 2%Mg. C can be 10% and 50% deformation. Figures 4.66-4.83 shows Pareto Charts consisting of three variables.

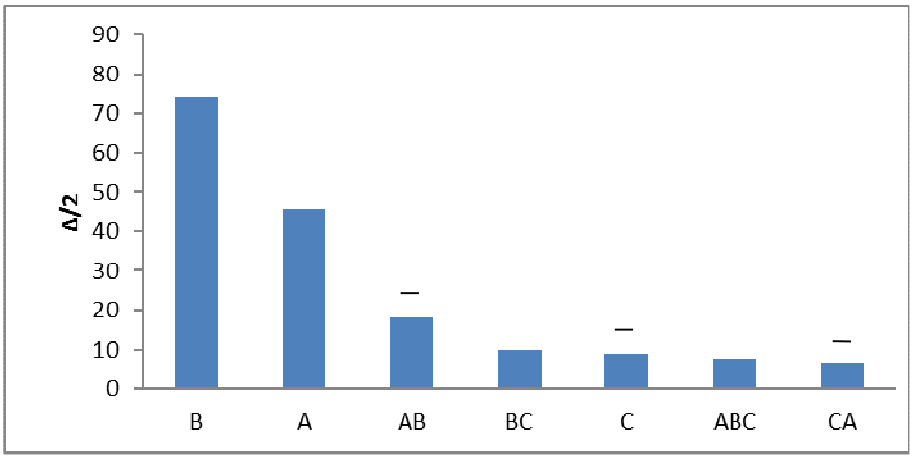

Figure 4.66: Pareto Chart of variables A=Cu (6, 2), B= Mg (2, 0), C= Homo/As Cast (Bar denotes negative effect).

From Figure 4.66, it can be observed that effect of magnesium was more significant compared to copper. However, the combined effect of copper and magnesium was negative, which mean in combined form those elements lowered hardness. Homogenization had a lower and negative effect on hardness. Effect of copper, magnesium and homogenization treatment in combination was positive but less significant on hardness. If the magnesium content is increased from 0% to 2%, a positive increase in half-effects reveals it’s most significant impact on hardness for the alloys considered. Increase of copper content from 2% to 6% also has a positive effect on hardness; however, this is not as significant as that for magnesium.

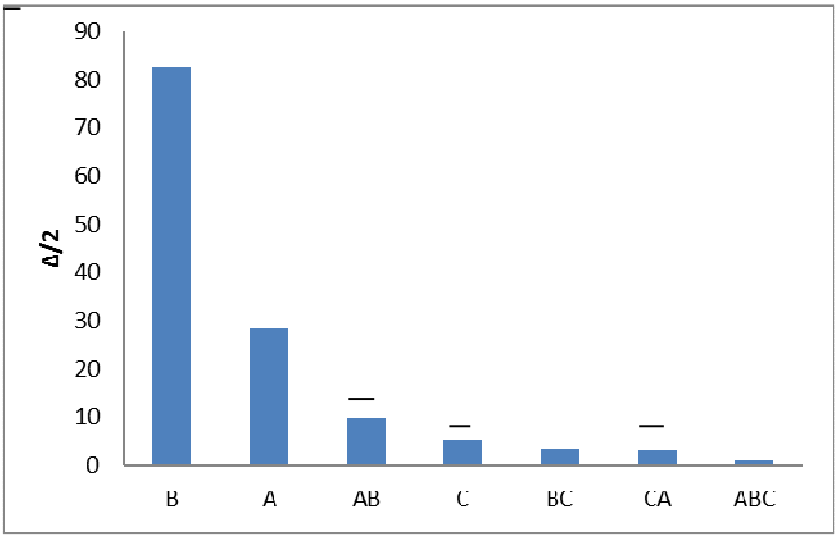

Figure 4.67: Pareto Chart of variables A=Cu (4, 2), B= Mg (2, 0), C= Homo/As Cast (Bar denotes negative effect).

Figure 4.67 revealed that effect of magnesium was highly significant compared to copper. However, the combined effect of copper and magnesium was negative, which means; in combined form those elements lowered hardness. Homogenization had a lower and negative effect on hardness. Effects of copper, magnesium and homogenization treatment in combination was positive but negligible on hardness. If the magnesium content is increased from 0% to 2%, a positive increase in half-effects reveals it's most significant impact on hardness for the alloys considered. Increase of copper content from 4% to 6% also has a positive effect on hardness; however, this is not as significant as that for magnesium.

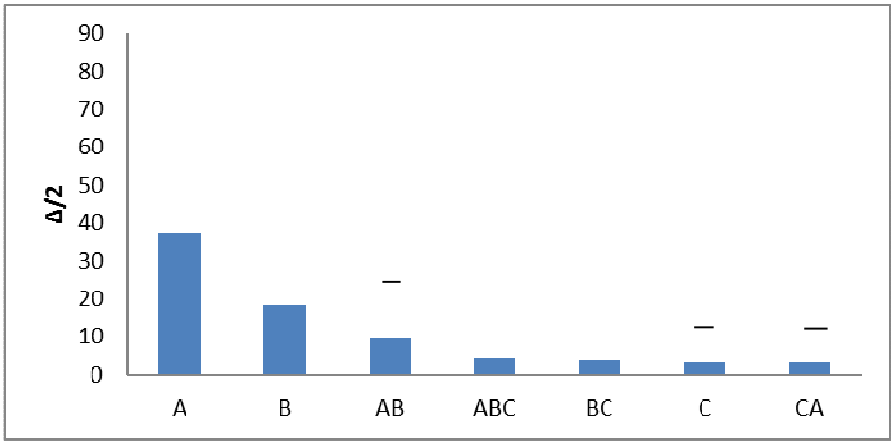

Figure 4.68: Pareto Chart of variables A=Cu (6, 2), B= Mg (2, 1), C= Homo/As Cast (Bar denotes negative effect).

From Figure 4.68, it can be observed that effect of copper was more significant compared to magnesium. However, the combined effect of copper and magnesium was negative, which means; in combined form those elements lowered hardness. Homogenization had a lower and negative effect on hardness. Effect of copper, magnesium and homogenization treatment in combination was positive but less significant on hardness. If the copper content is increased from 2% to 6%, a positive increase in half-effects reveals it's most significant impact on hardness for the alloys considered. On the other hand, increase of magnesium content from 1% to 2% has a positive but not a notable effect on hardness.

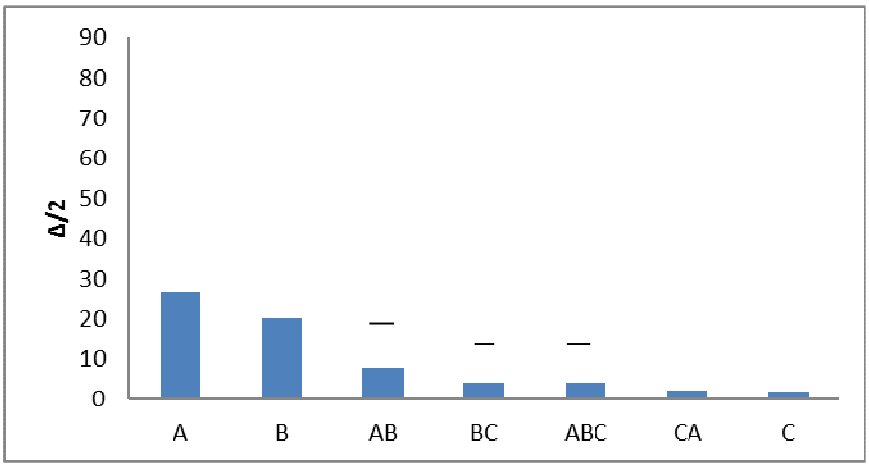

Figure 4.69: Pareto Chart of variables A=Cu (4, 2), B= Mg (2, 1), C= Homo/As Cast (Bar denotes negative effect).

From Figure 4.69, it can be observed that effect of copper was more significant compared to magnesium. However, the combined effect of copper and magnesium was negative, which means; in combined form those elements lowered hardness. Homogenization had a lower but positive effect on hardness. Effect of copper, magnesium and homogenization treatment in combination was negative and less significant on hardness. With increasing copper content from 2% to 4%, a positive increase in half-effects reveals it's most significant impact on hardness for the alloys considered. On the other hand, increase of magnesium content from 1% to 2% has a positive but its effect is not as significant as that for copper on hardness.

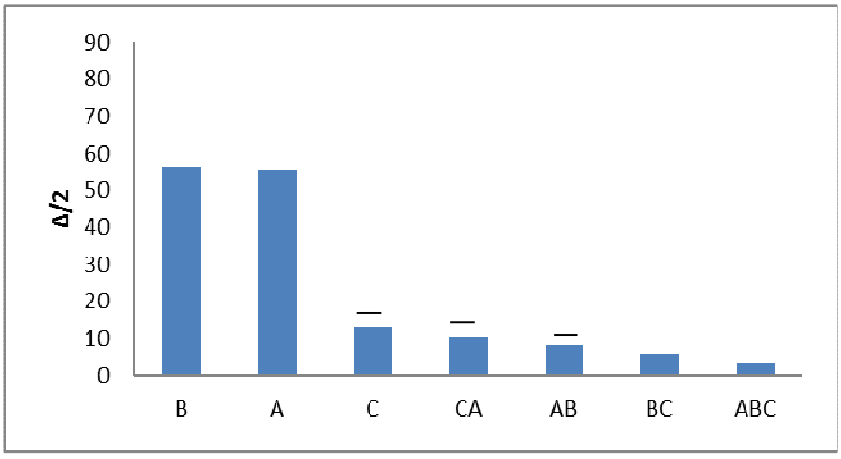

Figure 4.70: Pareto Chart of variables A=Cu (6, 2), B= Mg (1, 0), C= Homo/As Cast (Bar denotes negative effect).

From Figure 4.70, it can be observed that effects of magnesium and copper were very close on hardness. However, the combined effect of copper and magnesium was negative, which means; in combined form those elements lowered hardness. Homogenization had a lower and negative effect on hardness. Effect of copper, magnesium and homogenization treatment in combination was positive but less significant on hardness.

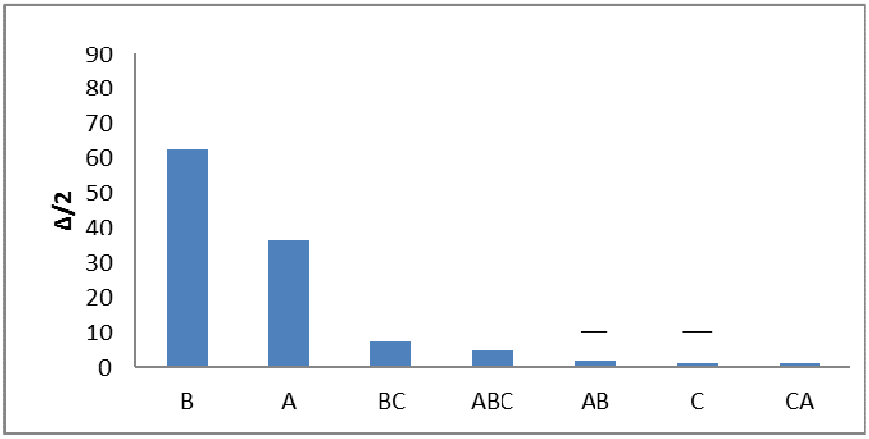

Figure 4.71: Pareto Chart of variables A=Cu (4, 2), B= Mg (1, 0), C= Homo/As Cast (Bar denotes negative effect).

From Figure 4.71, it can be observed that effect of magnesium was more significant compared to copper. However, the combined effect of copper and magnesium was negative, which means; in combined form those elements lowered hardness. Homogenization had a lower and negative

effect on hardness. Effect of copper, magnesium and homogenization treatment in combination was positive but less significant on hardness. If the magnesium content is increased from 0% to 1%, a positive increase in half-effects reveals it's most significant impact on hardness for the alloys considered. Increase of copper content from 2% to 4% also has a positive effect on hardness; however, this is not as significant as that for magnesium.

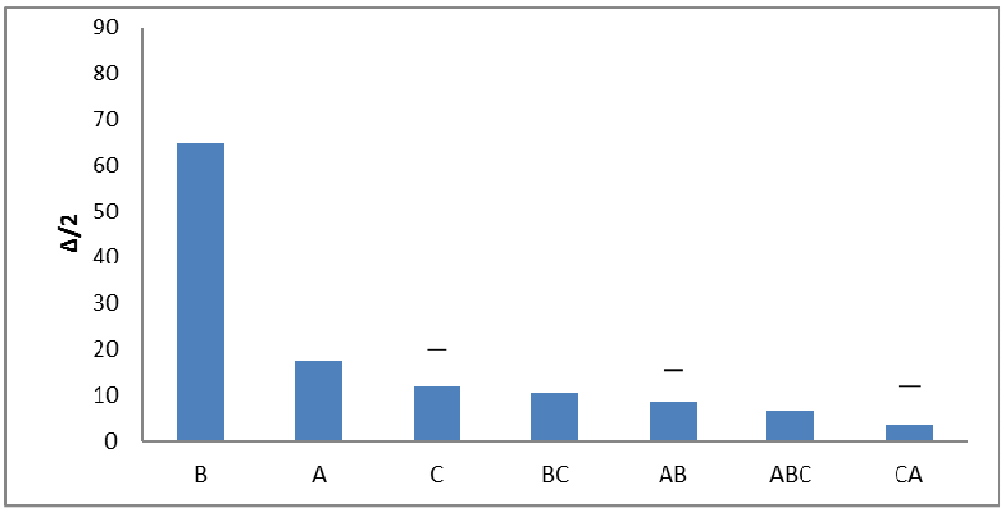

Figure 4.72: Pareto Chart of variables A=Cu (6, 4), B= Mg (2, 0), C= Homo/As Cast (Bar denotes negative effect).

From Figure 4.72, it can be observed that effect of magnesium was much more significant compared to copper. However, the combined effect of copper and magnesium was negative, which means; in combined form those elements lowered hardness. Homogenization had a lower and negative effect on hardness. Effect of copper, magnesium and homogenization treatment in combination was positive but less significant on hardness. If the magnesium content is increased from 0% to 2%, a positive increase in half-effects reveals it's most significant impact on hardness for the alloys considered. Increase of copper content from 4% to 6% also has a positive effect on hardness; however, this is not as significant as that for magnesium.

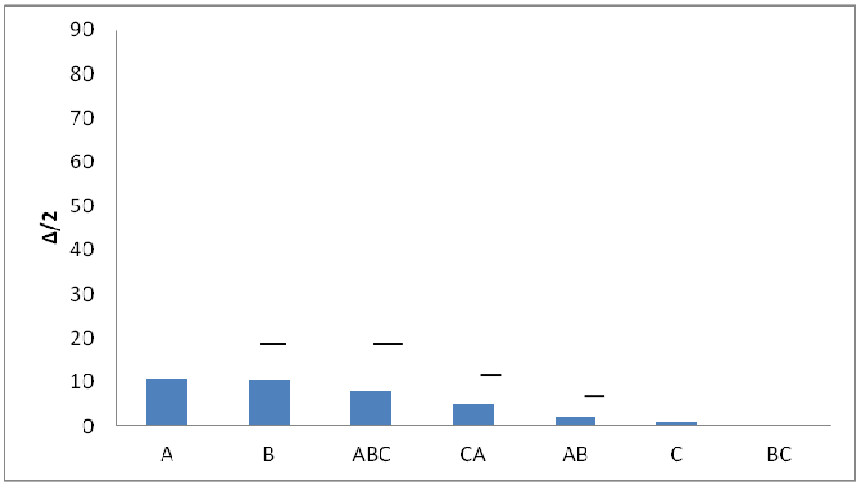

Figure 4.73: Pareto Chart of variables A=Cu (6, 4), B= Mg (2, 1), C= Homo/As Cast (Bar denotes negative effect).

From Figure 4.73, it can be observed that effects of magnesium and copper were very close on hardness. However, the combined effect of copper and magnesium was negative and less significant, which means; in combined form those elements lowered hardness. Homogenization had a lower and negative effect on hardness. However, effect of copper, magnesium and homogenization treatment in combination was highly significant on hardness.

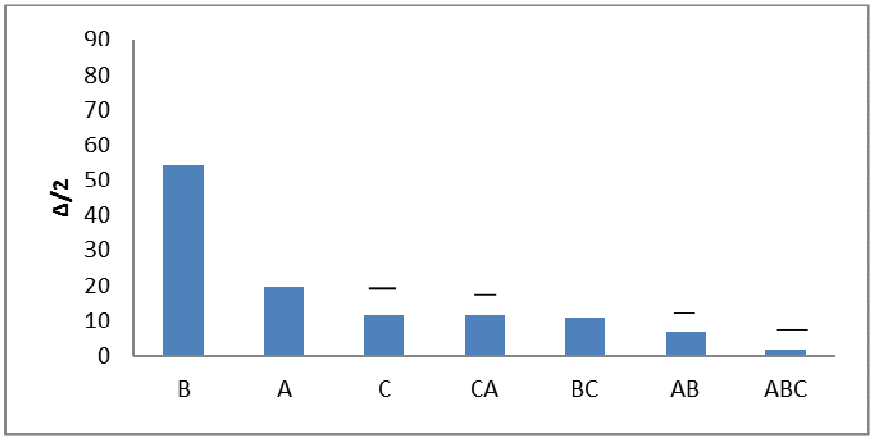

Figure 4.74: Pareto Chart of variables A=Cu (6, 4), B= Mg (1, 0), C= Homo/As Cast (Bar denotes negative effect).

From Figure 4.74, it can be observed that effect of magnesium was much more significant compared to copper. However, the combined effect of copper and magnesium was negative, which means; in combined form those elements lowered hardness. Homogenization had a lower

and negative effect on hardness. Effect of copper, magnesium and homogenization treatment in combination was negative and negligible on hardness. If the magnesium content is increased from 0% to 1%, a positive increase in half-effects reveals it's most significant impact on hardness for the alloys considered. Increase of copper content from 4% to 6% also has a positive effect on hardness; however, this is not as significant as that for magnesium.

In summary, from these (Figures 4.66-4.74) Pareto Charts, it is clear that magnesium has a large impact on hardness of Al-Cu-Mg alloys. This effect dominates when we compare between alloys containing no magnesium and with magnesium. But for alloys both containing magnesium about 1% and 2%, the addition of copper dominates rather than magnesium. However, when combined responses from variables are considered, the effect is not very significant. Also, homogenization tends to soften the material as predicted from phase analyses.

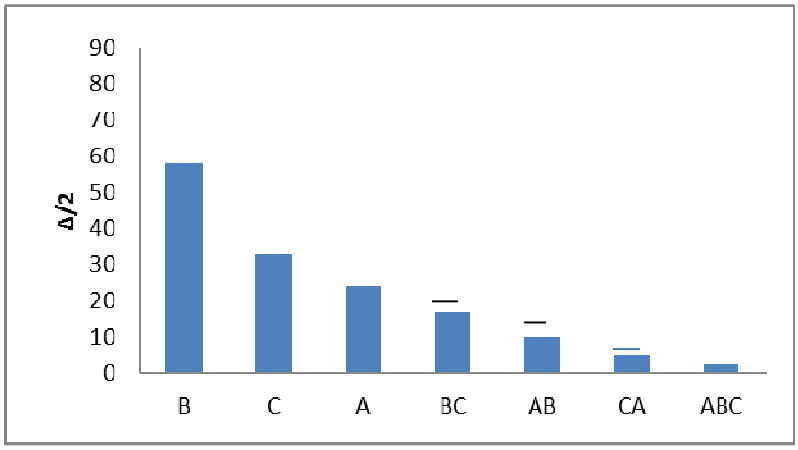

Figure 4.75: Pareto Chart of variables A=Cu (6, 2), B= Mg (2, 0), C= Deformation (50%/10%) (Bar denotes negative effect).

From Figure 4.75, it can be observed that effect of magnesium was much more significant compared to copper and deformation. However, the combined effect of copper and magnesium was negative, which means; in combined form those elements lowered hardness. Deformation had a positive and significant effect on hardness. Effect of copper, magnesium and deformation in combination was positive but less significant on hardness. When the magnesium content is increased from 0% to 2%, a positive increase in half-effects reveals it's most significant impact on hardness for the alloys considered. Increase of copper content from 2% to 6% also has a positive effect on hardness; however, this is not as significant as that for magnesium.

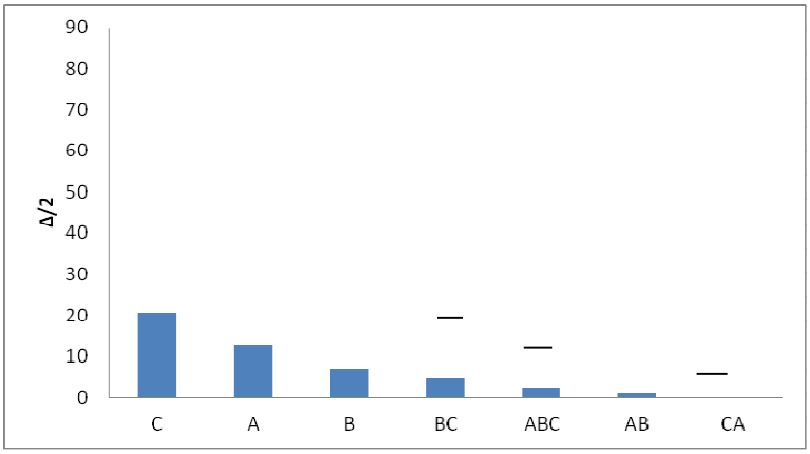

Figure 4.76: Pareto Chart of variables A=Cu (6, 2), B= Mg (2, 1), C= Deformation (50%/10%) (Bar denotes negative effect).

From Figure 4.76, it can be observed that effect of deformation was much more significant compared to copper and magnesium. However, the combined effect of copper and magnesium was less significant. Effect of copper, magnesium and deformation in combination was negative and less significant on hardness. If the amount of deformation is increased from 10% to 50%, a positive increase in half-effects reveals it's most significant impact on hardness for the alloys considered. Increase of copper content from 2% to 6% also has a positive effect on hardness and with increasing magnesium content from 1% to 2%, hardness value tends to rise; however, this is not as significant as that for copper.

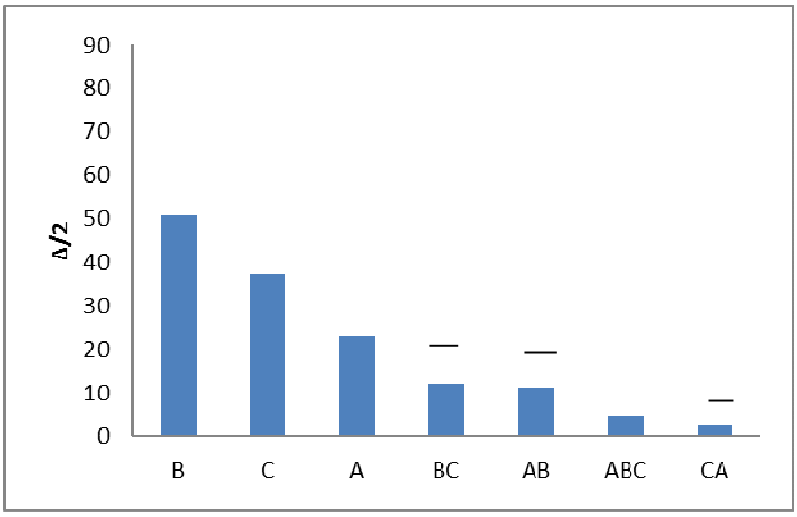

Figure 4.77: Pareto Chart of variables A=Cu (6, 2), B= Mg (1, 0), C= Deformation (50%/10%) (Bar denotes negative effect)

From Figure 4.77, it can be observed that effect of magnesium was more significant compared to copper and deformation. However, the combined effect of copper and magnesium was negative, which means; in combined form those elements lowered hardness. Deformation had a positive and more significant effect than copper on hardness. Effect of copper, magnesium and deformation in combination was positive but less significant on hardness. When the magnesium content is increased from 0% to 1%, a positive increase in half-effects reveals it's most significant impact on hardness for the alloys considered. Increase of copper content from 2% to 6% also has a positive effect on hardness; however, this is not as significant as that for magnesium.

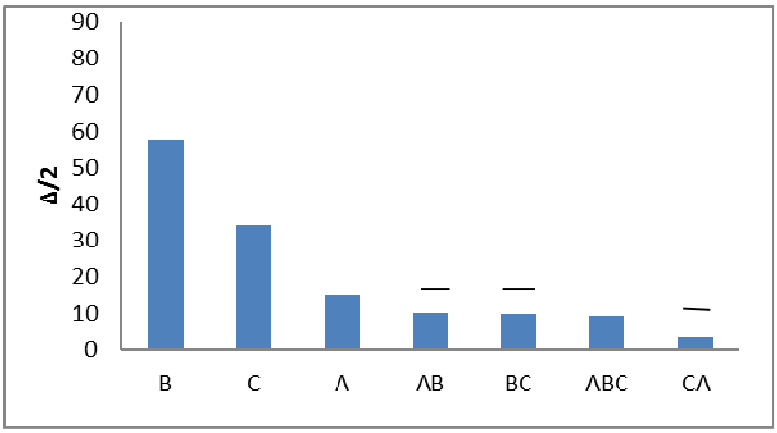

Figure 4.78: Pareto Chart of variables A=Cu (4, 2), B= Mg (2, 0), C= Deformation (50%/10%) (Bar denotes negative effect).

From Figure 4.78, it can be observed that effect of magnesium was more significant compared to copper and deformation. However, the combined effect of copper and magnesium was negative, which means; in combined form those elements lowered hardness. Deformation had a positive and significant effect on hardness. Effect of copper, magnesium and deformation in combination was positive but less significant on hardness. When the magnesium content is increased from 0% to 2%, a positive increase in half-effects reveals it's most significant impact on hardness for the alloys considered. Increase of copper content from 2% to 4% also has a positive effect on hardness; however, this is not as significant as that for magnesium.

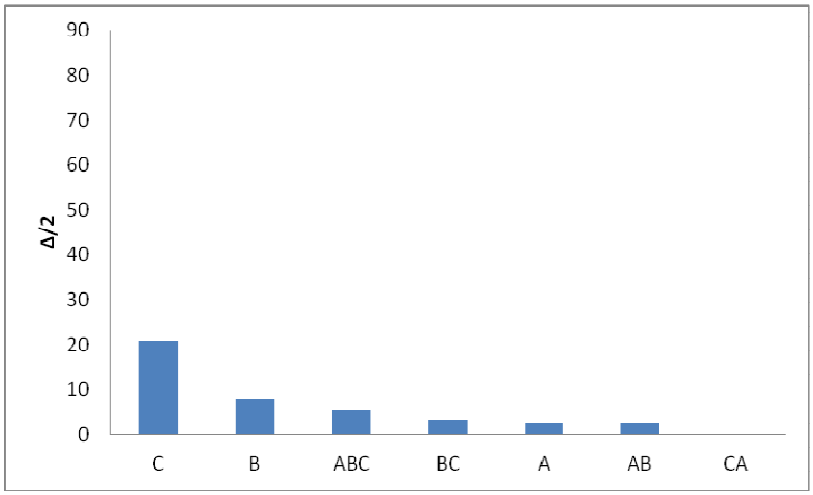

Figure 4.79: Pareto Chart of variables A=Cu (4, 2), B= Mg (2, 1), C= Deformation (50%/10%) (Bar denotes negative effect).

From Figure 4.79, it can be observed that effect of deformation was much more significant compared to magnesium and copper. However, the combined effect of copper and magnesium was less significant. Copper had a positive but less significant effect on hardness. Effect of copper, magnesium and deformation in combination was positive and significant on hardness. If the amount of deformation is increased from 10% to 50%, a positive increase in half-effects reveals it's most significant impact on hardness for the alloys considered. Increase of magnesium content from 1% to 2% also has a positive effect on hardness and with increasing copper content from 2% to 4%, hardness value tends to rise; however, this is not as significant as that for magnesium.

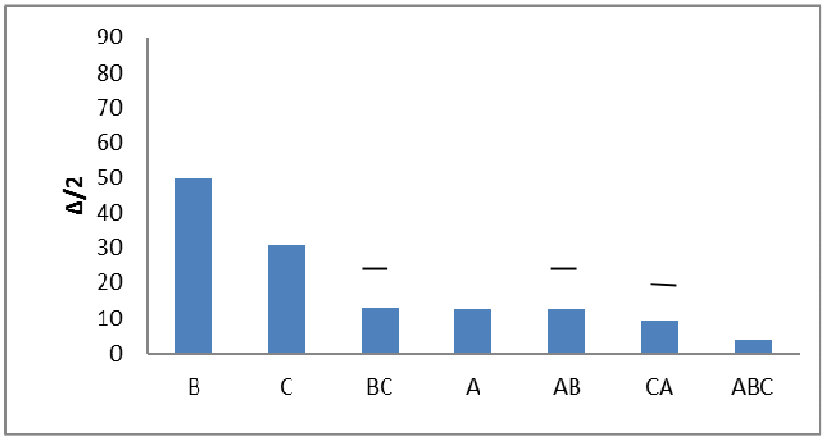

Figure 4.80: Pareto Chart of variables A=Cu (4, 2), B= Mg (1, 0), C= Deformation (50%/10%) (Bar denotes negative effect).

From Figure 4.80, it can be observed that effect of magnesium was more significant compared to deformation and copper. However, the combined effect of copper and magnesium was negative, which means; in combined form those elements lowered hardness. Deformation had a positive and significant effect on hardness. Effect of copper, magnesium and deformation in combination was positive but less significant on hardness. When the magnesium content is increased from 0% to 1%, a positive increase in half-effects reveals it's most significant impact on hardness for the alloys considered. Increase of copper content from 2% to 4% also has a positive effect on hardness; however, this is not as significant as that for magnesium.

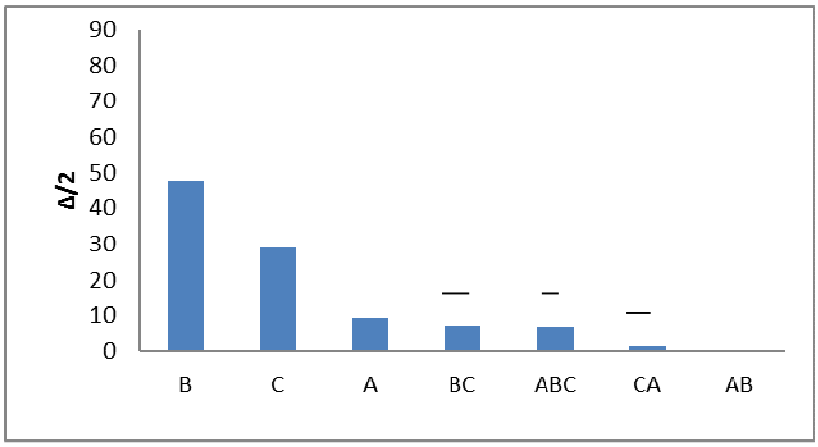

Figure 4.81: Pareto Chart of variables A=Cu (6, 4), B= Mg (2, 0), C= Deformation (50%/10%) (Bar denotes negative effect).

From Figure 4.81, it can be observed that effect of magnesium was more significant compared to deformation and copper. However, the combined effect of copper and magnesium was very negligible. Deformation had a positive and significant effect on hardness. Effect of copper, magnesium and deformation in combination was negative and less significant on hardness. When the magnesium content is increased from 0% to 2%, a positive increase in half-effects reveals it's most significant impact on hardness for the alloys considered. Increase of copper content from 4% to 6% also has a positive effect on hardness; however, this is not as significant as that for magnesium.

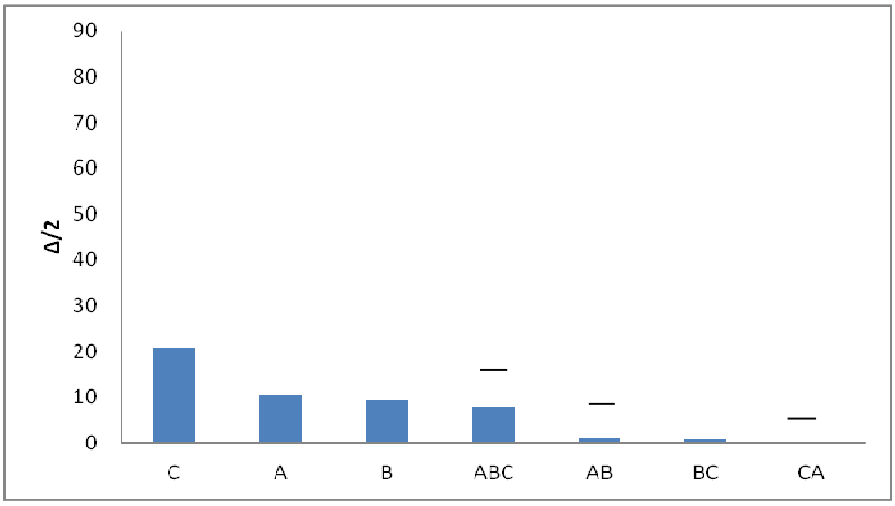

Figure 4.82: Pareto Chart of variables A=Cu (6, 4), B= Mg (2, 1), C= Deformation (50%/10%) (Bar denotes negative effect).

From Figure 4.82, it can be observed that effect of deformation was much more significant compared to copper and magnesium. However, the combined effect of copper and magnesium was negative, which means; in combined form those elements lowered hardness. Effect of copper, magnesium and deformation in combination was negative but significant on hardness. If the amount of deformation is increased from 10% to 50%, a positive increase in half-effects reveals it's most significant impact on hardness for the alloys considered. Increase of copper content from 4% to 6% also has a positive effect on hardness and with increasing magnesium content from 1% to 2%, hardness value tends to rise; however, this is not as significant as that for copper.

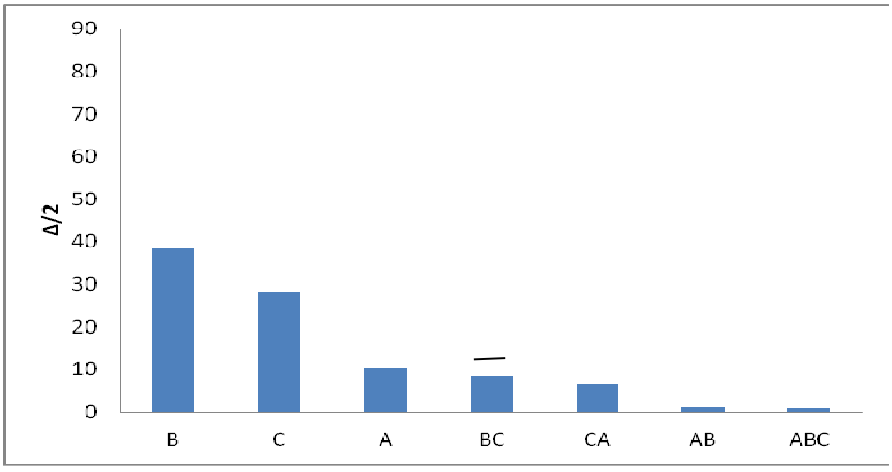

Figure 4.83: Pareto Chart of variables A=Cu (6, 4), B= Mg (1, 0), C= Deformation (50%/10%) (Bar denotes negative effect).

From Figure 4.83, it can be observed that effect of magnesium was more significant compared to deformation and copper. However, the combined effect of copper and magnesium was negligible. Deformation had a positive and significant effect on hardness. Effect of copper, magnesium and deformation in combination was positive but less significant on hardness. When the magnesium content is increased from 0% to 1%, a positive increase in half-effects reveals it's most significant impact on hardness for the alloys considered. Increase of copper content from 4% to 6% also has a positive effect on hardness; however, this is not as significant as that for magnesium.

In summary, from these (Figures 4.75-4.83) Pareto charts it is clear that both magnesium and extent of deformation affects hardness of Al-Cu-Mg alloys to a large extent. The effect of magnesium dominates when variables were compared between alloys containing no magnesium and with magnesium. But for alloys containing magnesium about 1% and 2%, the extent of deformation dominated rather than magnesium addition. Copper has lesser effect on hardness compared to magnesium and extent of deformation.

CHAPTER 5
CONCLUSION

This study emphasizes the effect of alloying elements and deformation on microstructure and hardness of aluminum alloys with varying amount of copper and magnesium. Results obtained from this research can be summarized as follows:

(i) Homogenization treatment causes dissolution of low melting point phases in to the matrix and thus reduces hardness of aluminum alloys.
(ii) CALPHAD modeling predicted the weight fractions of phases formed during solidification and homogenization. The major phase was Al_2Cu (except alloy A0, where there was a phase of Al_7Cu_4Ni, which can accommodate different amounts of nickel or copper because these two elements have atomic similarity. If more copper is substituted, it will tend to reduce the stability of other copper containing phases such as Al_2Cu).
(iii) EDX results also assured the formation of Al_2Cu phase (white phase) and Al_7Cu_2M and Mg_2Si phases (black phase).
(iv) Except alloy A0, the results from image analysis (taking account the associated error from standard deviation) closely match with modelling predictions.
(v) In the alloys investigated addition of copper increases copper containing phases Al_2Cu and Al_7Cu_2M. Similarly, with increasing magnesium content fraction of Al_2CuMg and Mg_2Si phases were also found to increase.
(vi) From DTA results it was evident that addition of alloying elements lowers liquidus and solidus temperatures of alloys which were also predicted precisely in modeling.
(vii) Deformation causes an increase in hardness than non-deformed homogenized alloy due to changes in dislocation density. Deformation increases the number of dislocations by interactions of dislocation during deformation and other defects, which cause an enhancement of hardness values. High dislocation density results in a large number of dislocation interactions which results in high strength and hardness.

(viii) Deformation also changes the microstructure by destroying the necklace like shape of Al-Cu-Mg phases. For this reason, with larger amount of deformation, the increment of hardness may not be very significant.

(ix) Solution treatment at 500 °C results a decrease in phase fraction in the microstructure compared to that without any solution treatment.

(x) With increasing amount of deformation, hardness continues to increase for different magnesium addition. Also, the higher the magnesium content, the greater is the hardness. Addition of copper results an increase in hardness of homogenized aluminum-copper-magnesium alloy.

(xi) Solution treatment also decreases the hardness of aluminum alloys due to dissolution of Al_2Cu and Mg_2Si phases in aluminum matrix.

(xii) ANOVA modeling concludes that magnesium addition and amount of deformation affect hardness of Al-Cu-Mg alloys to a large extent compared to addition of copper and homogenization treatment.

REFERENCE

1. H.N. Girisha and K.V. Sharma, “Effect of Magnesiun on Strength and Microstructure of Aluminum Copper Magnesium Alloy”, International Journal of Scientific & Engineering Research, ISSN 2229-5518, Vol. 3(2), 2012.
2. A. Zhu, B. M. Gable, G. J. Shiflet, E. A. Jr. Starke, “Trace element effects on precipitation in Al–Cu–Mg–(Ag, Si) alloys: a computational analysis”, ActaMaterialia 52, pp. 3671–3679, 2004.
3. I. J. Polmear, *Light Alloys*, Arnold, 1995
4. http://www.efunda.com/materials/alloys/aluminum/aluminum.cfm, Date Accessed: 16/12/2012
5. R.E. Sanders, “Technology Innovation in aluminum Products”, The Journal of the Minerals, 53(2):21–25, 2001.
6. http://aluminium.matter.org.uk/content/html/eng/default.asp?catid=214&pageid=2144417044, Date Accessed 17/11/2012
7. J. R. Brown, S- Foseco Non-Ferrous, Foundryman’s Handbook, Eleventh edition, Source: e0750642866 element
8. J.A. Omotoyinbo and I.O. Oladele, “Effect of Plastic Deformation and Magnesium Content on the Mechanical Properties of 6063 Aluminum Alloys”, Journal of Minerals and Materials Characterization and Engineering”, Vol. 9, No. 6, pp 539-546, 2010.
9. D. Apelian, Aluminum Cast Alloys: Enabling Tools for Improved Performance, North American Die Casting Association, Wheeling, Illinois, 2009.
10. D. Apelian, “Aluminum Cast Alloys: Enabling Tools for Improved Performance”, NAZCA, 2009.
11. S.H. Avner, “Introduction to Physical Metallurgy”, McGraw-Hill Book Company, Second Edition, ISBN 0-07-002499-5, 1974

%.

12. http://chem240.cs.uwindsor.ca/resources/Lecture-Notes/240_l19_supp.pdf, Date Accessed: 17/11/2012
13. http://www.matter.org.uk/matscicdrom/manual/ap.html, Date Accessed 17/11/2012
14. V. S. Zolotorevsky, N.A. Belov, M. V. “Glazoff,Casting Aluminum Alloys” Elsevier, First edition, 2007
15. http://www.keytometals.com/page.aspx?ID=CheckArticle&site=ktn&NM=235, Date Accessed: 17/11/2012
16. L. Kaufman and H. Bernstein, “Computer Calculation of Phase Diagrmas with Special Reference to Refractory Metals”, Academic Press, New York, 1970.
17. C. Wolverton, X. Y. Yan, R. Vijayaraghavan and V. Ozolins, "Incorporating first-principles energetics in computational thermodynamics approaches", Acta Materialia, Vol.50, pp. 2187-2197, 2002.
18. W. J. Golumbfskie, “Modeling of the AL-Rich Region of the Al-Co-Ni-Y System via Computational and Experimental Methoda for the Development of High Temperature AL-Based Alloys”, December 2005.
19. J. Grobner, R.S. Fetzer, A. Pisch, C. Colinet, ET. Al., “Phase Equilibria, Calorimetric Study and Thermodynamic Modeling of Mg-Li-Ca Alloys”, Thermochimica Acta 389, 85-94, 2002.
20. S. G. Fries and T. Zantzen, “Compilation of CALPHAD Formation Enthalpy Data Binary Intermetallic Compounds in the COST 507 Gibbsian Database”, Thermochimica Acta 314, 23-33,1998.
21. S. J. Golumbfskie, “Modeling of the Al-Rich Region of the Al-Co-Ni-Y System Via Computational and Experimental Methods for the Development of High Temperature Al Based Alloys”, 2005.
22. B. Sundman, B. Jansson and J.-O. Andersson, "The Thermo-Calc Databank System", CALPHAD, Vol.9, pp. 153-190, 1985.
23. J. Gro¨bner, D. Mirkovic´, R. Schmid-Fetzer, “ Monotectic four-phase reaction in Al–Bi–Zn alloys”, Acta Materialia 53, 3271–3280, 2005.
24. http://www.calphad.com/calphad_method.html, Date Accessed: 16/12/2012

25. N. Saunders, “The Modeling of Stable and Metastable Phase Formation in Multi-Component Al-Alloys”, 9th International Conference on Aluminum Alloys, Brisbane, Australia, 2-5 August, 2004.
26. N. Saunders and A. P. Miodownik, “CALPHAD – Calculation of Phase Diagrams”, Pergamon Materials Series vol.1, ed. R. W. Cahn, Elsevier Science: Oxford, 1998.
27. N. Saunders, “The Application of Calculated Phase Equilibria to Multi-Component Aluminum alloys”, J.JILM, 51, pp. 141-150, 2001.
28. P. Kolby, “Proc. 4th Int. Conf. on Al-alloys: Their Physical and Mechanical Properties”, vol.3, eds. T.H. Sanders Jr. and E.A. Starke Jr., Georgia Institute of Technology, 2, 1994.
29. L. Kaufman, “Computer Aided Innovation of New Materials II”, (eds.M. Doyama, J. Kihara, M. Tanaka and R. Yamamoto), Elsevier Science, Amsterdam, 683, 1993.
30. M. Hillert, “Computer Modelling of Phase Diagrams”, (ed.L.H.Bennett), TMS, Warrendale, PA, 1, 1986.
31. G. Eriksson and K. Hack: Met. Trans. B, 21B, pp. 1013, 1990.
32. I. Ansara, Int.Met.Reviews, 22, 20, 1979.
33. C. W. Bale and G. Eriksson: Canadian Met. Quarterly, 29, pp. 105, 1990.
34. S-L Chen, K-C Chou, YA Chang, “On a new strategy of phase diagram calculation, 1. Basic principles”, CALPHAD, 17:237.Y., 1993.
35. A. Chang, S. Chen, F. Zhang ET. Al, “Phase Diagram Calculation: Past, Present and Future”, Progress in Materials Science 49, 313–345, 2004.
36. K-C Chou, YA Chang, “A study of ternary geometrical models”, Ber Bunsenges Phys Chem 93, pp. 735, 1989.
37. YM. Muggianu, M. Gambino, JP. Bros. J Chimie Physique, pp. 72-83, 1975.
38. H. Liang, “Thermodynamic modeling and experimental investigation of the Al-Cu-Mg-Zn quaternary system”. Ph.D. Thesis, University of Wisconsin, Madison, WI., 1998.
39. S. Daniel, YA. Chang, unpublished work, University of Wisconsin, Madison, WI., 2001.
40. X-Y Yan, YA Chang, F-Y Xie, S-L Chen, F Zhang, S Daniel, “Calculated phase diagrams of aluminum alloys from binary Al-Cu to multicomponent commercial alloys”. J Alloy Compounds;320:151–60, 2001.

41. N. Saunders, A. P. Miodownik and J.-Ph. Schillé, “Modelling of the Thermo-Physical and Physical Properties for Solidification of Ni-based Superalloys” Liquid Metal Procession 2003, Nancy, France, 2003.
42. N. Saunders, Z. Guo, A. P. Miodownik and J-Ph. Schillé, “Thermo-Physical and Physical Properties for Use in Solidification Modeling of Multi-Component Alloys”, DOI: 10.1002/3527603506.ch10, Published Online: 3 May 2005.
43. Q. Chen and B. Sundman,” Computation of Partial Equilibrium Solidification with Complete Interstitial and Negligible Substitutional Solute Back Diffusion”, Materials Transactions, Vol. 43, No. 3, pp. 551-559, 2002.
44. http://www.ndted.org/EducationResources/CommunityCollege/Materials/Structure/linear defects.htm, Date Accessed :10/06/2012
45. U. Messerschmidt and M. Bartsch, “Generation of dislocations during plastic deformation”, Materials Chemistry and Physics 81, pp. 518–523, 2003.
46. P. Schall, M.Feuerbacher, M.Bartsch and U.Messerschmidt, “Dislocation density evolution upon plastic deformation of Al-Pd-Mn single quasicrystals”, Philosophical Magazine Letters, Vol. 79, No. 10, 785-796, 1999.
47. F.C. Frank, W.T. Read, Phys. Rev. 79, pp. 722, 1950.
48. J.S. Koehler, Phys. Rev. 86, pp. 52, 1952.
49. E. Orowan, “Dislocations in Metals”, American Institute of Mining and Metallurgy Engineering, New York, p. 103, 1954.
50. M. R. Khan, Irfanullah and F. Rehman, Beneficial Effect of Heat Treatment on Mechanical Properties and..Microstructure of Aluminum Alloys Used in Aerospace Industry, *J Pak Mater* Soc, 2008, 9-14, Vol. 2 (1)
51. J. Gubicza, N.Q. Chinh, Z. Horita, T.G. Langdon, Effect of Mg Addition on Microstructure and Mechanical Properties of Aluminum, Materials Science and Engineering, 2004, 55–59, Vol. A 387–389
52. R.S. Rana and R. Purohit, Effect of Magnesiun Enhancement on Mechanical Property and Wear Behaviour of LM6 Aluminum Alloy, International Journal of Scientific & Engineering Research, 2012, ISSN 2229-5518, Vol. 3(7)

53. C.T. Wu, S.L. Lee, M.H. Hsieh, Effect of Cu Content on Microstructure and Mechanical Properties of Al-14.5Si-0.5Mg Alloy, Materials Characterization, 2010, 1074-1079, Vol. 61
54. C.T. Wu, S.L. Lee, M.H. Hsieh and J.C. Lin, Effect of Mg Content on Microstructure and Mechanical Properties of Al-14.5Si-0.5Mg Alloy, Metallurgical and Materials Transactions *A*, 2010, 751-757, Volume 41A
55. G. Wang, X. Bian, W. Wang and J. Zhang, Influence of Cu and Minor Elements on Solution Treatment of Al-Si-Cu-Mg Cast Alloys, Materials Letters, 2003, 4083-4087, Vol. 57
56. C.H. Caceres, M.B. Djurdjevic, T.J. Stockwell and J.H. Sokolowski, Effect of Cu Content on the Level of Microporosity in Al-Si-Cu-Mg Casting Alloys, Scripta Materialia, 1999, 631-637, Vol. 40(5)
57. S. C. Wang and M. J. Starink, "Precipitates and Intermetallic Phases in Precipitation Hardening Al–Cu–Mg–(Li) Based Alloys", Int. Mater Rev., Vol. 50, pp 193-215, 2005.
58. L. Lasa and J.M. Rodriguez-Ibabe, "Characterization of the Dissolution of the Al_2Cu Phase in Two Al–Si–Cu–Mg Casting Alloys Using Calorimetry", Materials Characterization, Vol. 48, Issue 5, pp 371-378.
59. S. O. Adeosun, O. I. Sekunowo, S.A. Balogun, L.O. Osoba, "Effect of Deformation on the Mechanical and Electrical Properties of Aluminum-Magnesium Alloy", Journal of Minerals & Materials Characterization & Engineering, Vol. 10, No.6, pp.553-560, 2011.
60. A. Abdulhaqq, P. Hamid, S. Ghosh,, O. Jain, and R. Subrata, "Processing, Microstructure and Mechanical Properties of Cast in-situ Al (Mg,Mn)-Al_2O_3(MnO2) Composites" Metallurgical and Materials Transactions A, Vol. 36A, pp 221, 2005.
61. N. Roy, A. Samuel and F. Samuel, Metallurgical and Materials Transactions, Vol. 27A, pp. 415-429, 1996.
62. D. Lassance, M. Schmitz, F. Delannay and T. Pardoen, "Linking Microstructure and High Temperature Ductility in Aluminum alloys AA6xxx." Seminar paper available online at: www.hallf.kth.se/forskning/ecf15/ECF-proceedings/Lassance, 2002.
63. R. Valiev, N. Krashkov and K. Tsenev, "Plastic Deformation of Alloys with Submicron-grained Structure." Materials Science and Engineering A, Vol.153, Issue 3, pp.172-196, 1991.

64. http://www.csse.monash.edu.au/~smarkham/resources/anova.htm,DateAccessed: 10/05/2013
65. Anscombe, F. J. "The Validity of Comparative Experiments". Journal of the Royal Statistical Society, SeriesA(General) 111 (3), pp.181–211, 1948.

APPENDIX A

Table A.1 Simulation data for alloy C2

'Temperature (C')	'LIQUID'	'AL'	'AL7CU2M'	'AL2CU'	'MG2SI'	'S_AL2CUMG'
700	100					
690	100					
680	100					
670	100					
660	100					
650	100					
640	100					
638.7433	100	4.63E-06				
630	67.5409	32.4591				
620	48.04095	51.95905				
610	36.47183	63.52818				
600	28.79525	71.20476				
590	23.27874	76.72127				
580	19.05544	80.94457				
573.8901	16.89531	83.10469	0			
570	15.24418	84.60605	0.149766			
560	11.75811	87.86323	0.378659			
550	8.901755	90.60996	0.488283			
540	6.352494	93.10493	0.54258			
530	3.925008	95.50509	0.569899			
526.0802	2.978262	96.44529	0.576445	5.35E-06		
522.988	0	97.58805	0.584641	1.827311		
520		97.2873	0.585127	2.12757		
510		96.35705	0.586624	3.056324		
500		95.52968	0.587942	3.882377		
490		94.78968	0.589097	4.621223		
480		94.12476	0.590108	5.285134		
470		93.52502	0.59099	5.883989		
468.6923		93.45097	0.591096	5.957931	0	
460		92.87642	0.591765	6.472609	0.059204	
450		92.29137	0.592435	6.998642	0.117553	

440		91.77611	0.593011	7.464624	0.166258	
430		91.32078	0.593503	7.879564	0.206155	
420		90.91715	0.593924	8.250784	0.238139	
410		90.55825	0.594281	8.584293	0.26318	
400		90.23808	0.594583	8.885033	0.282308	
391.7935		90.00064	0.594796	9.110245	0.294326	0
390		89.94009	0.594837	9.121679	0.295732	0.047668
380		89.62255	0.595046	9.175616	0.302712	0.304077
370		89.33636	0.595223	9.214916	0.308409	0.545097
360		89.07818	0.59537	9.241993	0.31303	0.771432
350		88.84514	0.595492	9.258896	0.316752	0.983718
340		88.63477	0.595593	9.267369	0.319731	1.182538
330		88.44489	0.595677	9.268901	0.322097	1.368439
320		88.27359	0.595744	9.264766	0.323962	1.541941
310		88.11918	0.595799	9.256059	0.32542	1.703544
300		87.98015	0.595843	9.243718	0.326551	1.853735
290		87.85516	0.595878	9.22855	0.327419	1.992992
280		87.74298	0.595906	9.211248	0.32808	2.121783
270		87.64251	0.595927	9.192409	0.328578	2.240573
260		87.55274	0.595944	9.172543	0.328949	2.349819
250		87.47275	0.595957	9.152088	0.329222	2.449978
240		87.4017	0.595967	9.131416	0.329421	2.541499
230		87.33879	0.595974	9.110843	0.329565	2.62483
220		87.2833	0.59598	9.090636	0.329666	2.700415
210		87.23457	0.595984	9.071017	0.329737	2.768691
200		87.19196	0.595987	9.052169	0.329786	2.830095
190		87.1549	0.595989	9.034239	0.329819	2.885055
180		87.12283	0.59599	9.017341	0.329841	2.933998
170		87.09525	0.595991	9.001563	0.329856	2.977341
160		87.07168	0.595992	8.986964	0.329865	3.015496
150		87.05169	0.595992	8.973579	0.329871	3.048869
140		87.03486	0.595992	8.961424	0.329874	3.077855
130		87.0208	0.595993	8.950491	0.329876	3.10284
120		87.00917	0.595993	8.940759	0.329877	3.1242
110		86.99964	0.595993	8.932187	0.329878	3.142298
100		86.99192	0.595993	8.924723	0.329879	3.157484